Determination Of Optimal Counter-Mass Location In Active Prostheses For Transfemoral Amputees To Replicate Normal Swing

Michael Telwak
Marquette University

DETERMINATION OF OPTIMAL COUNTER-MASS LOCATION IN ACTIVE PROSTHESES FOR TRANSFEMORAL AMPUTEES TO REPLICATE NORMAL SWING

by

Michael Telwak, B.S.

A Thesis submitted to the Faculty of the Graduate School,
Marquette University,
in Partial Fulfillment of the Requirements for
the Degree of Master of Science

Milwaukee, Wisconsin

May 2013

ABSTRACT

DETERMINATION OF OPTIMAL COUNTER-MASS LOCATION IN ACTIVE PROSTHESES FOR TRANSFEMORAL AMPUTEES TO REPLICATE NORMAL SWING

Michael Telwak, B.S.

Marquette University, 2013

Transfemoral amputees suffer the loss of the knee and ankle joints, as well as partial or complete loss of many of the lower extremity muscle groups involved in ambulation. Recent advances in lower limb prostheses have involved the design of active, powered prosthetic knee and ankle-foot components capable of generating knee and ankle torques similar to that of normal gait. The associated onboard motors, conditioning/processing, and battery units of these active components result in increased mass of the respective prosthesis. While not an issue during stance, this increased mass of the prosthesis affects swing. The goal of this study is to develop and validate mathematical models of the transfemoral residual limb and prosthesis, expand these models to include an active ankle-foot, and investigate counter-mass magnitude(s) and location(s) via model optimization that might improve kinematic symmetry during swing.

Single- (thigh only, shank only) and multi-segment (combined thigh and shank) optimization of counter-mass magnitudes and locations indicated that a 2.0 kg counter-mass added 8 cm distal and 10 cm posterior to the distal end of knee unit within the shank segment approximated knee kinematics of able-bodied subjects. This location, however, induced artificial hip torques that reduced hip flexion during swing.

While such a counter-mass location and magnitude demonstrated theoretical potential, this location is not clinically realistic; mass can only be added within the prosthesis, distal to the residual limb. Clinically realistic counter-masses must also keep the total prosthetic mass to less than 5 kg; greater mass requires supplemental prosthetic suspension, would likely increase energy expenditure during ambulation, and contribute to increased likelihood of fatigue even with active prosthetic components. The ability to simulate the effects of active prosthetic components inclusive of varying placement of battery and signal conditioning units may advance the design of active prostheses that will minimize kinematic asymmetry and result in greater patient acceptance.

ACKNOWLEDGEMENTS

Michael Telwak, B.S.

First and foremost, I would like to thank my advisor, mentor, and teacher Dr. Silver-Thorn for helping me from the very start of my academic career at Marquette University. From picking classes as a freshman to revising my final drafts of my thesis as a graduate student, you have quite simply been the catalyst to my success. I do not know how I ever would have come this far without your help and guidance. To you I offer my most sincere gratitude!

I would also like to thank Dr. Voglewede for getting me interested in dynamics. You have been so generous with your time, and have been patient while working with me through the coding hurdles. Your approachability and disposition have made you a joy to work with.

To Dr. Harris, I would like to thank you for being a part of my committee. Your expertise and input has been beneficial to my understanding of my field.

To my family, William, Rosalie, and Zoriana Telwak, thank you for encouraging me to do my best. Your love and support have carried me through this process.

Kirsten. Gracias por todo. Soy porque eres.

Finally, I would like to acknowledge the Department of Biomedical Engineering at Marquette University for the financial support and Joel Kempfer of Kempfer Prosthetics Inc. for providing the loaner knee and foot units used in this study.

TABLE OF CONTENTS

LIST OF TABLES

LISTS OF FIGURES

CHAPTER 1: INTRODUCTION

Transfemoral amputees (TFAs) suffer the loss of the knee and ankle joints, as well as partial or complete loss of many of the lower extremity muscle groups involved in ambulation. To restore limb length and replace some of the lost lower limb functionality, physicians and prothetists prescribe a combination of components to form a functional prosthetic limb. Regardless of the selected components, lower limb prostheses lack the ability to fully restore normal gait and function.

Recent advances in lower limb prostheses have involved the design of active, powered prosthetic knee and ankle-foot components. These designs are able to generate knee and ankle torques similar to that of normal gait [1-11]. Onboard motors and conditioning/processing units located at the knee and ankle provide prescribed torques (and variable damping) based on various kinematic, kinetic, and/or neural control signals. In addition to the increased mass of the active components, the prosthetic limbs also must incorporate the mass of the battery. While not an issue during stance, the increased mass of the prosthesis affects swing.

Prior studies [12-19] have investigated the effects of mass magnitude and location on swing kinematics using passive prosthetic components. Both theoretical models and experimental analyses have shown that adding mass proximally on the shank segment improves kinematic symmetry during swing. For active prosthetic limbs, the addition of counter-weights to offset the mass of the distally positioned motors at the knee and ankle

may facilitate more kinematically symmetric gait, potentially improving acceptance of heavier prosthetic components.

The fundamental hypothesis motivating this study is that inclusion of strategically positioned counter-masses used in conjunction with heavier, active TF prosthetic components will improve kinematic symmetry during swing. The objectives of this study include the 1) development of computer models to simulate swing for an able-bodied lower limb and a TF residual limb and prosthesis with a Total Knee 2000 and an active ankle-foot (prosthetic components commonly prescribed for active TFAs), 2) evaluation of these computer models using normal gait data from the literature [20] as well as motion data from a physical model of the TF residual limb and prosthesis, and 3) use of these models to identify promising counter-mass magnitude(s) and location(s) to offset heavy, active prosthetic components such that hip and knee kinematic trajectories during swing match that of able-bodied subjects. These promising counter-mass locations might then serve as locations for the respective batteries and signal conditioning units of future active prosthetic limbs.

CHAPTER 2: BACKGROUND AND LITERATURE REVIEW

This chapter provides background information relevant to the understanding and development of models for able-bodied and TFA swing. Topics include able-bodied and TFA gait, lower extremity prosthetic components, passive and powered prosthetic knee and ankle mechanisms, and previous work regarding inertial loading of passive prostheses.

2.1 Able-Bodied Gait

Human locomotion is generally studied through gait analysis. The phases of the gait cycle, temporal and spatial parameters, lower extremity muscle activation, joint kinematics and kinetics, and energy cost of ambulation are used to quantify gait. Before summarizing TFA gait, an understanding of able-bodied gait characteristics is necessary.

2.1.1 The Gait Cycle

The gait cycle is generally divided into two periods: stance and swing. The time during which the foot is in contact with the ground is defined as stance. Stance begins with initial contact (heel strike) and ends with toe off. Swing is defined as the advancement of the limb without foot contact. This period extends from toe off until the subsequent heel strike. Stance and swing periods can be further subdivided into eight subcategories or phases of gait [21] (Figure 1). Stance phases include initial contact, loading response, mid-stance, terminal stance, and pre-swing; swing may be divided into initial, mid-, and terminal swing. These divisions allow gait to be described as a cyclic activity in terms of the associated muscle activity [21, 22].

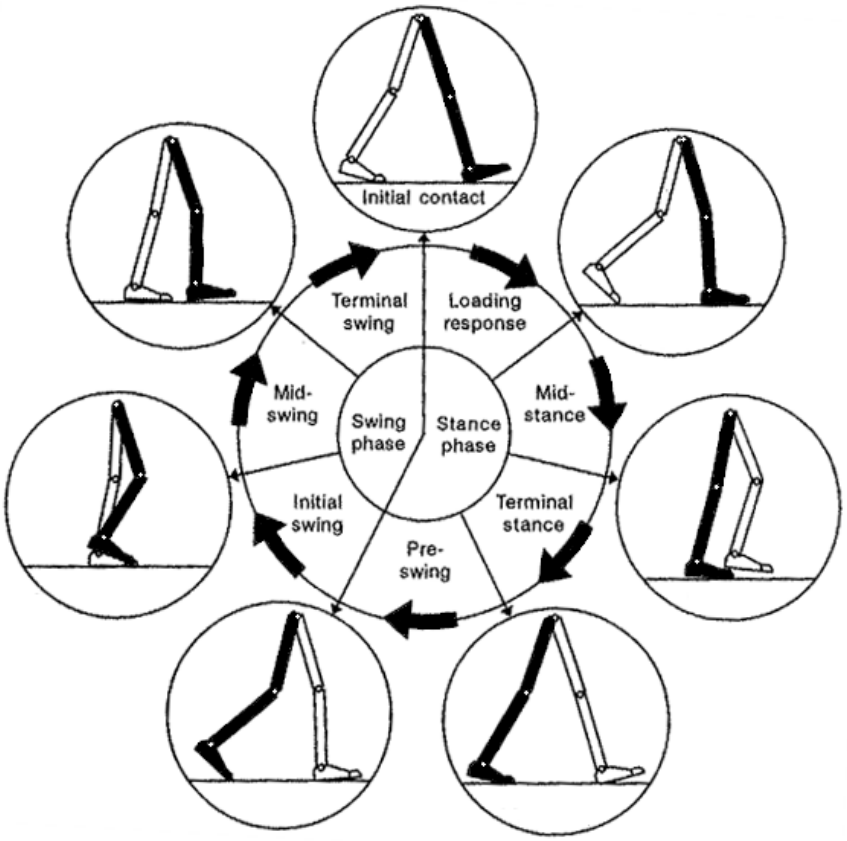

Figure 1: Phases of the gait cycle during stance and swing for the shaded limb. (Adapted from [21])

Initial contact is the first phase of stance. This phase is initiated when weight is accepted on the stance limb. Loading response follows with continued weight bearing through toe off of the contralateral limb. Mid-stance begins at contralateral toe off and ends when weight is aligned over the forefoot. Terminal stance is marked by heel rise of the ipsilateral foot and ends with initial contact of the contralateral foot. During this phase, forward progression of body weight extends past the base of support. Pre-swing is the final phase of the stance period. With initial contact of the contralateral foot, weight is rapidly transferred in preparation for ipsilateral swing.

Initial swing is the first phase of the swing period, beginning with ipsilateral toe off and continuing until the ipsilateral foot is adjacent to the contralateral foot. Mid-swing follows until the ipsilateral tibia is vertical, with passive limb progression resulting from momentum provided during initial swing. Terminal swing is the final phase of swing and the gait cycle; it begins with the tibia in a vertical position and ends with initial contact (heel strike) of the ipsilateral limb.

2.1.2 Temporal and Stride Parameters

Timing and duration of gait cycle events and periods, respectively, are quantified in terms of temporal and stride parameters. Temporal parameters include duration of stance and swing periods, as well as the duration of double and single limb support periods. A single gait cycle is composed of approximately 60% stance and 40% swing [21, 22]. The timing of the stance and swing periods and the phases within stance and swing (Figure 2) varies based on an individual's walking velocity. The gait cycle includes periods of double and single limb support. Double limb support is seen when both feet are in contact with the ground. This occurs within the first 10% of the gait cycle, during loading response as weight is shifted from the contralateral to ipsilateral limb. Single limb support accounts for the following 40% gait cycle, when the ipsilateral limb provides sole weight-bearing support and the contralateral limb is in swing. These periods of double and single limb support are then repeated for the contralateral over the full gait cycle.

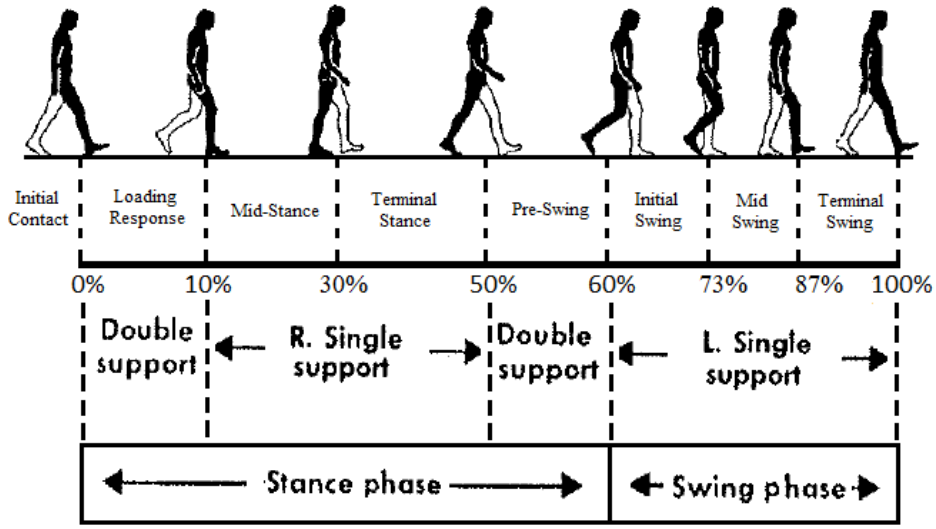

Figure 2: Gait cycle periods and phases, including single and double limb support durations. (Adapted from [23])

Stride parameters include step length, stride length, cadence, and velocity. Step length is the distance between initial contact of the ipsilateral limb to the subsequent initial contact of the contralateral limb. Stride length is the distance from initial contact of the ipsilateral limb to the subsequent ipsilateral heel strike; there are two steps in a single stride (Figure 3). Cadence is defined as the number of steps taken per unit time (often reported in minutes). Step length and cadence are used to determine the speed of progression, or gait velocity, reported as distance travelled per unit time [21, 22].

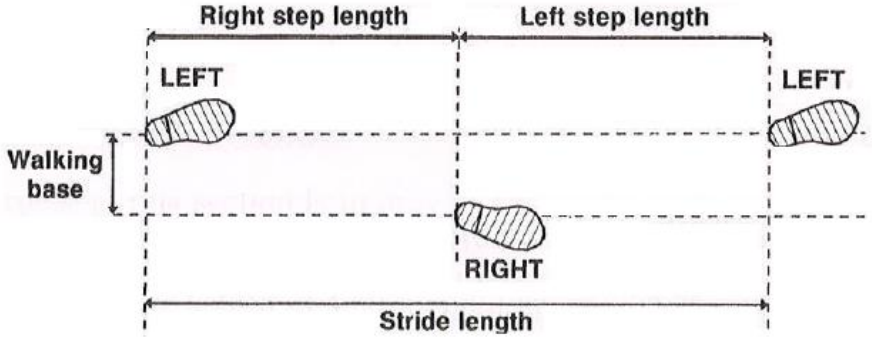

Figure 3: Step and stride length.
(Adapted from [21])

Cadence, stride length, and velocity for able-bodied gait are summarized in Table 1. These values represent mean values for both male and female individuals between the ages of 18-49, 50-64, and 65-80 years [21].

Table 1: Average Able-bodied Stride Parameters.
(Adapted from [21])

Age (years)	Sex	Cadence (steps/min)	Stride Length (m)	Velocity (m/s)
18-49	Male	113	1.55	1.46
	Female	118	1.32	1.30
50-64	Male	104	1.52	1.32
	Female	117	1.30	1.27
65-80	Male	103	1.41	1.21
	Female	116	1.20	1.16

2.1.3 Kinematics

Motion of the body during gait is typically described by joint angle kinematics. As the largest motion occurs in the sagittal plane, only sagittal plane joint kinematics are presented in this section. Normal, able-bodied kinematics for sagittal plane motion of the hip, knee, and ankle joint are summarized in Figure 4 [21].

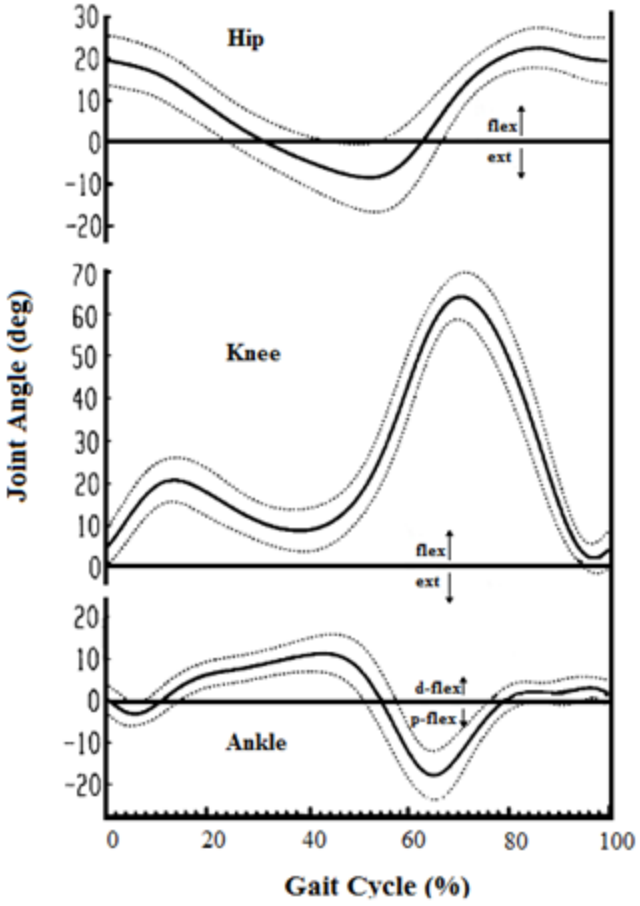

Figure 4: Sagittal plane joint kinematics (mean: solid line, s.d.: dotted) of the hip, knee and ankle during level overground walking for able-bodied subjects (N=16). (Adapted from [24])

Ankle motion throughout the gait cycle is noted by four distinct periods of plantar- and dorsiflexion. During initial contact through loading response, the ankle transitions from a neutral position to a plantarflexed position (first rocker about the heel). Ankle dorsiflexion then follows as the tibia rotates about the ankle during the second rocker with the advancement of the tibia during mid-stance. During the third rocker about the metatarsal heads, rapid plantarflexion occurs, providing push-off during terminal stance and pre-swing. Finally, ankle dorsiflexion occurs during mid- and terminal swing to ensure foot clearance [21, 22]. During the gait cycle, the ankle range of motion

transitions from 10° peak dorsiflexion during terminal stance to 15° peak plantarflexion in initial swing.

Knee motion during gait ranges from approximately 0° to 60° flexion, including two distinct periods of knee flexion, one during stance and one during swing, as shown in Figure 4. At initial contact, the knee is slightly flexed (~5°); knee flexion continues through loading response, peaking at approximately 20° to provide shock absorption during weight acceptance. By mid-stance, the knee is nearly extended for stability during single limb support. Knee flexion is initiated again during terminal stance and pre-swing to prepare the limb for swing, with peak flexion of approximately 60° during initial swing to assist with foot clearance. The knee then extends during mid- and terminal swing to prepare for initial contact [21, 22].

The sagittal plane motion of the hip is also illustrated in Figure 4. At initial contact, the hip is flexed approximately 20°. Gradual extension of the hip during stance provides forward progression from loading response to terminal stance, with peak hip extension of approximately 8° at terminal stance. Hip flexion is initiated during pre-swing, with approximately 25° peak flexion achieved at mid-swing and sustained through loading response to prepare for weight acceptance. Hip range of motion during gait ranges from 25° flexion to 10° extension, a range of nearly 35°; this hip motion is dependent on walking velocity [21, 22].

2.1.4 Muscle Activity

Muscle activity is assessed using surface EMGs for able-bodied gait (Figure 5), and must first be described before discussing joint kinetics.

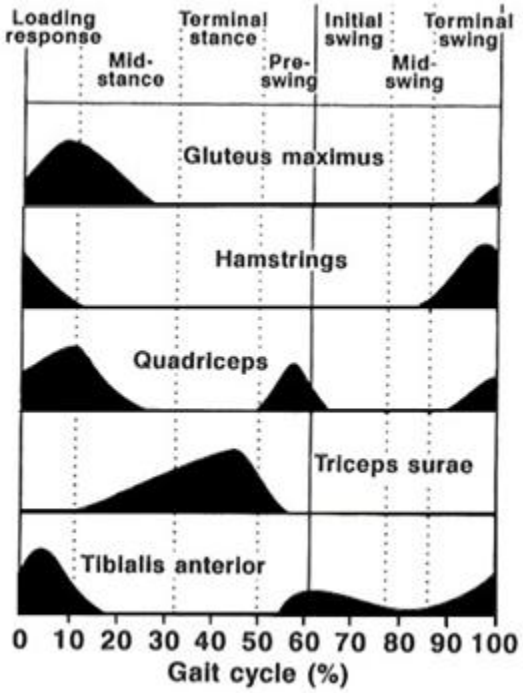

Figure 5: Muscle activity of the ipsilateral limb during the phases of the gait cycle. (Adapted from [21])

The gluteus maximus, a hip extensor, concentrically contracts from initial contact through mid-stance to extend the hip, stabilize the pelvis during weight acceptance, and provide forward progression. Reactivation of the gluteus maximus during terminal swing prepares the limb for initial contact during the subsequent gait cycle. Additional hip stabilization during weight acceptance is provided by the concentric contraction of the hamstrings during loading response. During terminal swing, the hamstrings activate again to decelerate the shank in preparation for initial contact [21, 22].

Quadriceps activity from initial contact through mid-stance provides shock absorption and knee extension during loading response to prevent knee buckling. During pre-swing, the rectus femoris of the quadriceps is again active to flex the hip in preparation for swing. Reactivation of the quadriceps during terminal swing stiffens the knee in preparation for weight acceptance [21, 22].

The triceps surae, which includes the gastrocnemius (knee flexor and ankle plantarflexor) and soleus (ankle plantarflexor only), is active from mid- through pre-swing to provide active push-off of the stance limb in preparation for swing. The tibialis anterior, an ankle dorsiflexor, is active during loading response to control foot flat and prevent foot slap. During swing, the tibialis anterior assists with foot clearance. Reactivation in terminal swing prepares the foot for the following gait cycle [21, 22].

2.1.5 Kinetics

Gait kinetics refer to the reaction forces and moments acting on the joints during ambulation, based on inverse dynamic calculations, kinematic data, ground reaction force data, and segment mass and inertia approximations. The joint moments are often normalized with respect to body mass to facilitate inter-subject comparison. The ankle, knee and hip flexion-extension moments for sixteen able-bodied subjects during level overground walking are summarized in Figure 6 [21].

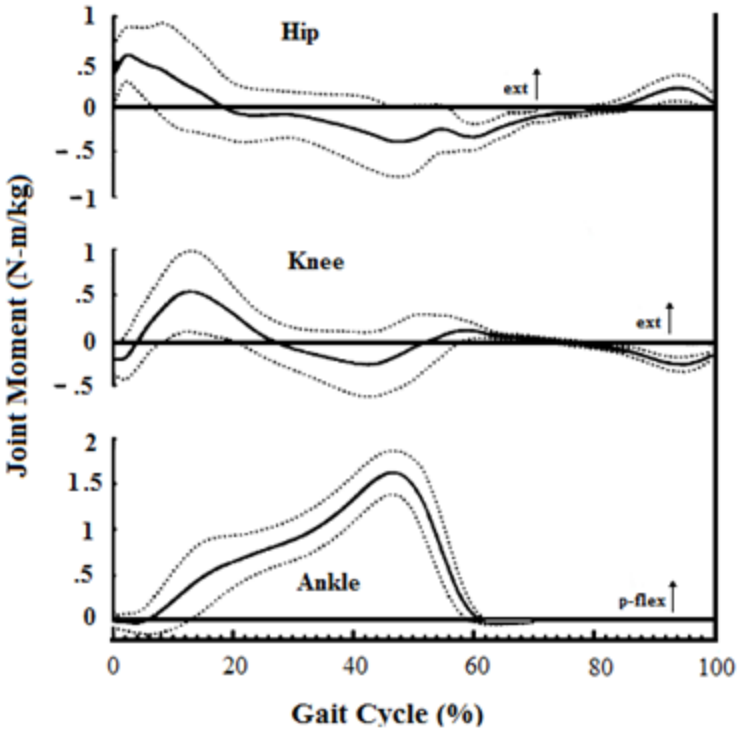

Figure 6: Lower extremity joint reaction moments (mean: solid line, s.d.: dotted) in the sagittal plane for sixteen healthy, able-bodied subjects during level overground walking at the subject's self-selected walking speed. (Adapted from [24])

Inverse dynamic calculation of these joint moments are performed by combining the inertial and gravitational forces with dynamic ground reaction forces at the foot to determine the joint reaction forces [24]. Moment balances, typically about the segment center of mass, can then be used to determine the torque at the respective joint. Assuming low frictional and ligament forces, these moments are the result of muscle activity during ambulation. This inverse dynamic analysis is typically conducted about the foot segment first, applying equal and opposite forces and moments about the more proximal segments, so as to complete the analysis of the full kinematic chain [24].

Clinicians, however, often use the relative location of the weight line and/or ground reaction force vector (GRFV) with respect to the lower extremity joints' centers

of rotation to pseudo-statically visualize joint moments and infer potential joint instability. Moments that are not inherently stable (e.g., prevented by a skeletal mechanical stop) require muscle activation for stability. For example, when the GRFV is posterior to the knee and anterior to the ankle centers of rotation (e.g., early stance), an unstable knee flexion moment and unstable ankle plantarflexion moment occur that require stabilization by the quadriceps and tibialis anterior, respectively (Figure 5) [21]. While providing useful insight to muscle activation, this clinical interpretation is based on a pseudo-static analysis and ignores inertial effects. This section describes the inverse dynamic approach to joint reaction moments while also identifying the muscles responsible for these moments.

The sagittal plane joint moments at the ankle, knee and hip for able-bodied subjects during level, overground walking are summarized in Figure 6. A plantarflexion moment at the ankle is observed from mid- to terminal stance, from approximately 10-60% gait cycle. This plantarflexion moment is provided by the triceps surae to provide active push-off for forward propulsion. A knee extension moment is present from loading response to mid-stance, at 10-30% gait cycle, followed by a flexion moment during terminal stance. These moments are provided by contraction of the quadriceps and hamstrings, respectively. An extension moment for the hip occurs during loading response through mid-stance. This moment is provided by the hamstrings and gluteal muscles. The moment reverses into flexion from terminal stance to mid-swing, via activity of the hip flexors and rectus femoris of the quadriceps [21].

For TFAs, the hamstrings and quadriceps are severed, and the triceps surae and anterior tibialis are lost. With no remaining musculature about the knee and ankle, TFAs must rely on remnant hip extensors and flexors and prosthetic knee stiffness and prosthetic limb alignment to stabilize the prostheses during stance and advance the prosthetic limb during swing [25, 26]. Active, powered prosthetic knee and ankle-foot components can compensate for this lost musculature by generating knee and ankle moments similar to that of able-bodied gait.

2.1.6 Energy Cost

As muscle activation is required to transition between stance and swing phases, energy is required for ambulation. A combination of anaerobic and aerobic metabolic pathways is responsible for providing muscles with the requisite energy. While a limited amount of energy is produced anaerobically, the aerobic process can supply a sufficient source of energy for prolonged activities [22]. As a result, oxygen is the primary energy source; its consumption during ambulation can be measured experimentally using spirometry techniques and is reported as volume of oxygen consumed per unit time, normalized with respect to body mass (e.g., $\frac{mL}{kg \cdot min}$). The energy cost takes the distance travelled into account and is found by dividing the rate of oxygen consumption by the walking velocity ($\frac{mL}{kg \cdot m}$) [22, 27].

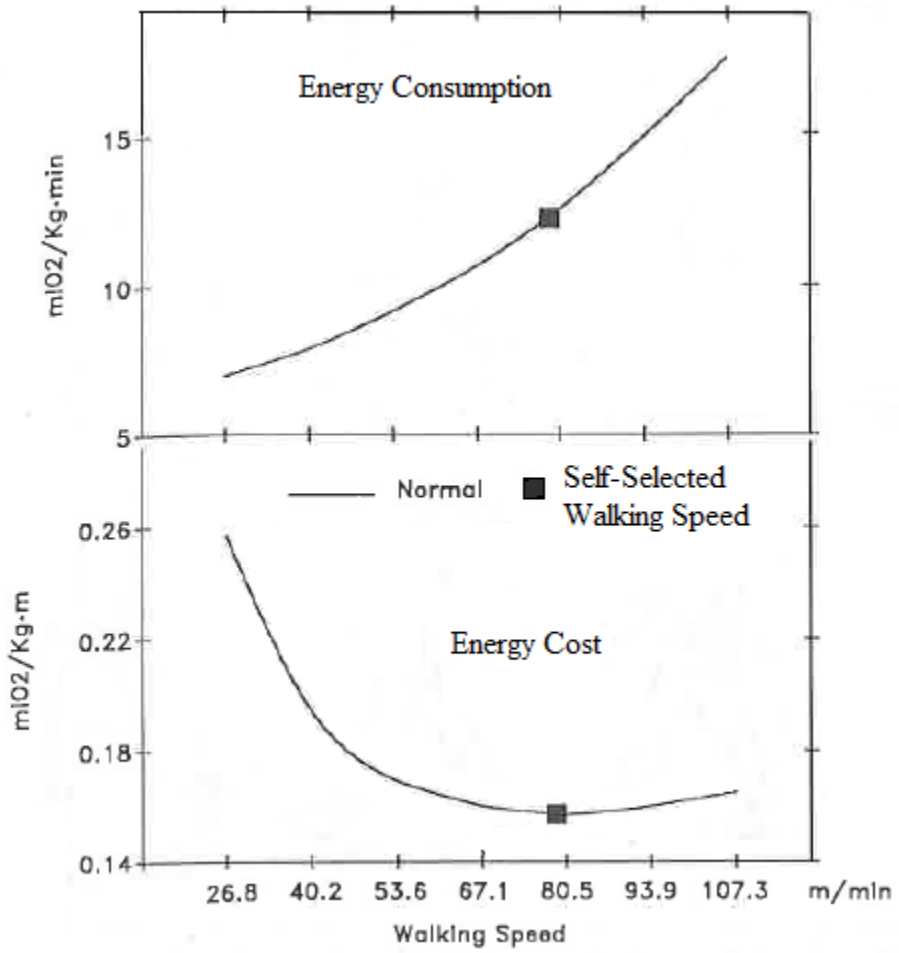

Figure 7: Effects of walking speed on energy consumption and cost of able-bodied subjects during level overground walking. (Adopted from [28])

Analysis of healthy able-bodied subjects during level overground walking demonstrates that energy consumption increases with walking speed. Energy cost indicates a parabolic relationship with greater energy cost observed at both slow and fast walking speeds; a local minimum is observed at the self-selected walking speed (approximately 80 m/min or 3.5-4 mph), as shown in Figure 7. While the above graphs demonstrate the dependence of energy consumption and cost on walking speed, specific

values vary with test protocol, spirometric instrumentation, and overground versus treadmill ambulation.

2.2 TFA Demographics and Surgery

The demographics and functional losses due to TF amputation surgery will be summarized in this section. This content will assist in describing the prosthetic componentry.

2.2.1 Demographics and Amputation Statistics

Nearly 1.7 million people in the U.S. are living with the loss of a limb, and 185,000 new amputations are performed each year [29]. Dysvascular diseases account for the majority, 82%, of all lower limb amputations; other causes include cancer, congenital disorders, and trauma. Of these amputations, 41% are performed at the transtibial and 39% at TF levels, excluding partial foot amputations [30]. These statistics show that there are over a quarter of a million people with TF amputation in the U.S.

2.2.2 Amputation Surgery and Relevant Anatomy

TFA involves amputation through the femur, loss of the knee and ankle joints, and partial or complete loss of lower extremity muscle groups. TF amputation may be performed at the supracondylar, mid-femur, or lesser trochanter level. Supracondylar level amputations result in a longer residual limb, while a subtrochanteric level amputation results in a short residual limb [31]. TF amputations can also be performed between these two levels, at the mid-femur level. The remnant femur must extend

proximally to the ischial pubic ramus (e.g., 3-5 cm) distal to the lesser trochanter to provide a sufficient lever arm for hip flexion/extension, ab/adduction, and internal/external rotation [31]. The remnant muscles of the hip (e.g., quadriceps and hamstrings) are then sutured together via myoplasty to provide continued muscle functionality and distal padding. Due to greater strength, the quadriceps are often cut shorter and have more slack than the hamstrings.

The resultant range of motion of the remnant hip is dependent on the length of the residual limb, the tautness of the remnant muscles, and the functional strength of the remaining musculature. A prosthesis can be prescribed to help restore lower limb functionality and ambulation. The respective prosthetic components are prescribed based on length of the residual limb, remnant hip muscle strength and voluntary control, and anticipated functional level (K-levels[*]). More complex knee and ankle-foot components are typically prescribed for active amputees (K3 and K4 level) to provide stance and swing phase control, facilitating variable cadence ambulation. These components, however, are typically passive and unable to fully restore the lost musculature. Consequently, the gait patterns for TFAs differ from that of an able-bodied person [32, 33].

[*] K levels are used to classify the ambulatory abilities of amputees. K3 and K4 level amputees are community ambulators who have the ability to walk at variable cadence and perform activities that may subject the residual limb and prosthesis to impact loads [34].

2.3 TFA Passive Prosthetic Components

To restore limb length and replace some of lost lower limb functionality, physiatrists prescribe a prosthetic limb. These TF prostheses include a socket which forms the mechanical interface between the residual limb and prosthesis, some form of prosthetic suspension, a knee joint, and an ankle-foot component. These components can then be linked through exoskeletal or endoskeletal designs.

Prosthetic component selection is based on the amputee's weight, activity level, and projected functional status or K-level [34]. All lower limb prostheses are fabricated, fitted, and aligned by a prosthetist to best restore normal gait and function.

2.3.1 Exoskeletal versus Endoskeletal Designs

Prosthetic components are linked together via either an exoskeletal or endoskeletal design. An exoskeletal design consists of a hard exterior, providing load transfer through the prosthetic exterior. Exoskeletal designs are perhaps more durable, but the prosthetic alignment or component changes cannot be easily performed. In contrast, pylons and tube clamp adaptors are used to link the prosthetic socket, knee, and ankle components in an endoskeletal design. Traditional pylons are rigid, hollow tubes made of stainless-steel, aluminum, titanium, or carbon fiber, making this design lighter. Endoskeletal designs more readily facilitate prosthetic alignment and component changes.

Shock-absorbing pylons are also available to reduce the forces transferred to the residual limb. Spring-like mechanisms within the pylon shorten telescopically under axial loading. Some designs also provide transverse rotation to reduce transmission of torsional loads and shear forces during ambulation over uneven terrain and/or rotational loading. These shock-absorbing pylons may be indicated for amputees who participate in high-impact activities (K4-level) [35, 36].

2.3.2 Sockets

The prosthetic socket acts as the mechanical interface between the residual limb and the prosthesis. These sockets are made of a plastic laminate formed over a plaster-positive model of the residual limb. Proper fitting is critical to provide stability and transfer loads from the remnant skeletal structure to the prosthesis through the soft tissue. An improper fit can lead to pain, edema, movement of the residual limb within the socket (pistoning), discomfort during ambulation, and potentially impaired remnant hip muscular function [28].

The two most common types of TFA sockets are the quadrilateral and ischial containment sockets. The objective of both designs is to use femoral flexion and adduction so as to have the hip extensors and abductors at a functional length. The design choice depends on the length of the patient's residual limb, functional strength of the remaining musculature, ability to balance, and prosthetist preference [28, 34, 35].

The quadrilateral socket, as the name implies, consists of four walls: posterior, anterior, medial, and lateral [35]. The posterior wall contains a small, horizontal shelf used as a weight bearing surface for the ischial tuberosity. The anterior wall extends superiorly to the ischial seat and provides pressure needed to maintain contact with the posterior wall. The medial wall of the socket provides a counterforce for the remnant tissues and musculature, while the lateral wall places the femur in adduction. This type of socket is typically recommended for patient with a long residual limb and strong remnant musculature.

The ischial-containment socket is typically prescribed for active TFAs with short, fleshy residual limbs. This socket contains a wide anterior-posterior and narrow medial-lateral dimensions to maintain adduction of the femur. Unlike the quadrilateral design, high posterior and medial walls encase the ischial tuberosity within the socket. This containment provides a mechanical lock between the ischium, trochanter, and lateral femur, preventing mediolateral translation and more effective distribution of forces on the residual limb [34, 35, 37].

2.3.3 Suspension System

The prosthetic suspension system keeps the prosthesis securely attached to the residual limb, maintaining the prosthesis in an optimal functional position while supporting the weight of the knee and ankle-foot components. Proper suspension assists in minimizing movement of the residual limb within the socket to achieve stable and efficient gait. The five types of suspension systems prescribed for TFAs include an

external hip joint and pelvic band, supplemental Silesian belt, supplemental total elastic suspension (TES) belt, suction suspension with expulsion valve, and liner suction with locking pin [34, 35].

The hip joint and pelvic band suspension consists of a metal pin joint positioned over the anatomic hip joint and attached to a leather-lined pelvic band resting on the iliac crest. Fixation of the joint in the sagittal plane provides rotational control and increases medial-lateral stability of the residual limb within the socket. This form of suspension is typically prescribed for TFAs with short residual limbs. Poor cosmetic appearance, increased weight, and potential discomfort in the seated position do not make this form of suspension highly favored [28, 34, 35].

A Silesian belt is another method of suspension which wraps around the pelvis and is anchored to the socket. This configuration provides supplemental rotational control of the residual limb within the socket. A Silesian belt is commonly used in combination with suction suspension for active TFAs with short residual limbs [28, 34, 35].

The TES belt is made of an elastic neoprene material. This method of suspension fits around the proximal socket and encircles the waist. The TES belt prevents excessive limb pistoning by distributing pressure over a greater area. This form of suspension may be comfortable for low activity levels, but the associated heat retention can be problematic for active TFAs. TES belts are typically used as a supplemental means of suspension as it provides easy donning and doffing of the prosthesis [28, 34, 35].

Suction suspension is the most frequently used form of suspension, providing total contact of the residual limb with the socket, improving prosthetic limb control, and enhancing proprioception during ambulation. The two types of suction suspension include the traditional suction with expulsion valve and more recent gel liner with locking pin. In traditional TF suction suspension, the residual limb is wrapped with an ace bandage or pull sock and placed into the socket. The bandage or sock is then removed through a hole located at the distal end of the socket. A one way air expulsion valve is then screwed into place, sealing the hole. Loading of the prosthesis allows additional air to escape, securing the residual limb within the socket. This suspension method requires that the residual limb volume is stable. For liner suction suspension system, a silicone liner with a distal locking pin provides a stable mechanical lock between the residual limb and prosthesis. The liner is rolled over the residual limb, creating a suction fit between the residual limb and silicone liner. The locking pin is then inserted into the socket, locking the residual limb in place via a mechanical linkage [28, 34, 35, 37].

2.3.4 Prosthetic Knees

Prosthetic knee components are designed to replicate able-bodied knee joint motion in the sagittal plane. These components must provide stability during weight bearing in stance and control limb advancement during swing. Prosthetic knees are characterized as either single-axis or polycentric, which can be further divided into stance and swing phase control. Improper design selection, fitting, or alignment may result in buckling of the knee during stance, inability to fully extend the prosthesis during swing,

or produce an altered gait pattern that increases energy expenditure. Thus, knee prescription by the physician and prosthetist is based on the consideration the functional capacity of an amputee and inherent prosthetic knee stability to produce effective gait.

The simplest stance phase controlled design is a mechanical locking knee joint. A slider pin keeps a single or polycentric knee-axis in full extension throughout the gait cycle; the lock can be disengaged for seating. This design provides maximum stance stability, but results in abnormal gait patterns due to restricted knee flexion during swing. To prevent excessive hip hiking, circumduction, or vaulting to assist with limb clearance, the overall length of the prosthesis is typically shortened. This design is most often used for gait training of new amputees, geriatric patients, or other TFAs with limited mobility and stability issues (e.g., K1-level) [28, 34].

In contrast, free single axis designs allow flexion and extension of the knee joint about one axis of rotation. Stability depends upon the position of the knee center of rotation with respect to the ground reaction force and strength of the remnant musculature. While the knee is capable of rotating freely during swing, weight-activated designs provide stability during stance by locking the knee during loading. Weight bearing of the prosthesis activates a locking pin to prevent undesired flexion or buckling of the knee. This lock releases at toe off for swing. These designs are often prescribed for TFAs with short residual limbs and inability to stabilize the knee during weight acceptance [28, 34].

Polycentric knee designs consist of a series of four or more links to provide a changing instantaneous center of rotation which simulates the anatomic knee joint more closely. Simple polycentric designs focus on cosmetic appearance by reducing limb length discrepancies for long TF residual limbs when seated. The geometry of the mechanism allows the prosthetic shank to tuck under the thigh in flexion. Individuals with both TFA and knee disarticulations may use polycentric knees. More complex designs take advantage of the changing instantaneous center to provide additional stance phase stability. During stance, the instantaneous center of rotation lies proximally on the socket and anterior to knee to create a locking moment, preventing knee flexion. The center rapidly descends to the height and location of an able-bodied knee joint during swing. This shift reduces the effort required to induce a knee flexion moment for swing. Geometric configurations of the design may also assist in toe clearance during swing with flexion. This type of knee is prescribed for TFAs who require inherent knee stability and/or minimized length discrepancies [28, 34, 38].

Swing phase control differs from stance phase control designs by controlling the speed of knee flexion and extension during swing. Knees provide smooth pendulum-like rotation of the shank, limit knee flexion and heel rise in early swing, and enable variable resistance to accommodate an amputee's self-selected walking speed. Early designs, such as a constant friction knee, are optimized for a single cadence and walking velocity. Advances in hydraulic and pneumatic designs, however, allow the knee to vary resistance for flexion/extension during swing. The variable resistance ensures that the prosthetic

limb reaches full extension during terminal swing for various cadences and walking velocities.

The simplest swing phase control, as mentioned above, is a constant friction mechanism. This design consists of a mechanical collar wrapped around a knee bolt; friction can be adjusted via a screw. An optimal frictional setting prevents excessive heel rise during terminal stance and limits knee flexion during swing. The major disadvantage of this design is that friction can only be optimized for a single walking speed. Increased walking speed results in terminal impact of the shank upon full extension [28, 34, 35].

Hydraulic and pneumatic swing phase controlled knees are cadence responsive. Fluid swing phase control is available for both single-axis and polycentric designs. The fluid mechanical properties regulate the resistance to knee flexion and extension. Piston components force fluid through narrow channels. As shear force is proportional to velocity, the resistance increases as cadence and walking speed increase. The number of channels allowing fluid flow can be adjusted by the prosthetist so as to support an optimal range of resistance for the subject's gait velocities. These designs are mostly prescribed for active TFAs with longer residual limbs who vary walking speed (K3 or K4-level) [28, 34, 39].

Some fluid controlled designs are able to provide both stance and swing phase control. During stance, the fluid mechanism prevents knee flexion during weight bearing. This feature allows TFAs to ambulate over uneven terrain with greater confidence [34].

Other prosthetic knee designs include microprocessor technology. Sensors transmit joint and force data to an onboard processor. Predictive algorithms adjust the resistance of mechanical, hydraulic, and/or pneumatic components to provide stance and swing phase control. While these advanced components allow TFAs to walk with improved gait, microprocessor controls remain passive, unable to provide active torque at the knee [34, 35].

2.3.5 Ankle-Foot Components

A prosthetic ankle-foot is the final component necessary for a functional prosthesis. While prosthetic ankle-foot designs are made to replicate a normal ankle (and perhaps the subtalar joint), these feet are unable to duplicate the complex biomechanical functionality of the anatomic ankle and subtalar joint. Most foot designs focus on performance during stance to provide shock absorption and control plantarflexion during loading response, a solid base of support during weight transfer and forward progression, and limited push-off for transition into swing [34]. Variations in foot designs produce changes in functional characteristics important to determining the most effective foot for an amputee.

Prosthetic feet may be divided into three main categories: non-articulating, articulating, and dynamic response or energy storage and return (ESAR). The ESAR feet may be articulating or non-articulating.

The simplest and most commonly prescribed non-articulating foot is the Solid Ankle Cushioned Heel (SACH) foot. This lightweight foot is composed of dense and flexible foam surrounding a rigid keel. Compression of the heel cushion at initial contact simulates plantarflexion and provides shock absorption, while the solid keel prevents excessive heel rise at terminal stance. Due to lack of propulsion force during pre-swing, the SACH foot is most appropriate for limited community and household ambulators (K1- K2 level) [34, 35].

Articulating ankle-foot designs permit motion of the ankle joint in one or more planes. The simplest design is the single-axis foot which contains an ankle joint with rubber bumpers limiting plantarflexion and dorsiflexion to 15° and 5-7°, respectively. A single-axis design provides excellent shock absorption and rapid foot flat at initial contact. This response contributes to enhanced knee stability by reducing the required knee flexion moment. Single-axis feet are commonly prescribed for TFAs who require knee stability due to weak hip extensors or short residual limbs [34].

Multi-axis feet are similar to single-axis designs but also provide motion in the transverse and coronal planes. Active amputees who frequently walk on uneven terrain find multi-axis foot designs advantageous. These added degrees of freedom allow the foot to conform to various surfaces and absorb shear forces and torques which would be otherwise transferred to the residual limb. The increased design complexity, however, tends to make articulated multi-axis feet heavier than non-articulated designs [34, 35].

Dynamic response or ESAR feet are the final category of passive prosthetic feet. These designs are made with carbon fiber and other composite materials which absorb energy through deformation of the keel at heel strike and return a fraction of the energy during pre-swing. This response and ability to fine tune stiffness enables amputees to walk with less difficulty. Dynamic response feet are especially beneficial for high level, active amputees (K3-K4 level) as these designs adapt to increased cadence and walking speed. While most ESAR feet are non-articulating, some designs (e.g., Tru-Step by College Park) combine dynamic response with multi-axis capabilities, enabling stabilization over uneven terrain while still providing energy return during late stance [34, 35].

2.4 TFA Gait

Although TFA gait is dependent on prosthetic alignment and componentry, the general temporal and stride parameters of TFA gait can be contrasted with that of able-bodied gait during level, overground walking. This section discusses the impact of amputation on TFA gait and provides the rationale for powered knee and foot-ankle prosthetic designs.

2.4.1 Temporal and Stride Parameters

TFAs exhibit a significantly longer gait cycle duration than able-bodied subjects [32, 33], due to temporal asymmetry between the sound and prosthetic limbs and potential confounding medical conditions (Table 2). TFAs tend to have shorter stance duration, with prolonged swing duration, on the prosthetic versus sound limb [33, 40].

When compared to able-bodied subjects, these amputees also spend more time in double limb support, with prolonged single support on the sound limb due to the decreased stance duration on the prosthetic limb [32, 33].

Table 2: Mean temporal and spatial data collected from 10 unilateral, traumatic TFAs and 30 able-bodied subjects during level overground walking. (Adapted from [33])

	Able-bodied Subjects	TFA	
Cycle Duration (sec)	1.06	1.38	
Double-Limb Support Duration (sec)	0.12	0.18	
		Sound	Prosthetic
Stance Duration (sec)	0.65	0.94	0.80
Swing Duration (sec)	0.41	0.43	0.58
Step Length (cm)	78	64	72

Differences in gait velocity, cadence, and stride length are typically less for traumatic versus dysvascular TFAs (see Table 3), largely due to confounding medical conditions and the increased age of dysvascular amputees. Many dysvascular TFAs are unable to walk without crutch assistance [22]. The decreased cadence and walking speed of TFAs may be attributed to sound limb modulation [33] and/or the longer step length of the prosthetic limb due to prolonged sound limb stance duration [41].

Table 3: Mean self-selected walking speed, cadence, and stride of normal and unilateral TFAs (dysvascular and traumatic) during level overground walking. (Adapted from [42])

	Normal or Able-bodied	TFA Traumatic	TFA Dysvascular
Number of Subjects	5	15	13
Average Age (yr)	50	31	60
Self-Selected Walking Speed (m/min)	80	52	36
Cadence (steps/min)	116	87	72
Stride Length (m)	1.50	1.20	1.00

2.4.2 Kinematic

In addition to differences in temporal and stride parameters, differences in lower extremity joint kinematics have also been observed for TFAs with respect to able-bodied subjects, as seen in Figure 8 [25].

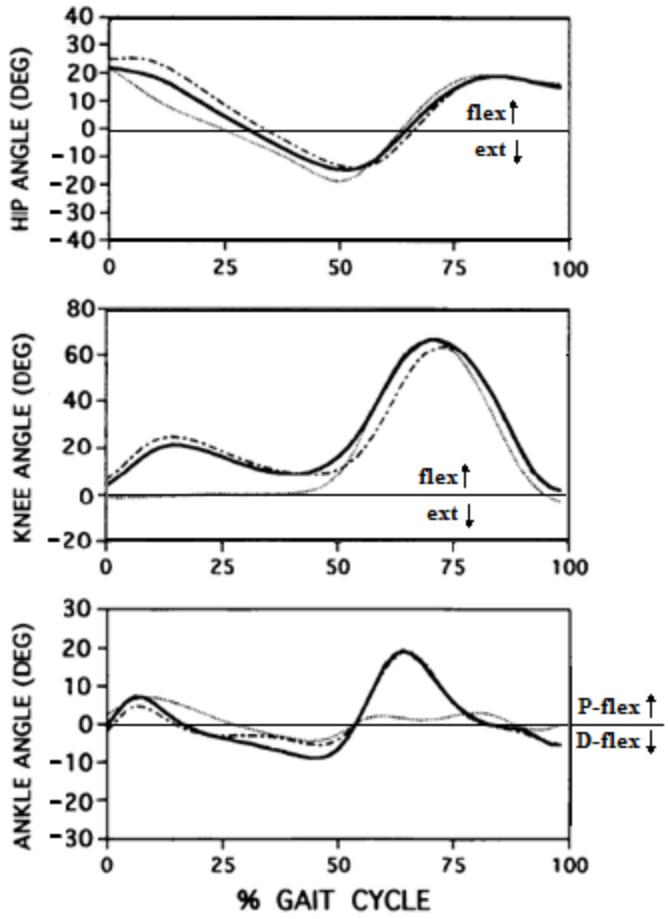

Figure 8: Sagittal plane joint kinematics for able-bodied subjects (solid black, N=8) and TFA [sound limb: dot-dash, prosthetic (Seattle Light Foot, Tehlin polycentric knee, Mauch SNS hydraulic unit) limb: grey, N=8] during level overground walking at the subject's self-selected walking speed. (Adapted from [25])

Although motion of the sound limb of TFAs is similar to that of able-bodied subjects, sagittal plane ankle kinematic data show less dorsiflexion during mid- to terminal stance (Figure 8). Excessive heel rise and reduced dorsiflexion during terminal-stance characterize prosthetic limb ankle kinematics for TFAs. These differences are due to the limited dorsiflexion/plantarflexion range of motion in most prosthetic ankle-foot units [22]. Prosthetic knee motion, however, shows excessive knee extension from loading response through mid-stance to prevent knee bucking during early stance [32, 43]. This knee motion, however, is strongly dependent on the specific prosthetic knee and

its alignment. Finally, hip kinematic data shows that residual limb hip extension starts earlier to initiate swing of the prosthesis [32, 33]. These kinematics are characteristic of TFA ambulating with passive prosthetic componentry; active, powered prostheses may enable TFAs to walking with a more symmetric gait that more closely replicated that of able-bodied subjects.

2.4.3 Muscle Activity

Muscle activity for TFAs differs from that of able-bodied subjects due to the partial or complete loss of many of the lower extremity muscle groups involved in ambulation. Sonja et al. [44] investigated the EMG activity of the remnant quadriceps and hamstring musculature for TFAs, as shown in Figure 9.

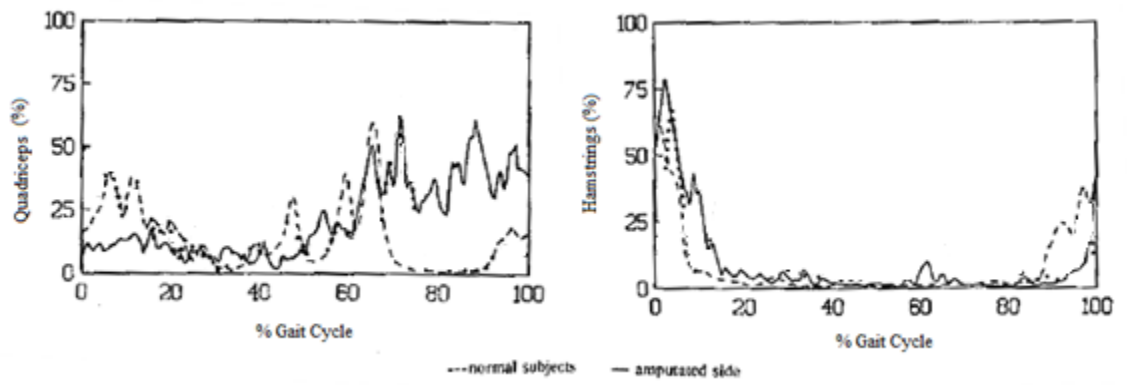

Figure 9: Quadriceps and hamstring muscle activation pattern for the residual limb (solid) of a TFA compared with able-bodied data (dashed, N= 11). (Adapted from [44])

Quadriceps activity for the residual limb remains low during stance. In pre-swing, the rectus femoris of the quadriceps activates to provide flexion of the hip in preparation for swing. The muscle remains active throughout swing to propel the prosthetic limb forward until initial contact.

During initial stance, stronger hamstring activity is needed to provide prosthetic limb stability and prevent the knee unit from buckling in weight bearing. Reactivation occurs at terminal swing; indicative to the TFA pulling the residual limb backwards to ensure that the prosthesis is in full extension.

Variations in these muscle activities were observed among subjects based on altered gait patterns and residual limb length. Particularly, constant high levels of quadriceps and hamstring activity were observed for high level amputees with short residual limbs [44].

2.4.4 Kinetics

Seroussi et al. [25] also investigated lower extremity joint kinetics using inverse dynamic modeling with modified mass and inertial properties of the prosthetics limb, as shown in Figure 10 [25].

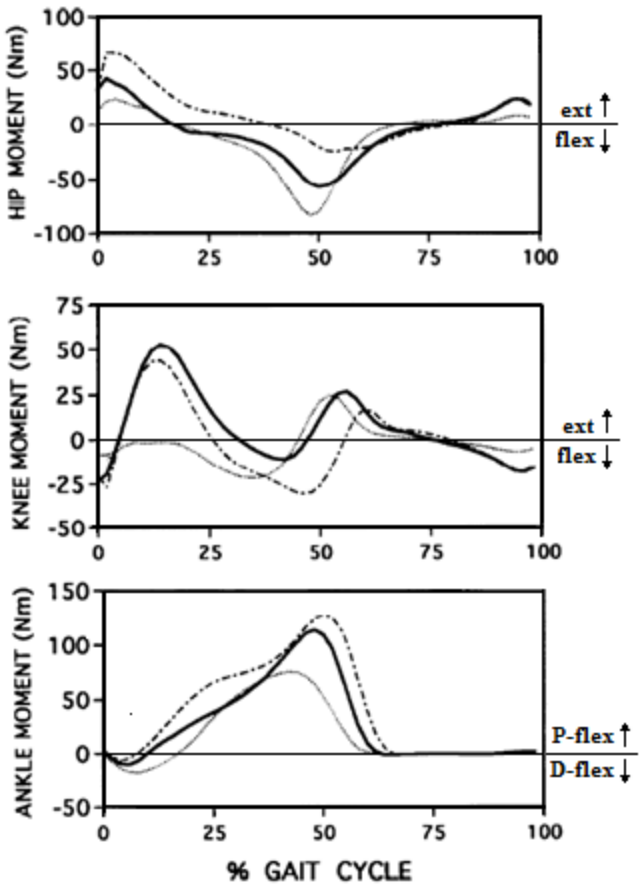

Figure 10: Sagittal plane kinetics for able-bodied subjects (solid black, N=8) and TFA [sound limb: dot-dash, prosthetic (Seattle Light Foot, Tehlin polycentric knee, Mauch SNS hydraulic unit) limb: grey, N=8] during level overground walking at the subject's self-selected walking speed. (Adapted from [25])

The passive prosthetic ankle-foot components are unable to provide the same plantar/dorsiflexion moments as for able-bodied individuals. This results in reduced ankle plantarflexion moment on the prosthetic side during stance. TFAs compensate for the lack of prosthetic propulsion by exerting a greater plantarflexion moment with the sound limb. This sound limb ankle moment is about 33% larger than that for able-bodied subjects [25]. Development of active, powered ankle-foot devices can provide the missing plantarflexion moment and potentially minimize compensatory mechanisms used by TFAs.

The prosthetic knee moment for a TFA wearing a passive prosthesis resembles that of able-bodied subjects during swing. However, prosthetic knee stance flexion and alignment stability, as well as the lack of knee flexion during stance, result in lack of a knee extensor moment during early to mid-stance (Figure 10) [25, 43]. In contrast, sound limb knee moments resemble that for able-bodied gait during stance; the prolonged sound limb single support duration delays the knee extension moment during late stance/early swing [25].

The hip moments for the sound and prosthetic limbs of TFAs resemble that of able-bodied subjects. However, the prosthetic limb hip extension moment during early stance is reduced due to the less effective remnant hip musculature; the hip flexion moment during terminal stance is elevated with respect to able-bodied gait to overcome stance flexion of the prosthetic knee unit and initiate swing. In contrast, the hip extension moment of the sound limb during early stance exceeds that for able-bodied gait; during terminal stance, the sound limb hip flexion moment is less than that for able-bodied gait. During pre-swing and swing, the hip moment of the sound limb resembles that for able-bodied gait [25, 43].

2.4.5 Energy cost

With the loss of a lower limb, ambulation for an amputee becomes increasingly difficult and requires greater energy expenditure. Studies have shown that oxygen consumption is higher for TFAs when compared to able-bodied subjects. Etiology of

amputation, age, walking velocity, length of residual limb, and prosthetic experience affect oxygen consumption, and can contribute to data variability [42]. The oxygen consumption and energy cost are summarized in Table 4 for dysvascular and traumatic TFAs.

Table 4: Oxygen consumption and energy cost (mean and s. d.) at self-selected walking speeds for able-bodied and unilateral TFAs during level overground walking. (Adapted from [42, 45])

	# Subjects	Oxygen Consumption (mL//kg-min)	Energy Cost (mL/kg-m)	Prosthetic Use (yr)
Able-Bodied	111	12.1	0.15	-
Dysvascular	13	12.6 ± 2.9	0.35 ± 0.06	1.2
Traumatic	15	12.9 ± 3.4	0.25 ± 0.05	9.8

Due to increased age and confounding health problems, dysvascular TFAs are not as successful prosthetic ambulators as traumatic TFAs and tend to walk at slower speeds, as indicated by the greater differences between TFAs for energy cost than for energy consumption. These differences in energy cost with amputation etiology may also be affected by prosthetic experience [27]. For both dysvascular and traumatic TFAs, energy costs greatly exceed that for able-bodied subjects [22, 45]. These elevated energy costs may be attributed to increased age, decreased health, lost musculature, prosthetic limitations, and gait asymmetries. Active prosthetic ankle-foot and knee components are in development to address these prosthetic limitations and perhaps decrease energy cost for TFAs during ambulation.

2.5 Powered Prosthetic Components

While passive prosthetic ankle-foot and knee units replace some of the functionality of ankle, subtalar, and knee joints, these devices are unable to provide similar ranges of motion and joint moments as seen in able-bodied subjects. Components are unable to provide dorsiflexion during swing to assist with foot clearance, plantarflexion during late stance to provide active push-off to initiate swing, and knee flexion during loading response for weight acceptance as seen through TFA gait analysis. The objectives of active prosthetic ankle-foot and knee designs are to generate large instantaneous power while providing sufficient torque to propel the prosthesis and the body forward, as done by triceps surae activity during late stance for non-amputees, as well as to provide controlled knee flexion to assist with shock absorption, as done by quadriceps and hamstrings [1-11].

Current passive prosthetic knees and ankle-foot components may integrate implicit and/or explicit combinations of spring(s) and damper(s). Variable cadence prosthetic knees for K3-K4 level TFAs incorporate hydraulic or pneumatic units for swing (and stance) phase control; these dampers may also be controlled using microprocessors [41, 46]. The resistance to knee extension (and flexion) is adjusted for the individual, providing both stance and swing phase control. Ankle-foot components typically integrate both stiff and compliant materials. Dynamic response ankle-foot components are designed to absorb energy during early to mid-stance, and release energy during late stance and toe off [47]. While hydraulic knee and dynamic response ankle-foot components result in improved function during both stance and swing, these knee

and ankle-foot components do not replicate the kinematics of the intact lower extremity [2, 9-11, 41, 46, 47].

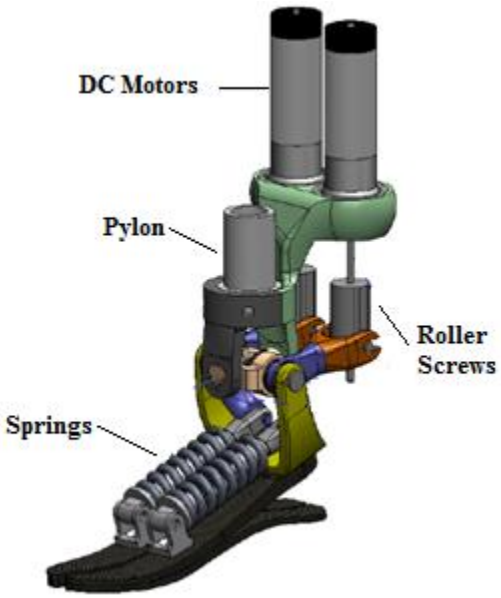

Figure 11: The SPARKy ankle-foot design by Hollander et al.
(Adapted from [2])

Hollander et al. developed the SPARKy (spring ankle with regenerative kinetics), a robotic tendon using helical springs in series with a ball screw mechanism [1, 2], as an active ankle-foot for transtibial amputees. A rotary motor actuates the spring at the ankle based on the subject's walking speed (Figure 11). While initial designs were bulky and inefficient, more recent models weigh 2.1 kg, provide greater power transmission, contain stronger motors, and allow for control of both inversion/eversion and plantarflexion/dorsiflexion [2]. To date, no amputee gait data validating this design has been published.

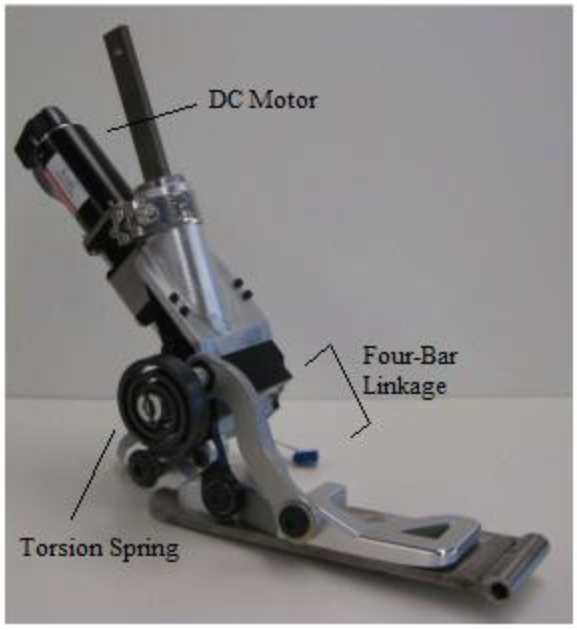

Figure 12: The powered ankle-foot design by Bergelin et al.
(Adapted from [4])

Bergelin et al. [3, 4] and Au et al. [5-8] also designed powered ankle-feet, designs that incorporate motors to modulate the stiffness of the spring components. Bergelin et al. [3, 4] utilized a four-bar linkage to transfer rotational energy stored in a torsion spring to provide active plantarflexion/dorsiflexion (Figure 12). While control systems for this design are still being refined, the total weight of this prosthesis is 2.23 kg, exclusive of the battery.

The designs by Au et al. [5-8] included a pulley system to modulate stiffness in linear springs located in the ankle. Finite-state controllers utilize heel/toe loading, ankle angle, and ankle torque to actuate ankle plantarflexion/dorsiflexion [6]. Subsequent designs utilized surface EMG electrodes on the remnant calf musculature of the transtibial residual limb to differentiate user intent [7]. The device, 4.5 kg inclusive of battery, has been verified for level overground walking and stair descent for a single

subject (Figure 13). This design is now commercially available, marketed as the BiOM (iWalk: Bedford, MA).

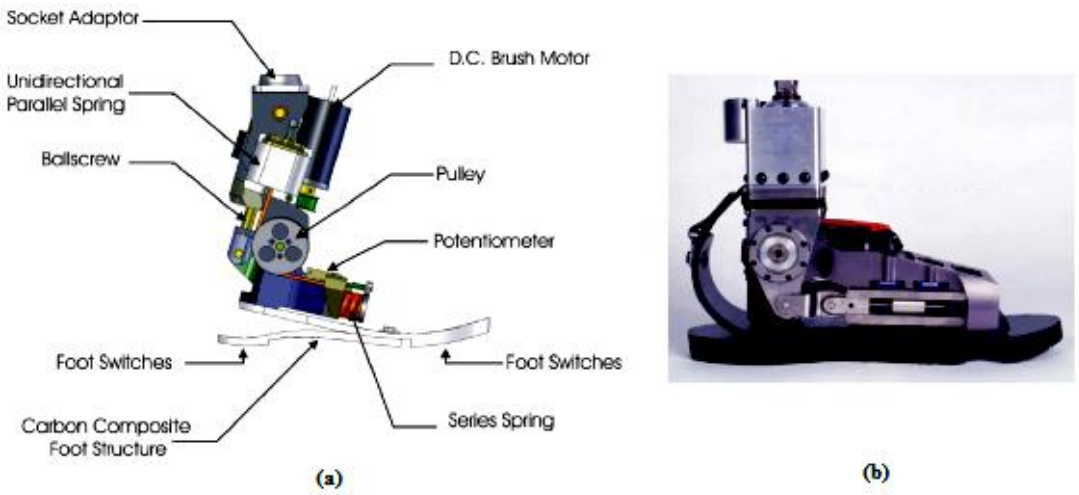

Figure 13: Initial prototype (a) and final (b) design of the BIOM powered ankle-foot. (Adapted from [8])

Unlike the active ankle-foot designs above, Sup et al. [9-11] developed a TF prosthesis incorporating both an active knee and ankle. Two motor-driven ball screws located proximally on the shank actuate slider-crank linkages to drive the knee and ankle (Figure 14). An additional spring component in parallel with the ankle ball screw provides the plantarflexion torque at toe off [10]. The moments and forces at the knee and ankle are measured using strain gauges, with on-board processors using this information to generate control signals to actuate the motors and control ankle position and torque [10, 11]. A self-contained version of the initial prototype was redesigned to integrate the processor and lithium ion battery within the prosthesis. This design was estimated to provide power for 9,000 steps; it weighs 4.2 kg inclusive of approximately 1kg for the battery and electronics [11]. Initial testing on a unilateral TFA resulted in similar knee and ankle kinematics as for able-bodied subjects during overground and uphill walking;

the subject's self-selected overground walking speed increased by 24% using the powered versus passive prosthesis [9, 11].

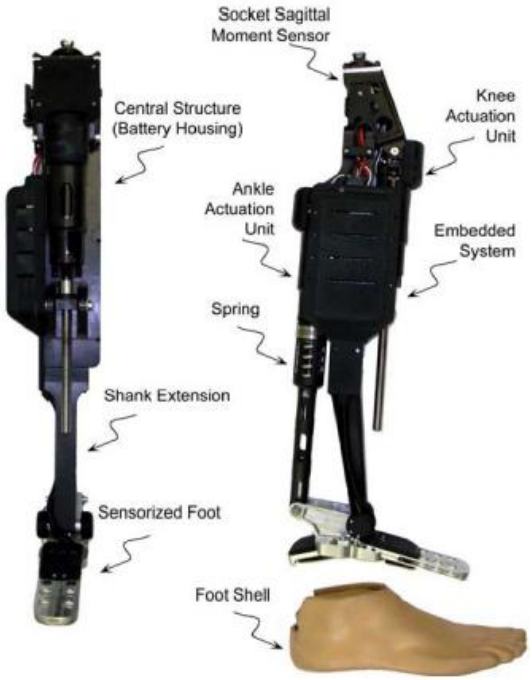

Figure 14: Powered knee and ankle-foot design by Sup et al.
(Adapted from [11])

These active prosthetic components have generated appropriate ankle and knee torques to provide enhanced temporal and kinematic symmetry and potentially reduced energy cost. Further development with respect to reduced mass, increased battery life, alternative control signals and algorithms are needed. The mass magnitudes and distribution of these active components and the associated power sources differ from that of the intact limb. The mass of these active components is concentrated at the joints themselves as the axes of rotation of the motors are positioned at the approximate location of the anatomic joint centers. Optimal locations for the power sources and control units, however, have not yet been assessed. While not a problem during stance,

the abnormal mass magnitude and distribution may adversely affect swing dynamics. Previous studies examining the effects of mass and inertial loading on limb kinematics can provide a foundation for the optimization analyses needed for this study.

2.6 Investigation of Inertial Properties of Passive Prosthetic Components

The addition of batteries and active components affects prosthetic mass and center of mass, thereby altering the inertial properties of the prosthesis. These inertial changes, in turn, affect lower extremity kinematics, especially during swing. Investigations of the effects of segment inertial properties on limb dynamics for TFAs have been performed for passive prosthetic components. Studies include both theoretical models and experimental gait analyses of swing. Functional parameters examined in these studies include lower extremity joint kinematics [12-16] and kinetics [16, 17], walking speed [14, 15, 18], and stride length [14], parameters that can be contrasted with that of able-bodied subjects [19]. These investigations are summarized in this section, highlighting the relevant methodology, key findings, and study limitations as relevant to this thesis.

2.6.1 Theoretical Models

Theoretical models investigating swing dynamics incorporate a pendular model of the lower limb, as swing is largely a passive activity. These models utilize the Lagrange method of dynamic analysis which minimizes energy transfer through conservation of energy (see Table 5).

Table 5: Summary of theoretical models investigating inertial property effects on lower limb dynamics.

Investigators	Mena et al. [12]	Tsai et al. [13]	Beck et al. [17]
Modeled Segments	3 segments: thigh, shank, foot	2 segments: TFA residual limb/socket, shank/foot	2 segments: TFA residual limb/socket, shank/foot
Initial Conditions	Initial position: hip, knee, ankle angles	Initial hip torque Initial position: hip, knee angles	Not stated
Independent Variable(s)	Segment inertia: nominal, ±10% nominal Initial conditions: angular velocity & joint moments	Segment inertia: 5 variations (Table 6) Initial conditions: hip torque Walking speeds: 0.69 m/s, 1.39 m/s, 1.88 m/s	Segment mass: shank-foot, 4 variations (Table 6)
Dependent Variable(s)	Joint kinematics: hip, knee, ankle angles	Deviation between TFA, able-bodied kinematics	Hip work
Conclusions	Joint motion more sensitive to decreased, not increased, inertial properties	More proximal shank-foot center of mass (COM) mimics able-bodied swing kinematics	More proximal shank-foot COM minimizes hip work during swing

Results of swing simulations confirm that varying shank segment inertia affects swing phase kinematics [12, 13, 17]. Decreasing both shank mass and shank inertia by 10% to 30% resulted in 10-15° deviations in sagittal plane hip and knee motion for TFAs compared to able-bodied gait [12]. Conversely, increasing these properties by 10% to 30% resulted in deviations of ±5° for the hip and knee and ±7° for the ankle for TFAs compared to able-bodied gait [12]. These findings were confirmed by Tsai et al. who showed that a shank COM that was more proximal (7 cm) resulted in TFA swing kinematics that more closely approximated able-bodied gait [13]. Tsai also noted that pure damping is unable to replicate able-bodied knee kinematics during swing at various walking speeds, although simulation models incorporating hydraulic knees are able to better replicate swing at variable cadences [13]. Beck noted that the more proximal

shank-foot COM resulted in decreased hip work during swing [17]. While the 4.7 kg shank foot modeled by Beck approximates that of an intact shank/foot, this mass is nearly 2 kg heavier than that of typical endoskeletal passive prosthetic components [18, 22].

No details regarding the prosthetic knee mass and its relative distribution into the thigh and shank segments were documented [12, 13, 17]. In addition, the initial conditions of all of these TFA models of swing were based on able-bodied, not TFA, gait data. Increases in prosthetic mass may also require further changes in residual hip muscle activity and joint torques, and as well as potential changes in lower limb kinematics affecting model initial conditions at toe off [13, 17]. Finally, none of these theoretical model results have been validated using gait analyses. These model limitations may therefore have introduced errors, limiting their clinical utility.

Table 6: Segment masses for TFA models of swing.

Investigators	Segment	Nominal (kg)	Light (kg)	Heavy (kg)	Heavy (kg)	Heavy (kg)
Tsai et al. [13]	Residual limb and socket	5.07	4.80	5.07	5.07	5.07
	Prosthetic shank and foot	3.09	1.30	3.09 + 1.5 kg (7 cm proximal to COM)	3.09 + 1.5 kg (7 cm distal to COM)	3.09 + 1.5 kg (at COM)
Beck et al. [17]	Residual limb and socket	7.6	-	-	-	-
	Prosthetic shank and foot	0.7	0.7 + 0.5*	0.7 + 1.5*	0.7 +2.5*	0.7 + 4.0*

* Additional mass spaced at 2 mm intervals along shank-foot segment

Regardless of these potential modeling limitations, all of these models and simulations indicate that it is advantageous to concentrate prosthetic mass more

proximally in the shank. Such placement is often difficult for active prosthetic components as onboard componentry are typically located distally to control the powered ankle-foot. Optimization analyses that investigate counter-mass magnitude and location may identify options that might compensate for this increased mass and distal distribution, providing improved functionality of active, powered lower extremity prostheses.

2.6.2 Experimental Analyses

Experimental analyses involving gait analysis of TFAs have also been conducted to investigate the effects of inertial parameter variations on gait. Experimental analysis to date has focused on manipulation of mass and moment of inertia of the shank-foot segment only [12, 13, 17, 22]. A summary of these investigations is presented in Table 7.

Table 7: Summary of experimental gait analyses of TFAs investigating effects of prosthetic inertia.

Investigators	Hale [15]	Gitter et al. [16]	Czerniecki et al. [18]	Tashman et al. [14]
#TFAs	6	8	8	1
Mean Nominal Shank-Foot Mass (kg)	1.17	3.30	3.30	1.90
Walking Speed	Self-selected	Self-selected	Self-selected	Self-selected, fast
Variables: Prosthetic shank-foot mass (kg)	Nominal, +1.75, +3.15, +4.13 (at COM)	Nominal, +0.68, +1.33 (at COM)	Nominal, +0.68, +1.33 (at COM)	Nominal, +0.83 (variable position: 18.7 to 31.7 cm distal to knee)
Output Variables of Interest	Mechanical Work of the Hip	Mechanical Work of the Hip	Metabolic Cost	Joint kinematics, cadence, stride length, & walking speed
Findings for Increased Mass	Increased hip work	Increased hip work	No significant statistical differences	Proximally located mass reduced the swing duration

Hale [15], Gitter et al. [16] and Czerniecki et al. [18] investigated the effects of increased mass at the prosthetic shank-foot COM for TFAs walking overground at their self-selected walking speeds. No supplemental suspension was necessary. As shank mass increased, the swing duration decreased (36.7%) [15], hip torque increased (71.3%) [15] and hip work increased (up to 29%) [16] – without any significant changes in metabolic cost [18]. In contrast, Tashman et al. [14] controlled the mass and varied the shank-foot segment COM for a single TFA. Cadence, stride length and walking speed were unaffected by variations in shank COM. Swing duration, however, was reduced by 8% for the more proximally located supplemental mass, reducing swing duration asymmetry

(19.5% to 9.1% for self-selected and 32.4% to 19.6% for fast walking) between the prosthetic and sound limbs [14].

The joint forces, moments and work in the aforementioned studies were estimated based on inverse dynamic models and are therefore dependent on the assumed prosthetic knee center of rotation, mass distribution and residual limb/prosthetic thigh COM. Analysis by Miller et al. indicated that inverse dynamic techniques which do not consider the knee complexity, but rather approximate the knee center as a point, produce errors in joint forces, moments, and powers [48]. Additional limitations of these gait analysis investigations of mass/inertial effects on TFA gait include the limited number of TFA subjects and study power. Further research is needed to better understand the effects of inertial loading on joint kinematics and kinetics, metabolic cost, temporal parameters, and kinematic and temporal asymmetry.

Despite the aforementioned limitations, these prior studies of both theoretical models and experimental analysis of TFA gait indicate that inertial properties of the prosthetic limb affect lower extremity joint kinematics, cadence, and walking speed - particularly during swing. The function of active, powered lower extremity prostheses might be enhanced by the inclusion of counter-mass locations of optimal magnitude and location.

2.7 Summary

This chapter presented an overview of able-bodied and TFA gait, including a review of both temporal and stride parameters, hip, knee, and ankle joint kinematics, and the corresponding joint reaction forces and moments as determined via inverse dynamic modeling. Finally, energy consumption and energy cost were also presented for these two populations.

The demographics of lower extremity amputees were summarized, as was an overview of amputation surgery, prosthetic fabrication, fitting and alignment. The rationale and options for prosthetic components for TFAs were summarized, including both passive and active designs These new active components are directly relevant to the research objectives and hypotheses of this study, namely that the mass of these active components must be optimized to minimize the impact on swing.

Previous investigations of inertial loading effects of passive prostheses using both theoretical models and experimental analysis were also reviewed. These investigations confirm the relevance and need of the proposed research

CHAPTER 3: METHODOLOGY

This chapter presents the dynamic models and optimization techniques used to determine counter-mass location in an active TF prosthesis. Computer models simulating swing include an able-bodied lower limb and a TFA residual limb and prosthesis with both single axis and polycentric prosthetic knee components. Model validation procedures are presented as is the optimization procedure to identify promising counter-mass magnitudes and locations.

3.1 Dynamic Modeling

The thigh, shank, and foot segments of the lower extremity for both the able-bodied and TFA residual limb and prosthesis were modeled as a double pendulum system. The ankle was fixed at a neutral orientation as passive prosthetic ankle-foot components often do not provide explicit ankle dorsiflexion/plantarflexion, particularly during swing. Sagittal plane motion of the limb was defined using a fixed two-dimensional Cartesian coordinate system with origin located at the hip joint (Figure 15). Thigh (ψ_T) and shank (ψ_S) segment angles were defined with respect to the horizontal and used to determine hip (θ_H) and knee (θ_K) angles (Equations (1 and (2). Counter-clockwise rotation (hip flexion and knee extension) represents positive angular displacement. The ankle angle between the foot and shank segments was fixed at 90˚.

$$\theta_H = 90° - \psi_T \quad (1)$$

$$\theta_K = (\psi_T - \psi_S) \quad (2)$$

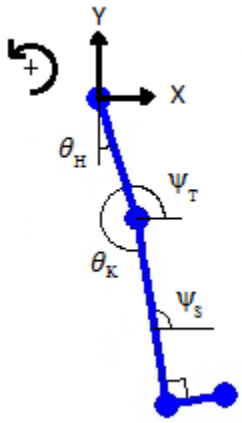

Figure 15: Double pendulum model of the lower limb including hip, knee, and ankle joints. Thigh (ψ_T) and shank (ψ_S) angles are with respect to the horizontal. Hip (θ_H) motion is relative to vertical; knee (θ_K) motion describes the angle between the thigh and shank segments. Positive angle measures indicate hip flexion and knee extension. The ankle angle between the shank and foot segments is fixed at 90˚.

The equations of motion for these double-pendulum models were derived via the Lagrange method. These ordinary coupled, second-order differential equations were solved using ODE45 in MatLab® (R2012a, Mathworks; Natick, MA), a function that utilizes the 4^{th}-5^{th} order Runge-Kutta technique to approximate results with variable step sizes. Models were assessed and validated using swing kinematic and duration data from the literature (able-bodied) and physical model experimentation (TFA residual limb and prosthesis). Initial models were then manipulated to include additional mechanical components (e.g., springs and dampers) in an attempt to improve model performance. Model output included comparative plots of model versus literature/physical model hip and knee joint motion, as well as the root mean square (RMS) errors in hip (θ_H) and knee (θ_K) – Equation (3),

$$RMS = \sqrt{\frac{1}{n}\sum\left(\frac{\left|\varphi_{exp} - \varphi_{math}\right|}{\varphi_{exp}}\right)^2} \quad (3)$$

where φ is the angle of interest (hip, knee or shank) for the respective experimental and mathematical model; n is the number of data points. The RMS error in the shank (ψ_S) segment angle was also included as the knee angle is a function of the thigh and shank angles

3.1.1 Able-Bodied Lower Limb Model

The sagittal plane hip and knee motion data detailed in Winter [20] for able-bodied subjects served as the control data for the able-bodied models (AB). These data were collected using two-dimensional motion analysis (69.9 Hz) with reflective markers placed on anatomical landmarks. Raw marker kinematic data were filtered using a Butterworth low-pass filter (6Hz cut-off frequency) prior to calculation of segmental linear and angular kinematics [49, 50].

The thigh and lumped shank-foot segments of the lower extremity of an able-bodied subject (56.7 kg) [20] were modeled with pin joints at the hip and knee. Specific equations of motion are summarized in Appendix B. Mass and inertial parameters of the thigh and shank-foot segments, as well as the initial positions of the hip and knee at toe off, were based on Winter [49, 50] (Table 9). As swing is mostly a passive activity with the exception of ankle dorsiflexion [22], the initial knee and hip torque was assumed to be zero.

The initial model (AB-1) assumed frictionless pin joints at the hip and knee. The equations of motion and the resultant hip and knee angles were solved numerically.

The second model (AB-2) included rotary dampers and torsion springs at both the hip and knee joints. These rotary dampers, with rotational stiffness C_H and C_K at the hip and knee, respectively, were used to reduce excessive hip flexion during late swing and prevent knee hyperextension. The torsion springs, with rotational stiffness K_H and K_K at the hip and knee, respectively, were added to compensate for loss of rotation caused by the dampers, with resting (i.e., free length) spring positions set at neutral hip (vertical thigh) and knee (vertical shank) positions. The hip spring approximates the rectus femoris of the quadriceps, flexing the hip during initial swing, while the knee spring approximates hamstring activity used to decelerate the shank during terminal swing. These springs provide additional potential energy to the system during swing.

The third model (AB-3) included a time-varying damper at the knee (C_{K1} for $t < \tau$, C_{K2} for $t \geq \tau$), approximating the activation period of the hamstrings for shank deceleration. This time-varying damper was implemented by using a conditional statement in the ODE45 solver.

Parameter optimization for these three able-bodied models included the three damping (C_H, C_{K1} and C_{K2}) and two spring (K_H and K_K) coefficients, as well as the time at which the damping coefficient changed (τ) for AB-3 – see Table 8. These model

parameters were optimized using the *fmincon* function. Refer to section 3.2 for details regarding the specific optimization objective functions.

Table 8: Mechanical parameters included and optimized in the various able-bodied swing models

Model	K_H $\left(\frac{N\,m}{rad.}\right)$	K_K $\left(\frac{N\,m}{rad.}\right)$	C_H $\left(\frac{kg\,m^2}{s\,rad.}\right)$	C_{K1} $\left(\frac{kg\,m^2}{s\,rad.}\right)$	C_{K2} $\left(\frac{kg\,m^2}{s\,rad.}\right)$	τ (s)
AB-1	-	-	-	-	-	-
AB-2	X	X	X	X	-	-
AB-3	X	X	X	X	X	X
Bounds	0-10	0-10	0-10	0-10	0-10	0- 0.40

3.1.2 TFA Residual & Prosthetic Limb Model

The able-bodied double pendulum models were revised to simulate swing for TFAs. These models included approximations of the residual limb and various prosthetic componentry.

The initial model (TFA-1) incorporated a simple, uniaxial prosthetic knee. Optimization techniques similar to that implemented for the able-bodied swing models were used to estimate knee and hip damping. Optimization of these parameters was based on experimental motion data of a physical model of the TFA residual limb and prosthesis.

The segment parameters (segment mass, length, and center of gravity locations) for this TFA model were based on the aforementioned physical model (see Section 3.1.3). Planar mass moment of inertia (I) for each segment was calculated as [51]:

$$I = \frac{T^2 mgd}{4\pi^2} - md^2 \quad (4)$$

where T is the oscillation period, m is the segment mass, g is the acceleration due to gravity, and d is the distance between the pivot point and the center of mass (Figure 16). Motion analysis, during which markers were placed on the pivot point and segment center of mass, was used to record the period for each rotating segment.

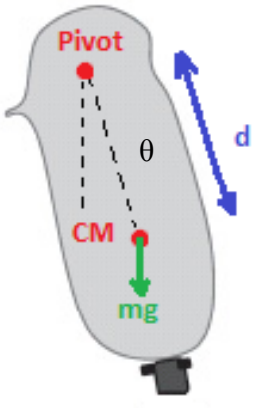

Figure 16: Moment of inertia reference points (circles) and distances for the thigh segment (residual limb/socket) of the TFA physical model. The segment was suspended at the pivot point and allowed to swing freely; rotation of the segment was measured using motion analysis.

The specific segments of this TFA model included the residual limb/socket/knee component (e.g., thigh segment) and pylon/foot (e.g., shank-foot segment), with each segment mass and moment of inertia determined as above (Table 9). The ankle was fixed at a neutral orientation as prosthetic ankle-foot components often do not provide dorsiflexion/plantarflexion, particularly during swing. The hip and knee joints for TFA-1 were assumed to be simple, planar single-axis pin joints. Initial positions approximated those used for physical model experimentation (Table 9). The corresponding initial

condition was zero rotational velocity at the hip and knee, approximating the "free fall" of the physical model swing. Rotary dampers with rotational stiffness C_H and C_K were used to approximate the remnant hip and prosthetic knee.

A second model of the TFA residual limb and prosthesis, TFA-2, was then created to include the Total Knee 2000® (Ossur; Foothill Ranch, CA – Figure 18), a polycentric, hydraulic knee unit, and an Axtion® (1E56, Otto Bock; Minneapolis, MN – Figure 17) ESAR foot. These prosthetic components more realistically represent components typically prescribed for an active TFA who might benefit from an active prosthesis. As with model TFA-1, rotary dampers C_H and C_K were used to replicate the viscous damping at the hip and knee joints. Additional Coulomb frictional forces producing a resistive moment ($M_{H\text{-}static}$ and $M_{H\text{-}kinetic}$) were incorporated at the hip joint as a function of time ($M_{H\text{-}static}$ for $t \leq \tau$, C_H and $M_{H\text{-}kinetic}$ for $t > \tau$) to simulate the friction acting on the metal uniaxial hip joint used to suspend the physical model (see Figure 20).

Figure 17: Diagram of the Axtion ESAR foot.
(Adapted from [52])

The third model, TFA-3, included an approximation of the powered, active prosthetic ankle-foot developed by Bergelin et al. [3] (Figure 12). The shank-foot inertial properties were modified to approximate that of the active ankle prosthesis. Damping components optimized for this model were identical to those of model TFA-2.

Figure 18: Diagram of the Total Knee 2000, hydraulic knee unit.
(Adapted from [53])

The SimMechanics toolbox in MatLab was used to characterize motion of the prosthetic limb with a Total Knee 2000. The mechanical joints and linkages of the knee component were visually defined and connected, creating a lower extremity "machine" based on specific linkage masses, lengths, and mass moments of inertia (Table 9 and Appendix C). As the individual linkages of the Total Knee 2000 could not be disassembled, each link was reconstructed in SolidWorks (SolidWorks 2011, Dassault Systemes SolidWorks Corp.; Waltham, MA) to compute the approximate center of mass location and inertial properties, assuming the knee was fabricated from stainless steel. The SimMechanics "machine" was then tested in a virtual environment using physical model initial conditions for visual verification of the dynamic motion.

Table 9: Thigh and shank-foot segment mass, proximal distance to COM, length, inertia, and segmental initial conditions based on able-bodied and physical model properties.

Model	Segment	Mass (kg)	Proximal Distance to COM (m)	Length (m)	Moment of Inertia (kg m^2)	ψ Segment Initial Positions (deg.)	Angular Velocity (rad/s)
AB 1-3	Thigh	5.67	0.136	0.314	0.058	82.70	3.29
	Shank-Foot	3.46	0.291	0.480	0.138	39.80	-2.41
TFA-1	Thigh w uniaxial knee	6.50	0.225 ± 0.002	0.518 ± 0.008	0.052 ± 0.006	72.97	0
	Shank-SACH Foot	1.09	0.348 ± 0.004	0.436 ± 0.001	0.022 ± 0.003	33.82	0
TFA-2	Thigh w TK 2000	6.80	0.130 ± 0.003	0.330 ± 0.003	0.075 ± 0.002	74.36	0
	Shank-Axtion Foot	1.15	0.344 ± 0.001	0.406 ± 0.002	0.0067 ± 0.0003	41.96	0
TFA-3	Thigh w TK 2000	6.80	0.130 ± 0.003	0.330 ± 0.003	0.075 ± 0.002	64.65	0
	Powered Ankle Foot	3.10	0.262 ± 0.004	0.444 ± 0.004	0.218 ± 0.006	45.82	0

Model optimization parameters included the respective damping coefficients and Coulomb frictional forces (C_H, C_K, $M_{H\text{-}static}$ and $M_{H\text{-}kinetic}$), as well as the time (τ) at which damping was activated (Table 10). These parameters were optimized using the *fmincon* function (see section 3.2).

Table 10: Mechanical parameters optimized in TFA models of swing.

Model #	$C_H \left(\frac{kg\ m^2}{s\ rad.}\right)$	$C_K \left(\frac{kg\ m^2}{s\ rad.}\right)$	τ (s)	$M_{H\text{-}static}$ (N m)	$M_{H\text{-}kinetic}$ (N m)
TFA-1	X	X	-	-	-
TFA-2	X	X	X	X	X
TFA-3	X	X	X	X	X
Bounds	0-10	0-10	0-0.40	0-10	0-10

3.1.3 Physical Model of TFA Residual & Prosthetic Limb

Physical models of the TFA residual limb and prosthesis were created to generate motion data during swing for parameter optimization of the TFA computer models. These physical models, as summarized in Table 11, included a hip joint, prosthetic socket with pseudo-residual limb (medium length), prosthetic knee, endoskeletal distal shank, and prosthetic ankle-foot. For each physical model, the prosthesis was suspended from a frame via the hip joint; this hip joint approximated that of the residual limb. The hip center of rotation for TFA-1 was displaced laterally due to the pelvic band; the hip center of rotation for the TFA-2 and TFA-3 models was internal to the socket, more closely approximating that of the remnant hip joint. These joint were connected to quadrilateral sockets filled with either sand or plaster of Paris to approximate the mass and density of the residual limb. Prosthetic knees were attached to the distal socket using a pyramid adapter; the pylon-shank was press fit to a tube clamp adaptor distal to the knee (see Figure 19 to Figure 21).

Table 11: Physical models of the TFA pseudo-residual limb and prosthesis

	TFA-1	TFA-2	TFA-3
Socket	Quadrilateral	Quadrilateral	Quadrilateral
Pseudo-residual limb	Sand	Plaster of Paris	Plaster of Paris
Pseudo- residual limb hip joint	Single Axis (Pelvic Band, waist belt, uniaxial hip joint)	Single Axis	Single Axis
Prosthetic knee	Uniaxial (unlocked manual locking knee)	Polycentric, hydraulic (TK 2000)	Polycentric, hydraulic (TK 2000)
Prosthetic foot-ankle	Single-axis ankle with SACH foot	Axtion	Powered Ankle

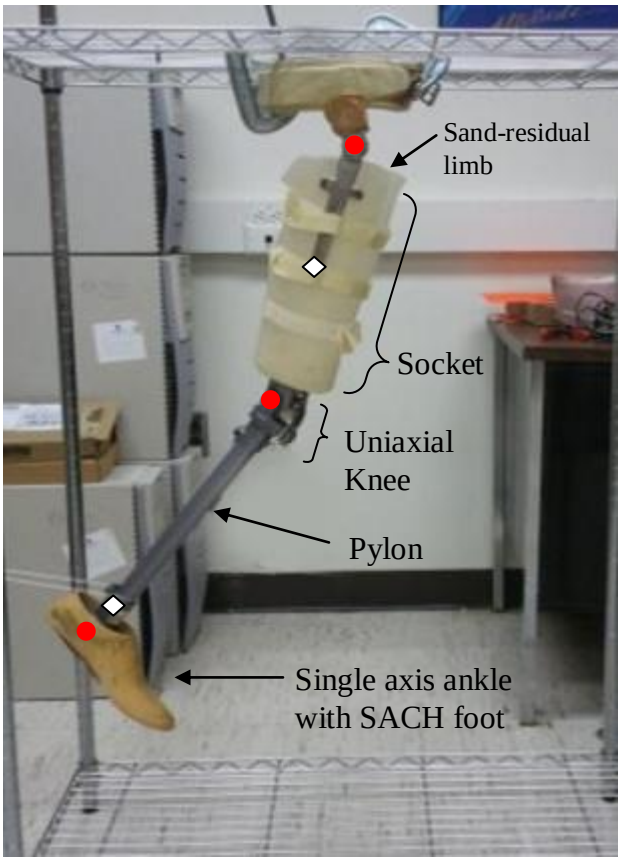

Figure 19: Physical model for experimental simulation of theoretical model TFA-1. The circles indicate marker locations for the hip, knee and ankle centers of rotation. The diamonds approximate the thigh and shank COMs; reflective markers were placed at these locations for motion analysis.

The initial position for each of the physical models approximated toe off [49, 50]. Segments were pulled posteriorly to the desired start angle (see Table 9, Figure 19) and then released. These initial conditions approximate a free falling pendulum with zero initial rotational velocity and no input knee or hip torque.

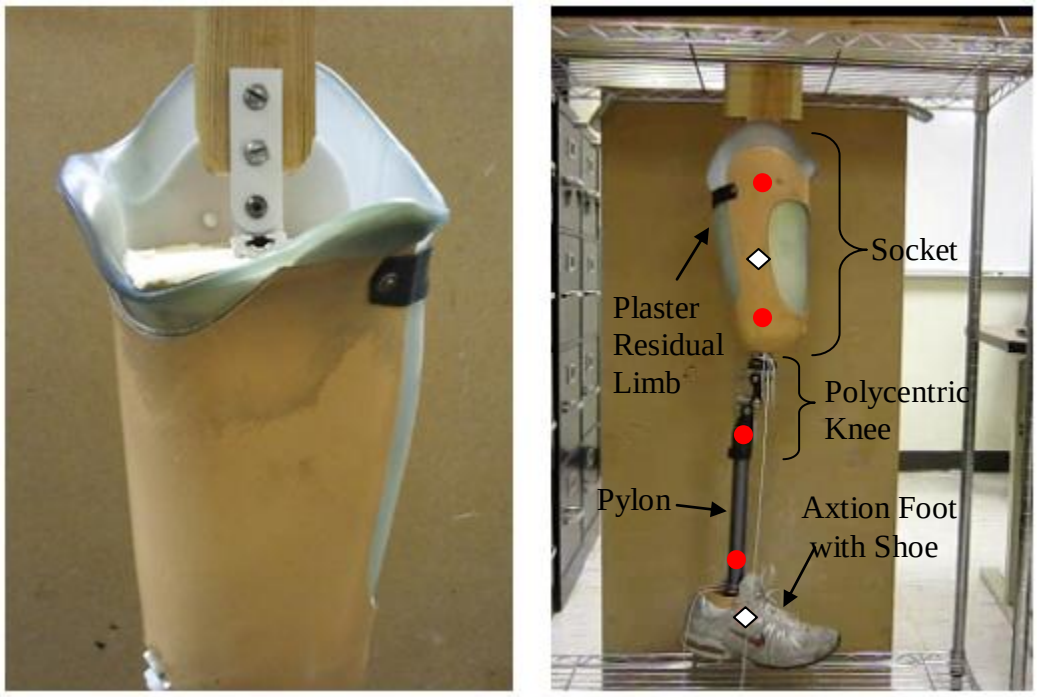

(a) (b)

Figure 20: The suspension (a) and pseudo-residual and prosthetic limb (b) for experimental simulation of the TFA-2 mathematical model. The circles indicate marker locations for the hip, knee and ankle joint centers. The diamonds approximate the thigh and shank segment COMs; reflective markers were placed at these locations for motion analysis.

Reflective markers were placed at the hip center of rotation, lateral socket (e.g., thigh), lateral shank (mid-pylon), and foot. For the physical model approximating TFA-1, markers were placed at the respective hip and knee centers of rotation of the uniaxial pin joints; a third marker was placed laterally on the center of rotation of the single-axis ankle (Figure 19). For physical models TFA-2 and TFA-3, two markers were placed on the lateral socket, one of which approximated the center of rotation of the thigh suspension system. Two additional markers were placed on the shank segment to approximate the instantaneous polycentric knee center of the Total Knee 2000 (Figure 20).

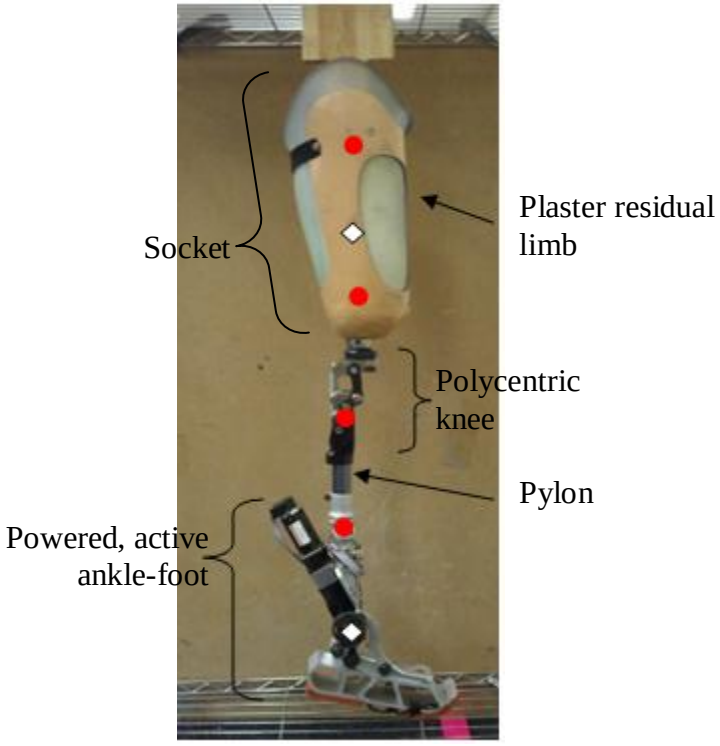

Figure 21: The physical model of the TFA-3 mathematical model. The circles indicate marker locations of the hip, knee and ankle joint centers. The diamond approximates the thigh and shank segment COMs; reflective markers were placed at these locations for motion analysis.

Marker motion data were acquired at 100 Hz using a 6 camera motion analysis system (Vicon 524, Oxford Metrics; Oxford, England). Direct linear transformation was performed to convert individual camera data to three-dimensional marker motion data, motion data that were then reduced to planar segment motion data. These kinematic data were filtered using the generalized cross-validation method (Woltering filter) [54]. Motion data were exported in binary c3d files to calculate sagittal plane Euler joint angles using MatLab. A minimum of ten motion trials were collected for each physical model.

3.2 Optimization Objective Functions

Spring and damper parameters for the various mathematical models were determined through optimization using the *fmincon* function in MatLab. Four different objective functions were investigated for minimization of error in the thigh and shank segment angles between the respective mathematical and corresponding physical models. The objective function that yielded the best approximation of the physical data with the mathematical model was then adopted for counter-mass investigations.

The first objective function ($OF_{diff\text{-}hor}$) was based on the difference between the physical and mathematical model thigh and shank angles measured with respect to a global horizontal reference frame. These differences in joint angle were then squared and summed in a RMS fashion – Equation (5):

$$OF_{diff-hor} = \sqrt{\frac{1}{n}\sum\left(\psi_{T-exp} - \psi_{T-math}\right)^2} + \sqrt{\frac{1}{n}\sum\left(\psi_{S-exp} - \psi_{S-math}\right)^2} \qquad (5)$$

where n is the number of data points, $\psi_{T\text{-}exp}$ and $\psi_{S\text{-}exp}$ are physical model segment angles, and $\psi_{T\text{-}math}$ and $\psi_{S\text{-}math}$ are mathematical model segment angles – both measured with respect to a global horizontal reference frame.

An alternative objective function ($\overline{OF}_{ROM-hor}$) was defined that normalized the difference in segment angles with respect to the range of motion (ROM) of the respective physical model segment during swing – Equation (6. Unlike $OF_{diff-hor}$, this objective

function is dimensionless. However, both the segment angles and the respective segment ROM used for normalization are defined with respect to a global horizontal reference frame. This function poses an issue as the differences in thigh versus shank segments are weighted non-uniformly – the segment with the smallest ROM will have a greater affect on optimization.

$$\overline{OF}_{ROM-hor} = \sqrt{\frac{1}{n}\sum\left(\frac{\left|\psi_{T-exp} - \psi_{T-math}\right|}{\psi_{T-\exp ROM}}\right)^2} + \sqrt{\frac{1}{n}\sum\left(\frac{\left|\psi_{S-exp} - \psi_{S-math}\right|}{\psi_{S-\exp ROM}}\right)^2} \quad (6)$$

where n, $\psi_{\text{T-exp}}$ and $\psi_{\text{S-exp}}$ are as defined previously for Equation (5, and $\psi_{\text{T-exp ROM}}$ and $\psi_{\text{S-exp ROM}}$ are ranges of the motion of the physical model segment angles during swing.

The third ($\overline{OF}_{hor-ref}$) and fourth ($\overline{OF}_{vert-ref}$) objective functions are also dimensionless. For both objective functions the difference in segment angles (defined with respect to a global horizontal reference frame) are normalized with respect to the instantaneous segment angle of the physical model. For objective function $\overline{OF}_{hor-ref}$, the instantaneous segment angle is also defined with respect to a global horizontal reference (e.g., ground) – Equation (7. For objective function $\overline{OF}_{vert-ref}$, the instantaneous segment angle is defined with respect to a global vertical reference (e.g., gravity) – Equation (8.

$$\overline{OF}_{hor-ref} = \sqrt{\frac{1}{n}\sum\left(\frac{\left|\psi_{T-exp} - \psi_{T-math}\right|}{\psi_{T-exp}}\right)^2} + \sqrt{\frac{1}{n}\sum\left(\frac{\left|\psi_{S-exp} - \psi_{S-math}\right|}{\psi_{S-exp}}\right)^2} \quad (7)$$

$$\overline{OF}_{vert-ref} = \sqrt{\frac{1}{n}\sum\left(\frac{\left|\psi_{T-exp} - \psi_{T-math}\right|}{\psi_{T-exp} - 90}\right)^2} + \sqrt{\frac{1}{n}\sum\left(\frac{\left|\psi_{S-exp} - \psi_{S-math}\right|}{\psi_{S-exp} - 90}\right)^2} \quad (8)$$

3.3 Optimization of Counter- mass Location and Magnitude

Subsequent model optimization using the validated TFA-3 mathematical model was then performed to identify potential counter-mass magnitude(s) and location(s). Sagittal plane hip and knee motion data detailed in Winter [20] for an able-bodied subject served as the control data for optimization of swing. For kinematic consistency, the mass and length of the residual limb/thigh segment and pylon length/shank segment in the TFA-3 model were scaled to approximate a TFA of similar build to the able-bodied subject in Winter.

Contrary to the TFA-3 mathematical model that approximates a free falling double pendulum, TFAs activate their hip musculature during swing. As such, hip joint moments simulating hip muscle activation from pre- to terminal swing were included, based on normalized hip moments of four TFAs wearing prostheses that incorporated the Total Knee 2000 [55]. These normalized hip torques were simulated in a piece-wise linear fashion, as shown in Figure 22.

The initial positions for this modified version of TFA-3 model approximated the thigh and shank positions at pre-swing (ψ_T= 78.1° and ψ_S= 42.9°), just prior to toe off, as documented in Winter [20]. Simulations were performed with hip torques of varying magnitudes applied from pre- through terminal swing until the resultant hip kinematics of

the TFA-3 model matched that of the control data (e.g., cosmetic TFA gait approximating that of an able-bodied subject).

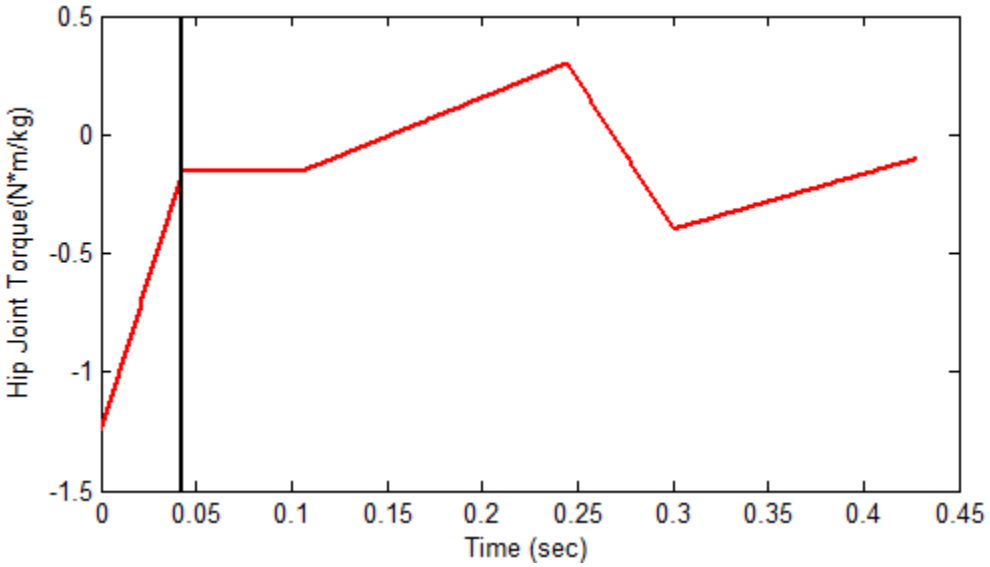

Figure 22: Piecewise linear approximation of normalized hip torque from four TFAs wearing a prosthesis incorporating a Total Knee 2000 [55]. The vertical line represents the transition from pre-swing (late stance) to initial swing.

Potential counter-mass magnitude(s) was first investigated by introducing point masses at the thigh only, the shank only, and both thigh and shank segments near the knee (Table 12). Magnitudes were determined through optimization with the selected objective function (e.g., $OF_{diff-hor}$, $\overline{OF}_{ROM-hor}$, $\overline{OF}_{hor-ref}$ or $\overline{OF}_{vert-ref}$) using the *fmincon* function in MatLab. Potential counter-mass magnitude was constrained to 0 to 2.0 kg to approximate the power source for an active ankle-foot prosthetic component.

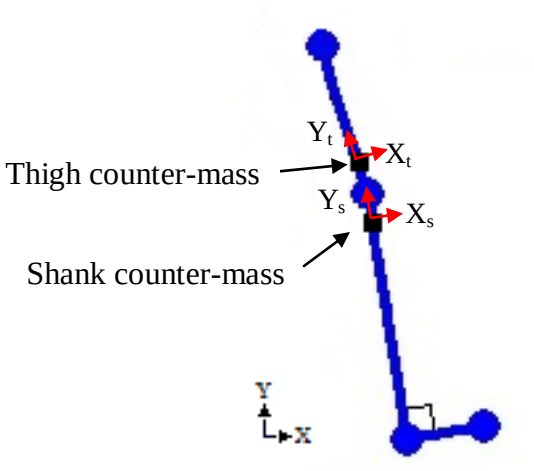

Figure 23: Potential counter-mass locations near the knee unit, at the distal thigh and proximal shank segments investigated via model optimization. Locations included both proximal/distal and anterior/posterior regions within the prosthesis in the XY plane.

Subsequent optimizations were then conducted to investigate altered counter-mass location(s) within the thigh segment only, the shank segment only, and both the thigh and shank segments. Initial position optimization was constrained to vary proximally or distally within the prosthesis (see Figure 23), within a large bounded region of ±1 m with respect to the distal end of the knee unit. These bounds were then further constrained to more realistic bounds corresponding to the actual thigh and shank segment lengths.

Further simulations were then performed exploring anterior/posterior placement of the counter-mass, constrained to a ±1 m by ±1 m area (within the XY plane, Figure 23) with respect to the distal end of the knee unit. These bounds were then tightened to approximate a more clinically relevant bound of ±0.10 m in the anterior/posterior directions and thigh and shank segment lengths. A positive (X,Y) location for a point mass indicates an anterior, proximal counter-mass; a negative (X,Y) location reflects a posterior, distal counter-mass.

Finally, optimizations were conducted to incorporate the inertial properties of the counter-mass, using the radius of gyration. The aforementioned optimizations assumed that the point masses did not affect the inertia of the system. The inertial tensor was assumed to be a planar ring (Equation (9) where M is the counter-mass and R is the radius of gyration:

$$I = MR^2 \tag{9}$$

This radial parameter was initially confined to 0 to 5 m relative to the long axis of the thigh and shank segments. This parameter space was then confined to a more clinically relevant 0 to 0.10 m region. These inertia effects were then included in the counter-mass location optimization in the proximal/distal (Y) and combined proximal/distal and anterior/posterior (XY plane) directions.

Table 12: Optimization trials and corresponding variables used to determine counter-mass magnitude(s) and location(s) for the thigh (T) and shank (S) segments. Y is proximal/distal position, X is anterior/posterior position, and R is the radius of gyration.

Optimization	Variables	Wider Bounds	Tightened Bounds
1	Mass (kg)	[0, 2]	[0, 2]
2	Mass (kg)	[0, 2]	[0, 2]
	Y (m)	[-1, 1]	T: [0, 0.33] S: [-0.37, 0]
3	Mass (kg)	[0, 2]	[0, 2]
	Y (m)	[-1, 1]	T: [0, 0.33] S: [-0.37, 0]
	X (m)	[-1, 1]	T: [-0.10, -0.10] S: [-0.10, -0.10]
4	Mass (kg)	[0, 2]	[0, 2]
	Y (m)	[-1, 1]	T: [0, 0.33] S: [-0.37, 0]
	R (m)	[0, 5]	T: [0, 0.10] S: [0, 0.10]
5	Mass (kg)	[0, 2]	[0, 2]
	Y (m)	[-1, 1]	T: [0, 0.33] S: [-0.37, 0]
	X (m)	[-1, 1]	T: [-0.10, -0.10] S: [-0.10, -0.10]
	R (m)	[0, 5]	T: [0, 0.10] S: [0, 0.10]

3.4 Summary

The thigh, shank, and foot segments of the lower extremity for both the able-bodied and TFA were modeled as a double pendulum system, with the ankle fixed at a neutral orientation. Initial positions and conditions approximated that of toe off. These equations of motion were solved numerically and validated using swing kinematic and duration data from the literature (able-bodied) and physical model experimentation (TFA).

The mass and inertia of the thigh and shank-foot segments were also based on the literature (able-bodied) and TFA physical models. The various mechanical parameters (rotary dampers and torsion springs) for the AB and TFA models were optimized in MatLab using four different objective functions. The objective function which best approximated terminal swing of the physical model was then adopted for counter-mass investigation. These promising counter-mass locations might then serve as locations for the respective batteries and signal conditioning units of future active prosthetic limbs.

Chapter 4: RESULTS

The following chapter presents the results associated with the respective research objectives of this study, namely: 1) development of computer models to simulate swing for an able-bodied lower limb and a TF residual limb and prosthesis, 2) validation or evaluation of these computer models using normal gait data from the literature as well as motion data from physical models of the TF residual limb and prosthesis, and 3) use of these models to identify promising counter-mass magnitude(s) and location(s) to offset large, active prosthetic components such that hip and knee kinematic trajectories during swing approximate that of able-bodied subjects.

4.1 Computer Models

Computer models approximating the lower limb of an able-bodied subject and a TFA were created to simulate swing phase kinematics. These models were then assessed and validated using swing kinematic and duration data from the literature (AB models) and physical model experimentation (TFA models).

4.2 Parameter Identification for Model Simulation

4.2.1 Kinematic Data Used for Parameter Optimization

4.2.1.1 Able-Bodied Swing Kinematics

As indicated previously, the sagittal plane swing phase kinematic data used for AB model validation were based on Winter[20]. These data are summarized in Figure 24 for the hip and knee joints. A swing duration of 0.386 seconds [20] was applied to all AB models, approximating the mean duration of the swing phase.

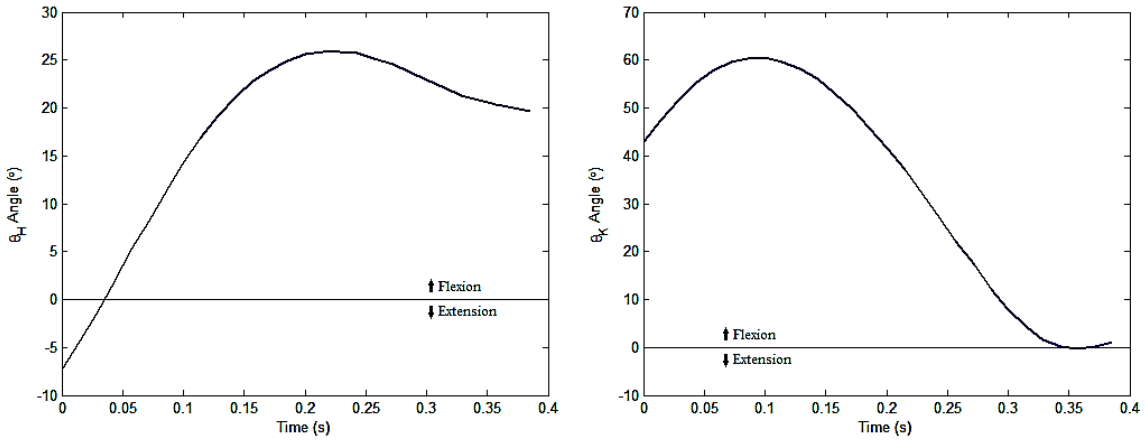

Figure 24: Sagittal plane hip and knee kinematics during swing (Winter [20]) used to optimize parameter values for AB models.

4.2.1.2 TFA Physical Model Swing Kinematics

The sagittal plane swing kinematics used for TFA model parameter optimization were based on the motion analysis data collected for various physical models of the TFA residual limb and prosthesis. Sagittal plane hip and knee kinematics during swing for the each physical model are summarized in Figure 25; the corresponding mean swing durations are presented in Table 13.

Table 13: Swing duration (initial release through full knee extension) for the TFA physical models.

Model #	Swing Duration (s)
TFA-1	0.36 ± 0.04
TFA-2	0.42 ± 0.01
TFA-3	0.42 ± 0.02

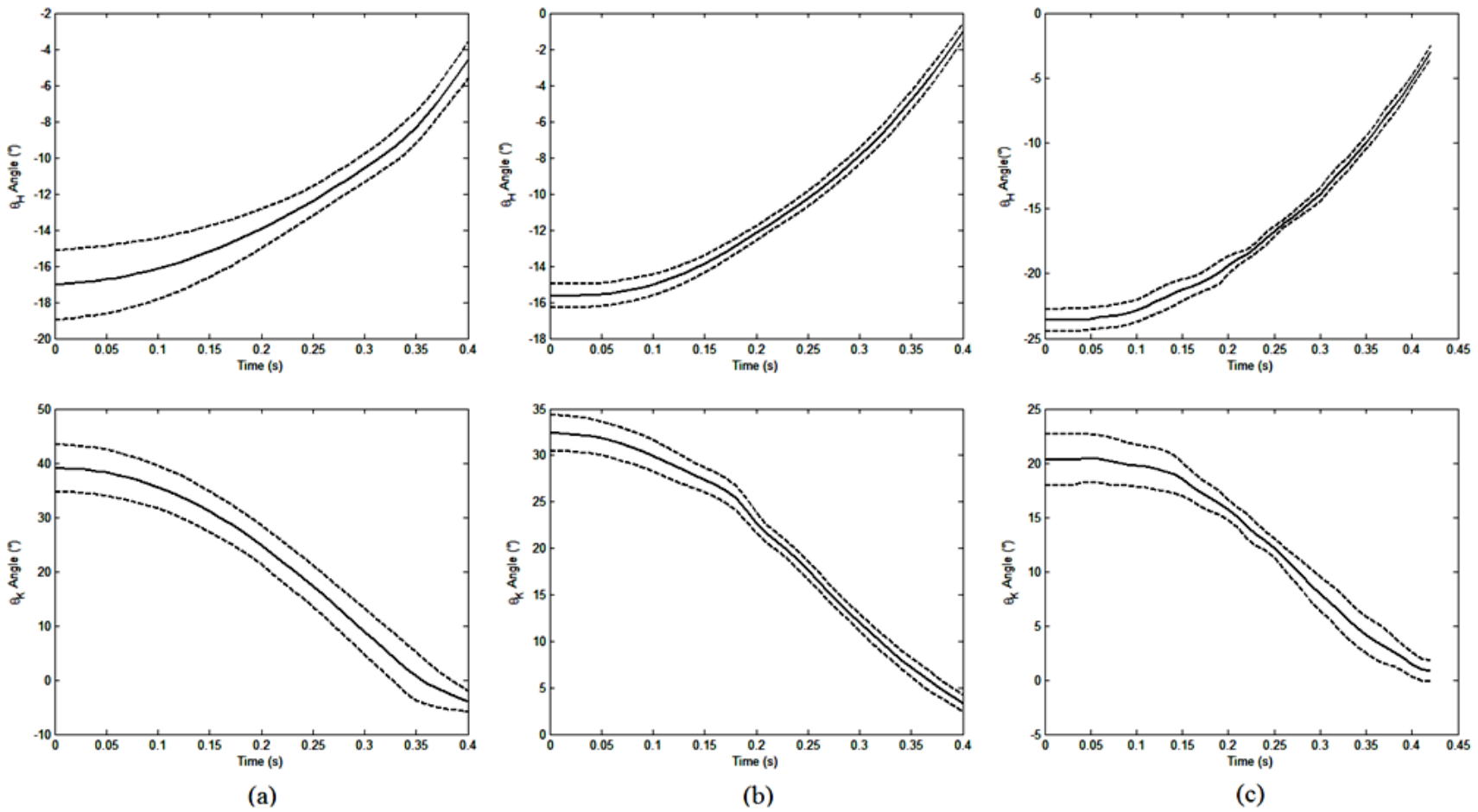

Figure 25: Mean sagittal plane hip and knee kinematics during swing for the various TFA physical models: model TFA-1 (a), model TFA-2 (b), and model TFA-3 (c) over 10 trials; the dashed lines represent one standard deviation about the mean.

4.2.2 Able-Bodied Model Parameter Identification

The optimized model parameters (using the $\overline{OF}_{vert-ref}$ objective function) for the AB-2 and AB-3 models are presented in Table 14. The corresponding RMS errors (see Equation (3) in hip and knee joint angles are summarized in Table 15 for each of the three AB models. Since the knee angle is dependent on both the thigh and shank segment angles (Equation (2)), the RMS error for the shank segment angle with respect to vertical is also presented.

The corresponding graphical comparison of these joint and segment angles for the respective mathematical model and literature data is shown in Figure 26. The double pendulum AB-1 model poorly approximated sagittal plane hip and knee motion during swing. Inclusion of rotational dampers at the hip and knee (model AB-2) resulted in improved simulation of knee flexion, although the simulated hip flexion during mid- and terminal swing remained poor. Inclusion of a time-variant damper at the knee (model AB-3) resulted in minimal, if any, improvement in simulation of hip and knee motion during swing with respect to model AB-2.

Table 14: Optimized mechanical parameters for AB-2 and AB-3 models.

Model Name	C_H $\left(\frac{kg\ m^2}{s\ rad.}\right)$	C_K $\left(\frac{kg\ m^2}{s\ rad.}\right)$	K_H $\left(\frac{N\ m}{rad.}\right)$	K_K $\left(\frac{N\ m}{rad.}\right)$	τ (s)
AB-2	0	0.9695	0	5.904	-
AB-3	0	1.297/0.9325*	0	5.609	0.1199

*Values for before and after knee damper activation

Table 15: Hip, knee, and shank RMS error values for AB-1, AB-2, and AB-3 models.

	RMS Error		
Joint or Segment	AB-1	AB-2	AB-3
θ_H	6.701	12.74	12.89
θ_K	21.04	12.86	13.18
ψ_S	15.16	1.776	1.981

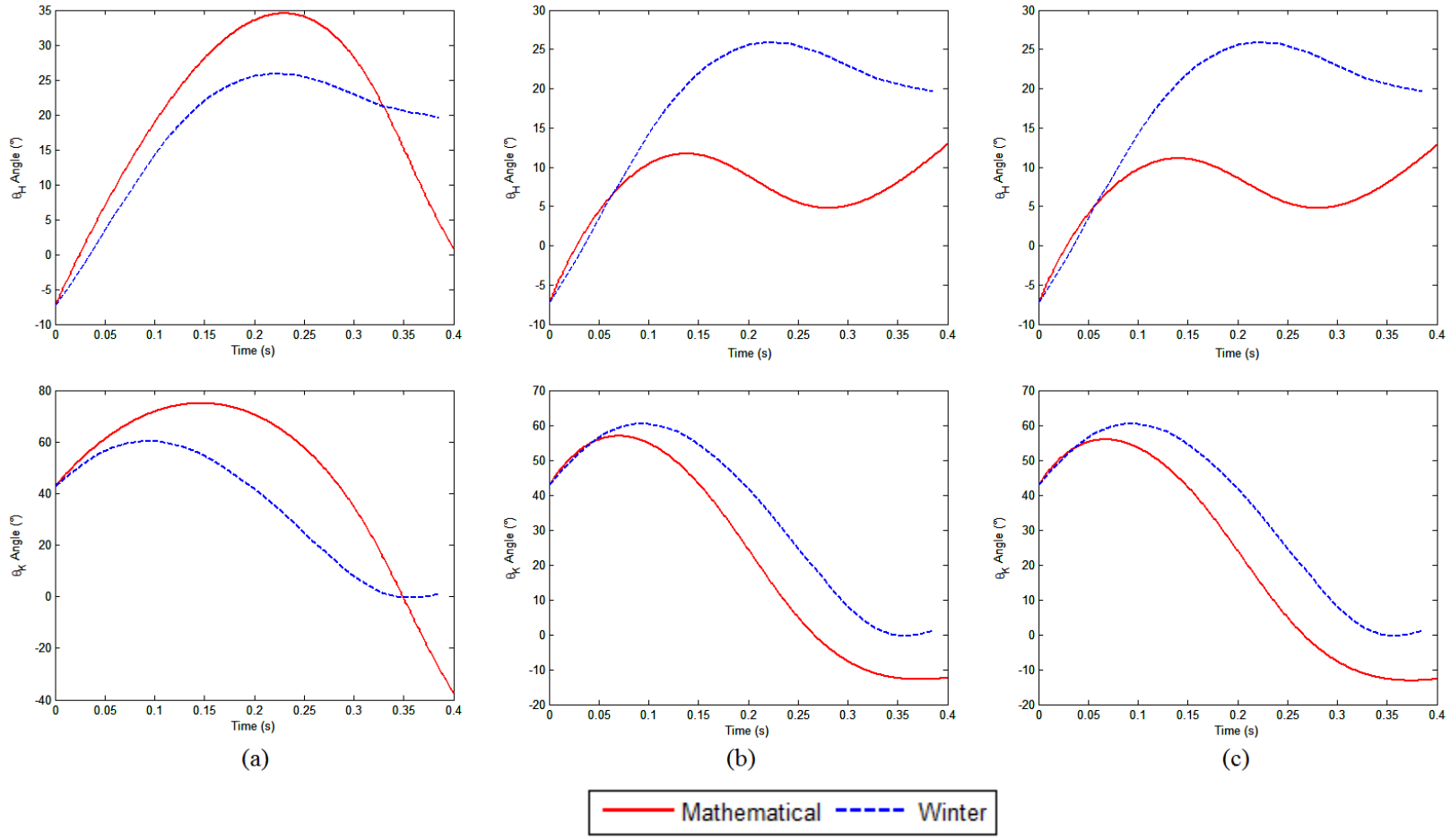

Figure 26: Comparison of simulated sagittal plane hip (top) and knee (bottom) joint angles during swing for AB-1 (a), AB-2 (b), and AB-3 (c) mathematical models contrasted with that of Winter [27]. Positive angles indicate flexion; negative angles indicate extension.

4.2.3 TFA Computer Model Parameter Identification

The respective model parameters of the three TFA computer models were optimized using swing kinematic data (see section 4.2.1.2) obtained for the corresponding physical models. The optimized model damping parameters for these models are summarized in Table 16 (based on objective function $\overline{OF}_{vert-ref.}$ as discussed in section 4.2.4). The corresponding RMS errors (see Equation (3) in hip and knee joint angles, as well as shank segment angle, are reported in Table 17.

Graphical presentation of these model simulations are contrasted with the physical model motion data in Figure 27. The viscous friction incorporated in model TFA-1 approximated the ball bearing hip joint and constant friction knee unit. The static and kinetic Coulomb frictional moments in models TFA-2 and TFA-3 approximated the pseudo-hip joint of the residual limb in these physical models. The transition from static to kinetic friction was implemented through a time-varying parameter (τ). The inclusion of these frictional moment parameters resulted in hip and knee joint motion matching that of corresponding TFA physical models.

Table 16: Optimized mechanical parameters for TFA-1, TFA-2, and TFA-3 models.

Model Name	C_H $\left(\frac{kg\,m^2}{s\,rad.}\right)$	C_K $\left(\frac{kg\,m^2}{s\,rad.}\right)$	τ (s)	$M_{H\text{-}static}$ (N m)	$M_{H\text{-}kinetic}$ (N m)
TFA-1	3.114	0.2177	-	-	-
TFA-2	0	5.38×10^{-4}	0	3.39×10^{-6}	1.106
TFA-3	0	6.50×10^{-4}	0	5.71×10^{-4}	2.531

Table 17: Hip, knee, and shank RMS error values for TFA-1, TFA-2, and TFA-3 models.

	RMS Error		
Joint or Segment	TFA-1	TFA-2	TFA-3
θ_H	0.653	0.109	0.637
θ_K	1.254	1.028	0.770
ψ_S	0.688	1.011	1.253

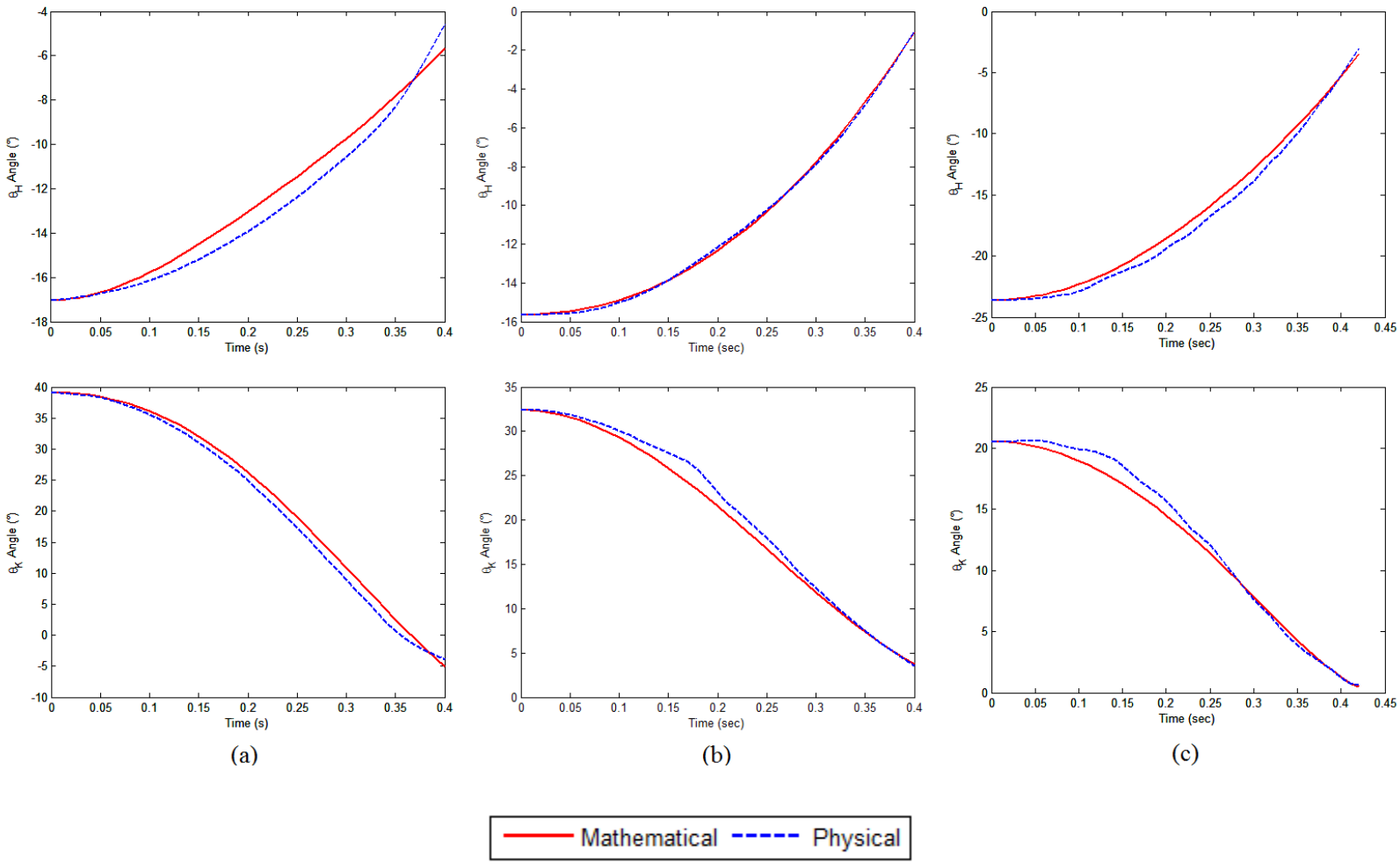

Figure 27: Comparison of simulated sagittal plane hip (top) and knee (bottom) joint motion during swing for TFA-1 (a), TFA-2 (b), and TFA-3 (c) models with respect to motion data of the corresponding physical models. Positive angles indicate flexion; negative angles indicate extension.

4.2.4 Objective Function Identification

Four different objective functions were investigated during optimization of the model parameters for each of the respective AB and TFA mathematical models. These results are summarized in Appendix D for all models. As the primary hypothesis motivating this thesis is identification of counter-mass magnitude(s) and location(s) for an active ankle-foot, the TFA-3 model was tested with the various objective functions to determine which best approximated the physical data. This function was then adopted for counter-mass investigations.

The optimized TFA model parameters for each of the respective objective functions are summarized in Table 18. Parameter optimizations appeared insensitive to initial parameter values and parameter bounds. The viscous knee damping parameter, C_K, appeared most sensitive to the objective function. The hip frictional moment also varied with objective function. These differences in the respective parameter values affected the observed versus physical model motion errors (see Equation (3), as summarized in Table 19. While the $\overline{OF}_{vert-ref}$ objective function resulted in the greatest errors in hip angle, it resulted in the smallest errors in knee angle – the functional parameter with the greatest clinical relevance as the knee must be fully extended during late swing in preparation for weight acceptance.

Table 18: Optimized mechanical parameters for the TFA-3 model using alternative objective functions.

Objective Function	C_H $\left(\frac{kg\ m^2}{s\ rad.}\right)$	C_K $\left(\frac{kg\ m^2}{s\ rad.}\right)$	τ (s)	$M_{H\text{-static}}$ (N m)	$M_{H\text{-kinetic}}$ (N m)
$OF_{diff-hor}$ (°) (Eqn (5))	0	$9.87x10^{-4}$	0	$8.18x10^{-3}$	3.041
$\overline{OF}_{ROM-hor}$ (-) (6)	0	$1.07x10^{-3}$	0	$4.16x10^{-3}$	3.131
$\overline{OF}_{hor-ref}$ (-) (7)	0	$1.11x10^{-3}$	0	$6.86x10^{-3}$	3.151
$\overline{OF}_{vert-ref}$ (-) (8)	0	$6.50x10^{-4}$	0	$5.71x10^{-4}$	2.531

Table 19: Hip, knee, and shank RMS error for model TFA-3 using alternative objective functions.

	RMS Error			
Joint or Segment	$OF_{diff-hor}$ (Eqn 5)	$\overline{OF}_{ROM-hor}$ (6)	$\overline{OF}_{hor-ref}$ (7)	$\overline{OF}_{vert-ref}$ (8)
θ_H	0.2694	0.2470	0.2433	0.637
θ_K	1.171	1.233	1.250	0.770
ψ_S	1.355	1.386	1.395	1.253

Simulated sagittal plane motion of the thigh and shank angles during swing for model TFA-3 is shown in Figure 28. While the objective functions are defined with respect to the independent thigh and shank segment angles, these objective function results are also presented in terms of the more clinically relevant and knee joint angles in Figure 29.

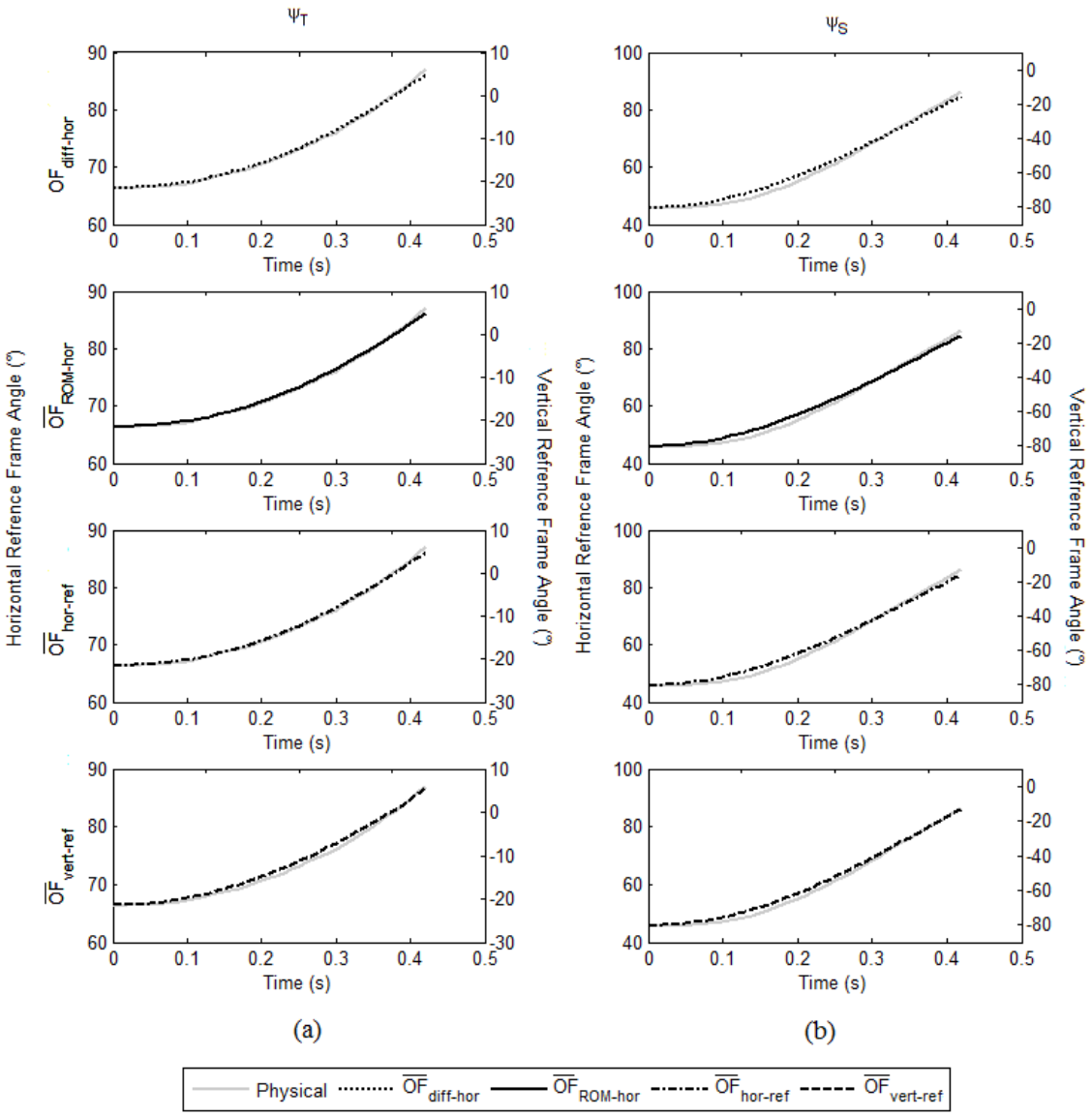

Figure 28: Comparison of simulated sagittal plane thigh (left) and shank (right) segment motion during swing for TFA-3 model for each objective function compared with the physical model. Both the horizontal and vertical frames of references for the objective functions are presented.

The resultant simulated sagittal plane motion of the hip was comparable for each objective function, with a maximum deviation of approximately 0.50° during mid-swing. Deviations in knee motion between the mathematical and physical models were greater, with differences of up to 1.7° observed during both initial/mid (~0.15 sec) and terminal (~0.35 sec) swing. Clinically, the knee position at terminal swing is of greater clinical importance as the knee must be fully extended in preparation for weight acceptance in early stance. As the objective function $\overline{OF}_{vert-ref.}$ resulted in more accurate simulation of knee position at terminal swing (< 0.1° error) than the other objective functions, this objective function was used for all subsequent optimizations.

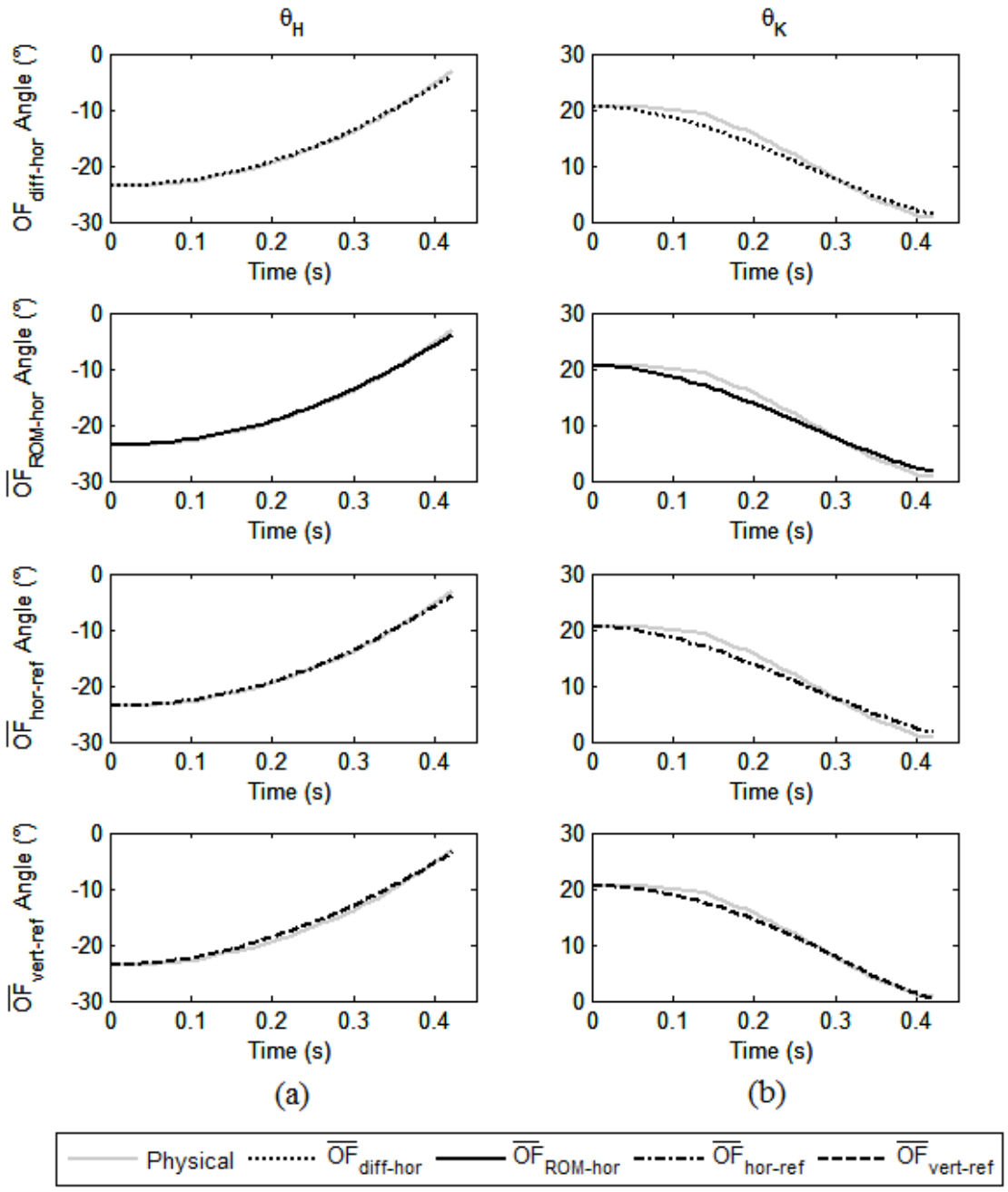

Figure 29: Comparison of simulated sagittal plane hip (left) and knee (right) joint motion during swing for TFA-3 model for each objective function compared with the physical model. Positive angles indicate flexion; negative angles indicate extension.

4.3 Counter-mass Magnitude and Location Optimization

Subsequent analyses and optimizations were conducted using model TFA-3 and $\overline{OF}_{vert-ref.}$ to identify promising counter-mass magnitude(s) and location(s) to offset large, active prosthetic components. Counter-masses were added to the thigh and the shank segments, near the knee unit; these mass magnitudes were constrained between 0 to 2.0 kg, approximating the mass of batteries and signal conditioning units for active prosthetic components. The corresponding counter-mass locations were then optimized to explore proximal/distal and anterior/posterior positions within the prosthesis.

The optimization results for counter-mass location within the thigh segment only are shown in Table 20. Results for both wider and tightened bounds indicated that counter-masses between 1.7 and 2.0 kg (upper mass bound) might be added ~30 cm proximal and 6.5 mm anterior to the proximal end of the knee unit (Figure 30). These counter-mass magnitudes and locations yielded a corresponding increase (~4%) in hip RMS error and a decrease (<1.5%) or improvement in knee RMS error (Table 23 and Table 24). These counter-mass optimization results are contrasted graphically in Figure 31a and Figure 32a.

Counter-mass optimization results within the shank segment only are presented in Table 21. Mass magnitudes ranged from 0.027 to 2.0 kg (upper mass bound); these counter-masses might be positioned ~2-12 cm distal to the distal end of the knee unit, or approximately mid-shank (Figure 30). These proximal-distal counter-mass optimizations (Y) yielded less than a 3% reduction in knee RMS error with respect to the nominal TFA-

3 model or control data (Table 23). However, when the counter-mass (~2.0 kg) was shifted posteriorly (10 cm) and distally (8.7 cm), e.g., X and Y, the RMS error for the knee was reduced nearly 60% (Table 21 and 24). These counter-mass optimizations within the shank are presented graphically in Figures 31b and 32b, illustrating enhanced simulation of knee motion during mid- through terminal (0.25-40 sec) swing. These counter-mass locations, however, induced a hip torque artifact that reduced the corresponding hip flexion during swing.

The final series of counter-mass optimizations were conducted such that the counter-mass locations were explored within both the thigh and shank segments (Table 22). Optimization determined that two masses, one in both thigh and shank segments, were recommended for optimal swing. Investigation of the proximal/distal locations indentified that a counter-mass within the thigh segment ranged from 1.5 to 2.0 kg, located ~31 cm proximal and 2.5 to ~8.8 cm posterior to the proximal end of the knee unit, while an 80 g counter-mass within the shank might be placed 8 to 12 cm distal to the distal end of the knee unit (Figure 30). Compared to the able-bodied data, these counter-mass optimizations resulted in a slight (< 4%) increase in hip angle errors and slight improvements (< 3%) in knee joint angles for the mass and proximal-distal (Y) optimizations. These corresponding RMS errors are presented in Table 23 and Table 24.

As the optimization space was expanded to include anterior-posterior and radial locations, results indicated that only the counter-mass in the shank segment should be manipulated; mass should be increased to 2.0 kg and placed ~8 cm distal and 10 cm

posterior to the distal end of the knee unit (Figure 30). This counter-mass location reduced knee RMS errors by nearly 40% compared to the able-bodied data (e.g., enhanced knee symmetry between the prosthetic and "sound" limbs). However, the corresponding hip RMS error was increased by a factor of 12 due to this counter-mass location inducing a hip torque artifact. These counter-mass effects on hip and knee angle are summarized graphically in Figure 31c and 32c, indicating that knee joint motion approximated that of able-bodied subjects from mid- through terminal (0.25-40 sec) swing.

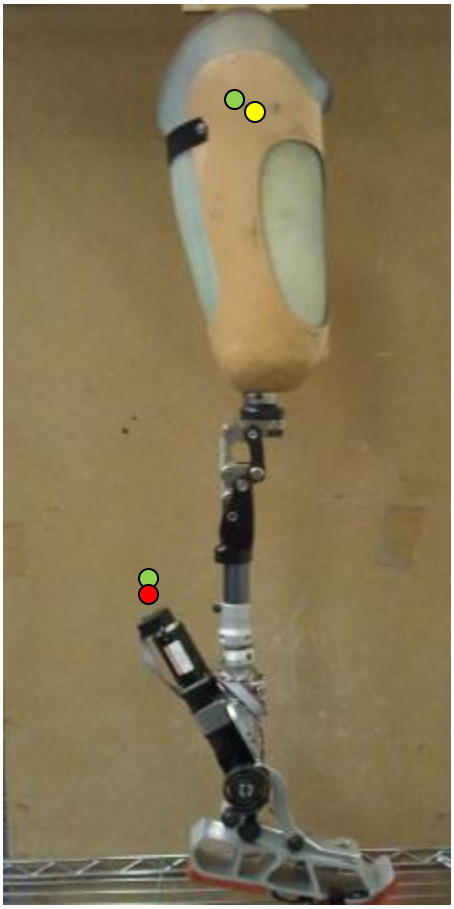

Figure 30: Relative locations for the optimized thigh only (yellow), shank only (red), and both thigh/shank counter-masses (green) are presented on the TFA-3 physical model.

Table 20: Optimization results and corresponding bounds for counter-mass locations in the thigh segment: Y corresponds to the proximal/distal position, X the anterior/posterior position, and R is the radius of gyration.

	Optimization Results				Optimization Bounds			
	Mass (kg)	Y (m)	X (m)	R (m)	Mass (kg)	Y (m)	X (m)	R (m)
Mass	0^{+}	-	-	-	[0, 2]	-	-	-
	0^{+}	-	-	-	[0, 2]	-	-	-
Mass Y	1.73	0.2923	-	-	[0, 2]	[-1, 1]	-	-
	1.73	0.2923	-	-	[0, 2]	[0, 0.33]	-	-
Mass Y, X	2.00^{+}	0.308	0.0066	-	[0, 2]	[-1, 1]	[-1, 1]	-
	2.00^{+}	0.308	0.0066	-	[0, 2]	[0, 0.33]	[-0.10, 0.10]	-
Mass Y, I	1.704	0.2923	-	$1.30\text{x}10^{-4}$	[0, 2]	[-1, 1]	-	[0, 5]
	1.704	0.2923	-	$1.30\text{x}10^{-4}$	[0, 2]	[0, 0.33]	-	[0, 0.10]
Mass Y, X, R	2.00^{+}	0.3079	0.0065	$9.52\text{x}10^{-6}$	[0, 2]	[-1, 1]	[-1, 1]	[0, 5]
	2.00^{+}	0.3079	0.0065	$9.52\text{x}10^{-6}$	[0, 2]	[0, 0.33]	[-0.10, 0.10]	[0, 0.10]

Table 21: Optimization results and corresponding bounds for counter-mass locations in the shank segment: Y corresponds to the proximal/distal position, X the anterior/posterior position, and R is the radius of gyration.

	Optimization Results				Bounds			
	Mass (kg)	Y (m)	X (m)	R (m)	Mass (kg)	Y (m)	X (m)	R (m)
Mass	0.0273	-	-	-	[0, 2]	-	-	-
	0.0273	-	-	-	[0, 2]	-	-	-
Mass Y	0.054	-0.125	-	-	[0, 2]	[-1, 1]	-	-
	0.054	-0.125	-	-	[0, 2]	[-0.37, 0]	-	-
Mass Y, X	2.00^{+}	-0.0265	0.2888	-	[0, 2]	[-1, 1]	[-1, 1]	-
	1.752	-0.086	-0.10^{+}	-	[0, 2]	[-0.37, 0]	[-0.10, 0.10]	-
Mass Y, R	0.054	-0.1243	-	0^{+}	[0, 2]	[-1, 1]	-	[0, 5]
	0.054	-0.1243	-	0^{+}	[0, 2]	[-0.37, 0]	-	[0, 0.10]
Mass Y, X, R	2.00^{+}	-0.0264	-0.29	$7.72\text{x}10^{-5}$	[0, 2]	[-1, 1]	[-1, 1]	[0, 5]
	2.00^{+}	-0.0875	-0.10^{+}	0^{+}	[0, 2]	[-0.37, 0]	[-0.10, 0.10]	[0, 0.10]

$^{+}$ Bound hit by optimization

Table 22: Optimization results for counter-mass location in the thigh (T) and shank (S) segments: Y corresponds to the proximal/distal position, X the anterior/posterior position, and R is the radius of gyration.

	Optimization Results				Bounds			
	Mass (kg)	Y (m)	X (m)	R (m)	Mass (kg)	Y (m)	X (m)	R (m)
Mass	T: 0^{+} S: 0.0273	-	-	-	[0, 2] [0, 2]	-	-	-
	T: 0^{+} S: 0.0273	-	-	-	[0, 2] [0, 2]	-	-	-
Mass Y	T: 2.00^{+} S: 0.0822	T: 0.3126 S: -0.1256	-	-	[0, 2] [0, 2]	[-1, 1] [-1, 1]	-	-
	T: 2.00^{+} S: 0.0822	T: 0.3126 S: -0.1256	-	-	[0, 2] [0, 2]	[0, 0.33] [-0.37, 0]	-	-
Mass Y, X	T: 2.00^{+} S: 2.00^{+}	T: 0.3071 S: -0.0083	T: -0.0884 S: -0.3138	-	[0, 2] [0, 2]	[-1, 1] [-1, 1]	[-1, 1] [-1, 1]	-
	T: 1.462 S: 2.00^{+}	T: 0.3087 S: -0.0834	T: -0.0257 S: -0.10^{+}	-	[0, 2] [0, 2]	[0, 0.33] [-0.37, 0]	[-0.10, 0.10] [-0.10, 0.10]	-
Mass Y, R	T: 2.00^{+} S: 0.0818	T: 0.3125 S: -0.0835	-	T: 0^{+} S: $2.88\text{x}10^{-4}$	[0, 2] [0, 2]	[-1, 1] [-1, 1]	-	[0, 5] [0, 5]
	T: 2.00^{+} S: 0.0818	T: 0.3125 S: -0.0835	-	T: 0^{+} S: $2.88\text{x}10^{-4}$	[0, 2] [0, 2]	[0, 0.33] [-0.37, 0]	-	[0, 0.10] [0, 0.10]
Mass Y, X, R	T: 2.00^{+} S: 2.00^{+}	T: 0.3071 S: -0.0084	T: -0.0884 S: -0.3137	T: 0^{+} S: 0^{+}	[0, 2] [0, 2]	[-1, 1] [-1, 1]	[-1, 1] [-1, 1]	[0, 5] [0, 5]
	T: 1.622 S: 2.00^{+}	T: 0.3104 S: -0.0780	T: -0.0341 S: -0.10^{+}	T: 0^{+} S: 0^{+}	[0, 2] [0, 2]	[0, 0.33] [-0.37, 0]	[-0.10, 0.10] [-0.10, 0.10]	[0, 0.10] [0, 0.10]

$^{+}$ Bound hit by optimization

Table 23: Hip, knee, and shank RMS error values for counter-mass magnitude and location optimization for the wider bounds: Y corresponds to the proximal/distal position, X the anterior/posterior position, and R is the radius of gyration.

		RMS Error					
Segment Optimized	Angle	Control	Mass	Mass Y	Mass Y, X	Mass Y, R	Mass Y, X, R
Thigh	θ_H	0.6873	0.6873	0.7195	0.7146	0.7190	0.7141
	θ_K	14.69	14.69	14.68	14.47	14.68	14.48
	ψ_S	14.50	14.50	14.48	14.47	14.48	14.47
Shank	θ_H	0.6873	0.6587	0.6820	8.493	0.6820	8.497
	θ_K	14.69	14.53	14.29	8.450	14.29	8.442
	ψ_S	14.50	14.46	14.40	6.918	14.40	6.917
Thigh & Shank	θ_H	0.6873	0.6586	0.6880	5.844	0.6870	5.850
	θ_K	14.69	14.53	14.26	8.016	14.26	8.015
	ψ_S	14.50	14.46	14.34	6.756	14.34	6.756

Table 24: Hip, knee, and shank RMS error values for counter-mass magnitude and location optimization for the tighter bounds: Y corresponds to the proximal/distal position, X the anterior/posterior position, and R is the radius of gyration.

		RMS Error					
Segment Optimized	Angle	Control	Mass	Mass Y	Mass Y, X	Mass Y, R	Mass Y, X, R
Thigh	θ_H	0.6873	0.6873	0.7195	0.7146	0.7190	0.7141
	θ_K	14.69	14.69	14.68	14.47	14.68	14.48
	ψ_S	14.50	14.50	14.48	14.47	14.48	14.47
Shank	θ_H	0.6873	0.6587	0.6821	8.488	0.6820	9.338
	θ_K	14.69	14.53	14.29	5.590	14.29	6.103
	ψ_S	14.50	14.46	14.40	8.898	14.40	8.424
Thigh & Shank	θ_H	0.6873	0.6586	0.688	8.392	0.6870	7.77
	θ_K	14.69	14.53	14.26	5.862	14.26	5.810
	ψ_S	14.50	14.46	14.34	8.39	14.34	8.411

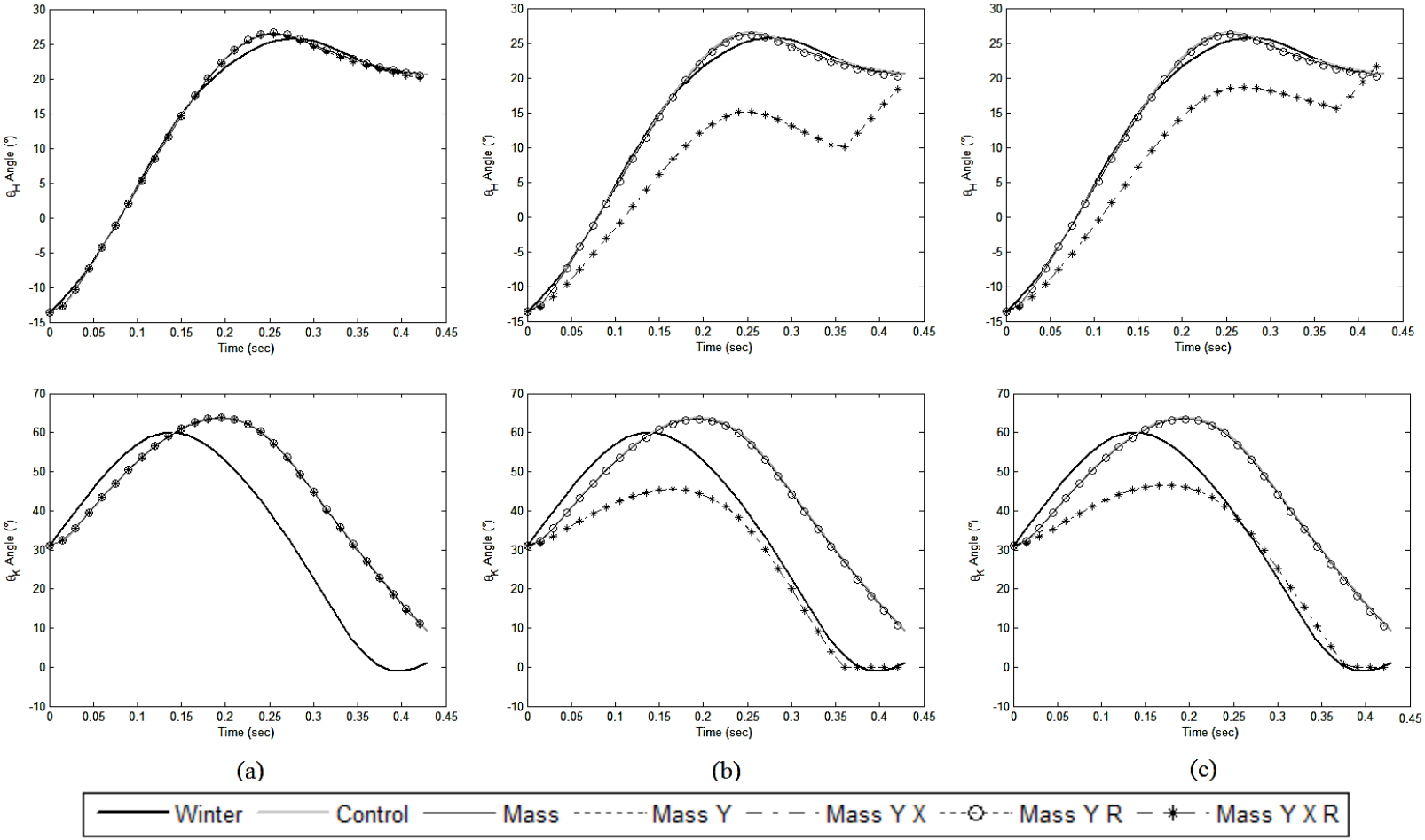

Figure 31: Hip (top) and knee (bottom) joint motion during swing for counter-mass magnitude and location optimization for the wider bounded region of the thigh only (a), shank only (b), and thigh and shank (c) segments. The counter-mass optimization results are contrasted with that for AB swing (thick black line) and nominal TFA-3 model (control – grey). Y corresponds to the proximal/distal position, X the anterior/posterior position, and R is the radius of gyration. Positive angles indicate flexion; negative angles indicate extension.

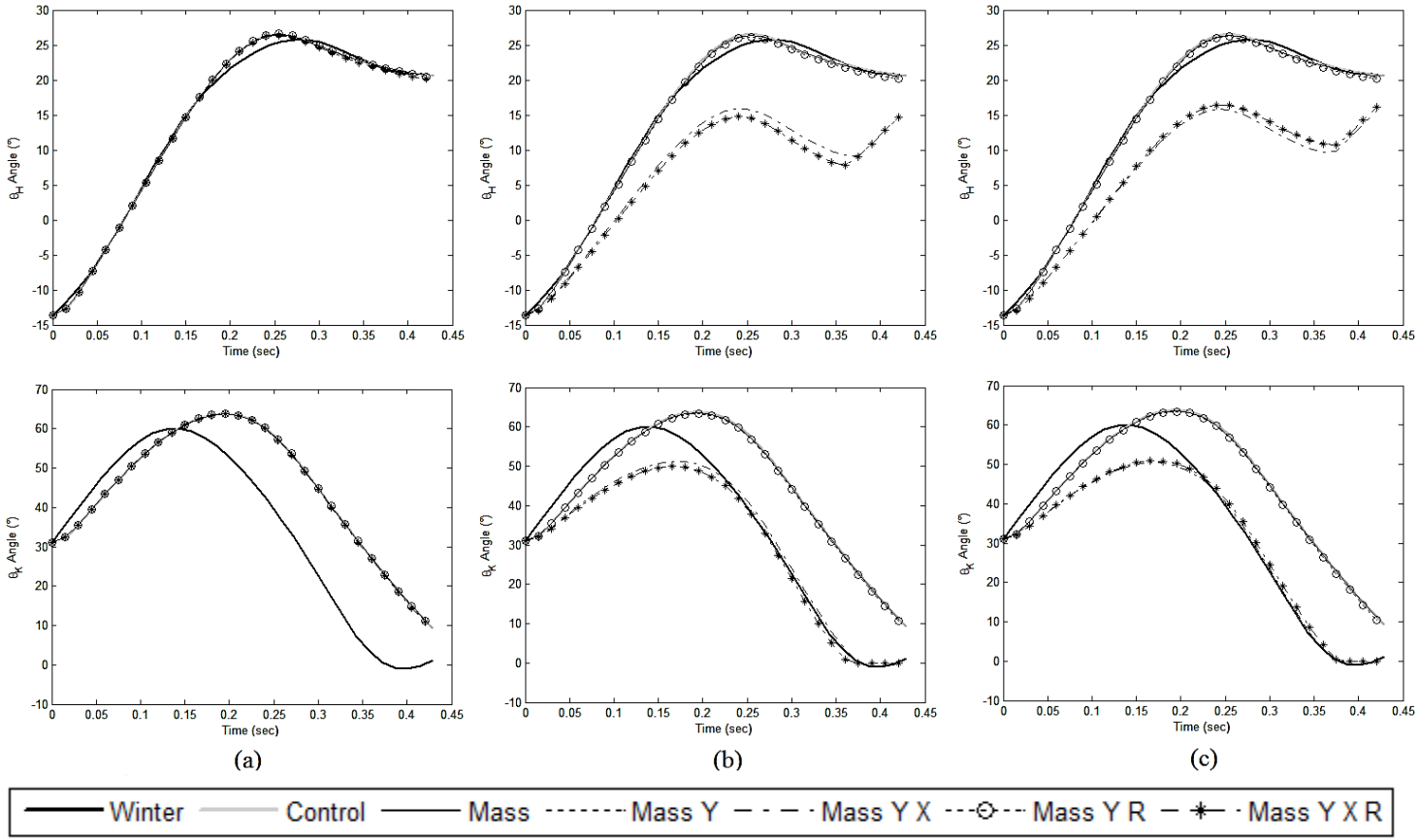

Figure 32: Hip (top) and knee (bottom) joint motion during swing for counter-mass magnitude and location optimization for a tighter bounded region of the thigh only (a), shank only (b), and thigh and shank (c) segments. The counter-mass optimization results are contrasted with that for AB swing (thick black line) and default TFA-3 model (control – grey). Y corresponds to the proximal/distal position, X the anterior/posterior position, and R is the radius of gyration. Positive angles indicate flexion; negative angles indicate extension.

4.4 Summary

The mechanical parameters of mathematical models approximating the lower extremity of an able-bodied and a TFA subject were optimized using hip and knee kinematic data during swing, as well as swing duration data, from the literature (AB models) and physical model experimentation (TFA models). The $\overline{OF}_{vert-ref}$ objective function was selected for subsequent counter-mass optimization analyses as this objective function resulted in reduced errors in knee position during terminal swing. Subsequent counter-mass magnitudes and locations optimizations indicated that batteries and/or signal processing units (up to 2.0 kg) for active lower limb prostheses might be positioned 8 cm distally and 10 cm posterior to the distal end of the knee unit, within the shank segment. While it is possible to add counter-masses 8 cm distal to the knee unit, counter-masses 10 cm posterior to this location would result in a non-cosmetic prosthesis and therefore represent a clinically unrealistic solution.

Chapter 5: DISCUSSION

The results of the mathematical models and the associated optimizations are discussed in the context of the research objectives and hypotheses. These results are also contrasted with prior investigations reported in the literature. Finally, the clinical impact of these results is summarized.

5.1 Parameter Identification

5.1.1 Able-Bodied Models

Based on lower limb muscle activity during ambulation, swing is primarily a passive activity for healthy, normal individuals [22], Figure 5. This conclusion was tested with the able-bodied (AB-1) model which indicated that comparable ranges of motion for the hip and knee can be simulated with a simple double pendulum. The lack of damping at both the hip and knee, however, caused excess hip and knee flexion (>20° - Figure 26a) at mid-swing and excess hip and knee extension (>20° - Figure 26a) at terminal swing. This simple mathematical model indicated that mechanical components may be necessary to limit hip and knee ranges of motion during swing. These additional mechanical components approximate the passive elastic properties of muscles and tendons.

Subsequent models (AB-2 and AB-3) of swing indicated that the inclusion of a rotary damper and torsion spring is required at the knee only. Components located at this position dynamically affect both hip and knee motion, similar to that of the biarticulating muscles crossing these joints (e.g., quadriceps and hamstrings). Optimized parameters

excessively reduced hip extension (>25° - Figure 26b) and slightly reduced knee flexion (<10°- Figure 26b) from mid- through terminal swing, compared to able-bodied gait. Hip and knee extension was slowed by the rotary damper while the torsion spring compensated for the loss of energy due to damping, helping to extend the shank. These components also approximated the slight muscle activity observed during terminal swing (Figure 5). The damper and spring approximate the quadriceps and hamstrings, stabilizing and decelerating the knee during terminal swing in preparation for weight acceptance at heel strike and loading response.

When a time-varying damper at the knee was included (model AB-3), results indicated that activation of the knee damper was not time dependent. Comparable (2.5%) knee errors resulted for both the constant and time-varying knee damping. The inclusion of the damping time constant or switch was to initiate greater hamstring activation to decelerate the shank during terminal swing (Figure 5). This optimized transition, however, occurred during initial swing (0.112 sec), approximately 0.15 sec earlier than that reported for hamstrings activation [21] and provided no physiological relevance.

Mechanical models of able-bodied gait, both stance and swing, have been developed previously. Van der Kooij's et al. two-dimensional model was a seven-link humanoid biped, inclusive of linear dampers and springs at the hips, knees, and ankle joints [55]. The respective damping coefficients and spring constants were evaluated using able-body joint kinematics, walking velocity, and stride length. The hip and knee joint damping and spring parameters were the same for both flexion and extension, 3

Nm/s and 35 Nm. While these values cannot be directly compared to the parameters evaluated in this study (~0.95 Nm/s-rad and 5.6 Nm/rad), results indicate that the spring component exhibits a greater influence on limb extension and control during swing simulation.

While these models demonstrated the feasibility of using mathematical double pendular systems to simulate lower extremity swing, the inability of the passive double-pendulum model may be due to the assumed fixed hip center of rotation. During able-bodied gait, the pelvis (e.g., hip frame of reference) translates anteriorly and rotates in the transverse and frontal planes. This motion may provide additional momentum assisting in hip flexion. The models also assumed unconstrained knee range of motion (e.g., contrary to the anatomic hyperextension stop), but did not affect results as simulation was halted when knee extension was achieved. In future model simulations, pelvic (e.g., hip center) translation and an anatomically accurate knee joint should be used to improve swing results.

5.1.2 TFA Physical Models

The properties of the TFA models were based on three different physical models. These physical models varied in terms of the approximation of the residual limb, the approximation of the remnant hip, and the incorporated prosthetic components (Table 11).

The first physical model (TFA-1) approximated a simplistic TFA residual limb and prosthesis. The mass and inertial properties of the residual limb were approximated by sand within the socket. Sand easily conformed to the shape of the socket, with a density (1.60 kg/L) [56] similar, although more dense, than that of soft tissue (1.05 kg/L) [20]. This increased density resulted in a residual limb which was approximately 15% heavier than the mass of thigh segment for an able-bodied subject [20]. The remnant hip for this model was simply the hip joint of the pelvic band suspension system. This exterior hip was more lateral and proximal that of the actual residual limb; for two-dimensional motion analysis, the lateral location likely did not impact results, although the more proximal location increased the effective length of the thigh segment. Finally, the prosthetic knee and ankle components used for the TFA-1 were a uniaxial knee and SACH foot, simple components not typically prescribed for more active K3/K4 level TFAs who might be candidates for active prostheses.

For the TFA-2 and TFA-3 physical models, the quadrilateral socket did not include a pelvic band/hip joint suspension system like that of TFA-1. To suspend the prosthetic limb, a pin joint approximating the remnant hip joint was placed within the socket. Plaster of Paris was used to fill the socket and approximate the residual limb (and secure the pseudo-hip joint at an approximate anatomic position). The density of this material, however, is significantly greater (2.63 kg/L) [57] than that of soft tissue, resulting is a residual limb mass that is ~20% higher. While the interior location of this joint better approximated that of the remnant hip, this location may have introduced an error in hip center of rotation as the hip marker was now placed on the lateral socket for

motion analysis (as done for able-bodied motion analysis). This lateral marker positioning, however, likely introduced minimal error in two dimensional motion analysis. The physical TFA-2 model incorporated prosthetic componentry more typically prescribed for active (K3/K4) TFAs: the Total Knee 2000 and Axtion foot. Model TFA-3 also incorporated the Total Knee 2000, but the Axtion foot was replaced by the active ankle-foot by Bergelin[3].

To simulate swing, the physical models were suspended by the hip joint, orienting the thigh and shank segments in a position approximating that at toe off, and releasing the prosthesis. The subsequent free fall of the residual limb/thigh and shank/foot segments then approximated swing. The primary challenges with this protocol were achieving consistent initial conditions approximating TFA toe off. Various methods of setting the initial limb position were attempted, taking care not to introduce extraneous forces or torques. The resultant initial positions for these physical models were approximately 16° hip extension and 20 to 40° knee flexion (Figure 25). This hip angle is consistent with that of TFA gait (approximately 15°, [25]). However, the initial knee angle was dependent on the mass of the shank-foot segment of the respective TFA physical model. This initial position was approximately 40° for TFA-1 and TFA-2 (similar to that for TFA gait, [25]) data. For the heavier active ankle-foot, the initial knee angle was only 20° knee flexion; as this ankle-foot has not been tested on TFAs, no gait data are available for comparison.

The results of the associated motion analysis of these swing trials were presented in Figure 25; the variation in segment/joint kinematics was minimal, with standard deviations less than 2° between trials. Contrary to that observed for TFA gait, swing of these TFA models did not result in hip flexion at terminal swing. Knee flexion was reduced, resulting in earlier extension and reduced swing duration with respect to the TFA gait data presented in Figure 8. Although these physical models do not accurately replicate TFA gait, these data allowed for the identification of the mechanical parameters needed to simulate the pendular motion of each model. These mechanical parameters were then used to conduct counter-mass optimization analyses to identify promising counter-mass magnitudes and locations.

5.1.3 Parameter Identification of TFA Mathematical Models

The requisite subset of mechanical components or parameters and their associated values were selected such that the TFA mathematical model approximated the observed physical model swing kinematics and duration. These values were then used for optimization analyses to identify potential counter-mass magnitude(s) and location(s).

The segment mass, center of gravity, and length were measured to estimate inertia as described in Chapter 3. These protocols were repeated three times. Although methods were relatively simple, up to 2% variability was observed between measurements (see Table 9). Segment inertia can be estimated using various techniques: geometric component estimation, CAD reconstruction, and experimentation. Inertia was determined using the experimentation method based on the composition and complexity of each

segment. The resultant variability in segment inertia, however, was due to finite resolution in measuring the associated period of swing for each segment, despite the use of motion and power spectrum analysis in the inertial estimates. To investigate the effects of errors in segment inertia, sensitivity analysis was conducted. As large as 10% variations in the inertial parameters of the thigh and shank segments resulted in differences of 10 to 20% in mechanical parameter values. The determined inertial parameters of the thigh and shank segments (Table 9, thigh: 0.052-0.075 kg-m^2 and shank: 0.0067-0.218 kg-m^2) were comparable to that of Tsai et al. (thigh: 0.070 kg-m^2 and shank: 0.055 kg-m^2) [13] and Hale (shank: 0.036 - 0.042 kg-m^2) [15], based on the pseudo-residual limb and prosthetic componentry (Table 11).

The respective damping coefficients at the hip and knee joints for each TFA model were reported in Table 16. For the TFA-1 model, this damping approximated that of the external single axis hip joint and constant friction knee unit. While data regarding prosthetic component specifications are not available, the magnitude of these damping coefficients appeared reasonable. Knee damping (0.2177 kg-m^2/s-rad.) was less than that at the hip (3.114 kg-m^2/s-rad.) due to the increased inertial load placed on the hip joint due to the sand-filled socket and distal prosthetic componentry. While damping was low at the knee, the non-zero optimized value indicates that damping should be included at both the knee and hip for simulation of swing kinematics. The damping parameter optimization results were insensitive to initial values or bounded ranges for a given optimization function, although these values varied slightly (hip: 3.11-4.15 kg-m^2/s-rad. and knee: 0.207-0.218 kg-m^2/s-rad.) between objective functions.

For the TFA-2 and TFA-3 models that incorporated the internal hip joint and polycentric, hydraulic Total Knee 2000, no viscous damping was necessary at the hip. This lack of damping indicated that other frictional forces were imparted on the system. Knee damping ($6.50x10^{-4}$ kg-m^2/s-rad.) was again minimal. Specific damping magnitudes, however, are not reported by the prosthetic manufacturer. The respective damping parameters for the hip and knee varied modestly (hip: 0 - 0.55 kg-m^2/s-rad and knee: 5.38 $x10^{-4}$ - $1.11x10^{-3}$ kg-m^2/s-rad - Table 18) for the different objective functions, reflecting the importance of objective function assessment in mechanical parameter estimation. The knee damping parameter was also sensitive to the varying mass and inertial properties of the passive (TFA-2) and active (TFA-3) ankle-foot, with an increased kinetic damping of nearly 20% for the heavy, active ankle-foot.

Additional frictional parameters were incorporated at the hip for TFA-2 and TFA-3 models to approximate the internal hip joint response. The metal-on-metal hip joint indicated that Coulomb (static and kinetic) friction forces, rather than viscous damping, are likely imparted on the system to create a resistive moment. The optimized static friction acting at the hip (TFA-2: $3.39x10^{-6}$ Nm and TFA-3: $5.71x10^{-4}$ Nm) was less the kinetic friction during swing. For both TFA-2 and TFA-3 models, the transition from static to kinetic friction occurred at the start of swing, indicating that static friction is negligible during swing. The increased kinetic friction for the TFA-3 (2.53 Nm) versus TFA-2 (1.11 Nm) model can be attributed to the increased distal mass of the active ankle-foot component.

Visual comparison of hip and knee kinematics for the mathematical models versus experimental motion data (Figure 27) indicated that the TFA-3 model was sufficiently accurate to investigate counter-mass magnitude and location optimization. Subsequent modeling techniques might incorporate might incorporate pelvic and hip motion profiles. The addition of these factors may result in joint kinematics comparable to actual TFA gait data, which is different from the passive motion determined for these physical models.

5.2 Objective Function Assessment

Four different objective functions were investigated for possible adoption in subsequent optimization analyses. These objective functions included dimensional and dimensionless forms, relative to either a global horizontal (ground) or global vertical (gravity) reference. Although optimization was required for mechanical parameter estimation for both the AB and TFA models, the TFA-3 model was used to assess the objective functions. The TFA-3 model incorporated prosthetic components typically prescribed for active TFAs, as well as an active ankle-foot necessitating potential counter-mass inclusion. Selection of the objective function was based on which function best approximated knee extension at terminal stance as clinically, the knee must be fully extended in preparation for weight acceptance in early stance.

The $OF_{diff-hor}$ function was also used by Tsai et al. [13] to investigate variations in prosthetic shank mass distribution in TFAs and quantify the error between model and

able-bodied gait data for the hip and knee joint angles during swing. Other studies investigating prosthetic mass effects were experimental; as such, these investigations assessed the effects of mass variation in terms of hip torque [15, 16], not mathematical modeling optimization.

The other objective functions were selected to investigate whether parameter estimation and the associated swing kinematics of the hip and knee might be improved if errors were normalized or expressed with respect to either horizontal or vertical reference frames. These varying reference frames resulted in non-uniform weighting of the hip and knee joint errors with respect to physical model data. The $\overline{OF}_{ROM-hor}$ objective function predominantly weighted the thigh segment with RMS errors (hip: 0.247 and knee: 1.23) comparable to that obtained with the $\overline{OF}_{hor-ref}$ objective function. This global horizontal reference frame weights initial swing joint errors more heavily than those in terminal swing. In contrast, the $\overline{OF}_{vert-ref}$ objective function predominantly weighted the knee or shank segment, resulting in increased hip (0.637) and decreased knee (0.770) RMS errors. Using an objective function based on a global vertical reference frame resulted in enhanced knee extension at terminal swing (Figure 29), a better clinical outcome.

For the various objective functions, differences in sagittal plane knee motion as much as 1.7° were observed during initial and terminal swing (Figure 29). Full extension of the knee at terminal stance is critical for weight acceptance during stance. As such, the $\overline{OF}_{vert-ref}$ objective function was selected for all subsequent analyses.

5.3 Potential Counter-mass Magnitude(s) and Location(s)

The purpose of this study was to identify promising counter-masses to offset the impact of the additional mass of active prosthetic components on hip and knee kinematic trajectories during swing. The specific research hypothesis was that manipulation of the prosthetic mass distribution can improve the kinematic and temporal symmetry of the residual limb and active prosthesis during swing. Initial TFA modeling indicated that a passive double-pendulum model is unable to simulate swing; the hip musculature must be incorporated. The activity of the remnant hip musculature for TFAs with the Total Knee 2000 incorporated in their prosthesis can be approximated using hip torque profiles reported in the literature.

5.3.1 Determination of Hip Torques

The hip moments, presented in Chapter 2, were estimated for TFAs using inverse dynamic modeling [25, 55, 58]. The kinetic data in Seroussi et al. (Figure 10, [25]) was for eight TFAs (section 2.4.4), while Hong et al. [58] investigated two TFAs using a quadrilateral socket, four-bar pneumatic knee, and ESAR foot. These resultant hip moments were consistent with the EMG data presented in Figure 9. For these TFA subjects, no hip moment was required at mid-swing, indicating that hip musculature is not required to propel the limb forward. The TFA-2 and TFA-3 models in this study resulted in reduced hip flexion compared to that of able-bodied subjects when an external hip moment was not incorporated. This potential disparity with Seroussi's and Hong's study may be attributed to fixing the hip joint center and differences in prosthetic knee

units: a Tehlin polycentric knee for Seroussi and four-bar knee for Hong versus the seven-bar hydraulic knee in the physical models of the current study.

Boyda et al. calculated hip moments for five TFAs wearing prostheses that incorporated a quadrilateral socket, Total Knee 2000, and ESAR foot [55]. These components were similar to those used in the TFA-2 model; the ESAR foot of Boyda's subjects was much lighter than the active ankle-foot of the TFA-3 physical model. These hip moments were approximated as a piecewise linear function (Figure 22) and applied to the TFA-3 model until the hip joint kinematics of the residual/prosthetic limb approximated that of a sound limb (e.g., that of an able-bodied subject). All other mechanical parameters identified in prior analyses remained unchanged. The inclusion of this hip moment resulted in reduced kinematic errors or improved kinematic symmetry for both the hip and knee. As residual limb hip moment appears critical to model performance, further study is needed to characterize the hip moment for TFAs wearing heavy, active prosthetic components. Motion of the pelvis should also be investigated to identify if the motion and associated momentum improves kinematic symmetry.

5.3.2 Significance of Counter-Mass Magnitude and Location Optimization

Potential counter-mass magnitude(s) and location(s) were investigated using the TFA-3 mathematical model and the $\overline{OF}_{vert-ref}$ objective function. As TFAs typically desire a normal, cosmetic gait pattern, sagittal plane hip and knee motion data for an able-bodied subject was selected as the control data for counter-mass optimization investigations. These potential counter-masses were constrained between 0 and 2.0 kg,

approximating the mass of power sources and/or conditioning units that might be incorporated in active ankle-foot prosthetic components.

Single- (thigh only, shank only) and multi-segment (combined thigh and shank) optimizations enabled identification of potential magnitude(s) and location(s) of counter-masses which might improve kinematic symmetry of swing. Contrary to previous studies reported in the literature that constrained the mass manipulations to the proximal/distal shank [14-18], this study expanded the solution space to include the thigh and proximal/distal, anterior/posterior and radial locations for each segment.

Investigations of counter-mass magnitude(s) and location(s) were first conducted with wide bounds to test the feasibility of the optimizations. These bounds were then refined to replicate more realistic prosthetic limb proximal/distal, anterior/posterior and radial regions; only the results from these tighter bounds will be discussed. The proximal/distal limits were selected based on the lengths of the respective thigh and shank segments. Limits of ±10 cm in the anterior/posterior and radial directions were set as greater distance from the central axis of the respective segments would result in non-cosmetic prosthesis.

The single-segment, thigh only counter-mass optimizations indicated that a 1.7 to 2.0 kg counter-mass can be added approximately 30 cm proximal and 6.5 mm anterior to the proximal border of the knee unit (Figure 30). This location, however, is not clinically feasible as such a counter-mass would be near the hip, *within* the socket, interfering with

residual limb placement in the socket. In contrast to other studies investigating mass manipulation effects on swing, this counter-mass magnitude resulted in a significantly heavier thigh segment (8.60 kg) {Tsai et al. (5.07 kg) [13], Beck et al. (7.60 kg) [17]}.

Optimization of counter-mass location of the shank segment resulted in potential increased knee symmetry for a counter-mass of 2.0 kg positioned approximately 8.0 cm distal and 10 cm posterior to the distal end of knee unit (Figure 30). This counter-mass location, however, induced an artificial hip torque that decreased hip kinematic symmetry during swing. Hip torque must seemingly be increased to compensate for this counter-mass, as proposed in other studies [15, 16], resulting in increased energy expenditure. Clinically, increased mass of the prosthetic shank, due to both the shank counter-mass and the active ankle-foot, may also require enhanced prosthetic suspension.

The inclusion of a 2.0 kg shank counter-mass will yield a shank segment with mass exceeding 5.0 kg, greater than the segment masses previously investigated in the literature [13-18]. Prior studies, however, only analyzed the effects of mass added at the shank center of mass (COM) [15-18]. These masses increased the mechanical work of the hip, consistent with the current study. Reduced shank mass and/or a more proximal COM have been reported to reduce swing time and result in joint kinematics which approximates able-bodied subject motion [13, 14]. In contrast, results of the current study indicate that a proximal and posterior shift in shank segment COM is necessary for enhanced kinematic symmetry of the knee. This difference can be attributed to increased mass of the powered prosthesis.

Multi-segment investigation of potential counter-mass within both the thigh and shank segments indicated that the two counter-masses should be located:

1) 31 cm proximal and 8 cm posterior (1.5 to 2.0 kg) to the proximal end of the knee unit in the thigh segment, and
2) 8 distal and 10 cm posterior to the distal end of the knee unit (2.0 kg)

as illustrated in Figure 30. These dual counter-masses resulted in improved kinematic symmetry at the knee (40% reduction in knee RMS error), but again resulted in a hip torque artifact that adversely affected hip kinematic symmetry (hip RMS error increased by a factor of 12). Clinically, these locations are not feasible; the thigh counter-mass is within the socket, interfering with the residual limb placement. The posterior positioning of the shank counter-mass may result in a non-cosmetic prosthesis and require enhanced prosthetic suspension. No comparison to the literature is possible as only the current study investigated multi-segment counter-mass placement.

The final counter-mass optimizations investigated the radial parameter properties for all optimization. Neither hip nor knee symmetry was enhanced for any radial contributions. The resultant radial parameters (1.30×10^{-4} to 9.52×10^{-6} m) indicate that the counter-masses may be approximated as point masses and that inertial effects can be ignored, consistent with results presented by Mena et al. [12].

While the TFA-3 mathematical model proved useful for investigation counter-mass optimizations, the resultant counter-mass locations and magnitudes have limited clinical potential. Counter-mass magnitudes were intended to approximate that of

batteries and signal conditioning units for active prosthetic components. The resultant locations, however, are either not feasible (e.g., within the residual limb) or are non-cosmetic (e.g., 10 cm posterior to shank). These preliminary results indicate that it may not be possible to position a counter-mass within a TF prosthesis that will offset a heavy active ankle-foot and improve kinematic symmetry of the hip and knee. However, future simulation inclusive of pelvic motion (e.g., hip joint center not fixed) and hip moments obtained during TFA gait with active ankle-foot units are needed to confirm this preliminary finding. Additional simulations might also be conducted to investigate counter-mass effects for an active knee, not an active ankle-foot. Finally, models might also be developed to investigate counter-mass effects for transtibial amputees wearing an active ankle-foot.

5.4 Study Limitations

One of the most significant limitations of this study was the lack of TFA hip kinetic data for a TFA using a prosthesis with an active ankle-foot. While data regarding the gait of TFAs have been reported [22, 23, 25, 32, 33, 43, 44, 55, 58], many studies involved kinematic analysis only [22, 23, 32, 33, 43]. A few studies [25, 55, 58] included inverse dynamic analysis to estimate joint moments; these studies, however, included limited subjects and only one study included subjects using a prosthesis that incorporated the Total Knee 2000 [55]. These prostheses, however, incorporated a lightweight, passive ESAR foot. As such, the subjects' hip moments likely differ from that which would result for a prosthesis with a heavy, active ankle-foot. The hip moments applied to the TFA-3 model may therefore be in error. Gait analysis data for TFA subjects wearing a prosthesis with the Total Knee 2000 in combination with an active (or at least comparably weighted) ankle-foot component are needed. Model optimizations could then be re-run to further investigate whether counter-masses might be included to improve kinematic symmetry.

Another related study limitation included ignoring pelvic motion by fixing the hip joint in space. During gait, the pelvis translates anteriorly and rotates in the transverse and frontal planes. This motion provides additional energy and momentum assisting in hip flexion. The reduction in hip flexion observed for both AB and TFA models may have been due to this assumption.

Lastly, these mathematical models were unable to compensate for the effects of the added counter-masses, correcting for their impact on model predicted hip torques. While the applied hip moment profile was applied for all counter-mass optimizations, these counter-masses often reduced hip flexion in terminal swing. TFAs would likely alter their gait and hip musculature activation to ensure the limb was in a stable position in terminal swing in preparation for weight acceptance in early stance.

5.5 Future Work

As mentioned previously, gait analysis trials are needed for TFA subjects wearing prostheses that incorporate the Total Knee 2000 and an active (or comparably weighted) ankle-foot component. Such analyses, in concert with inverse dynamic modeling, will provide better estimates hip torque for inclusion in the TFA-3 model. This model can also be updated to include pelvic translation and rotation observed during gait. These model inputs, as well as segment length and inertial properties, of respective test subject(s) can be used to conduct additional counter-mass optimization analyses.

Gait analysis trials may also be conducted to investigate the effects of the counter-masses magnitudes and locations identified in this study (e.g., kinematic symmetry, energy consumption, supplemental suspension needs). Such studies would also serve to validate the TFA-3 mathematical model, justifying its use to design new prostheses and/or components and modify existing prostheses so as to enhance TFA kinematic symmetry during swing.

Chapter 6: CONCLUSION

Transfemoral amputees (TFAs) suffer the loss of the knee and ankle joints, as well as partial or complete loss of many of the lower extremity muscle groups involved in ambulation. To restore limb length and replace some of lost lower limb functionality, physicians and prothetists prescribe a combination of passive components to form a functional prosthetic limb. Recent advances in lower limb prostheses have involved the design of active, powered prosthetic ankle-foot and knee components capable of generating ankle and knee torques similar to that of normal gait.

Onboard motors and conditioning/processing units located at the knee and ankle to provide the prescribed torques result in increased mass of the respective active components. The active prostheses also must incorporate the mass of the battery. While not an issue during stance, the increased mass of the prosthesis affects swing. The goal of this study was to develop mathematical models of the transfemoral residual limb and prosthesis, expand these models to include an active ankle-foot, and investigate counter-mass magnitude(s) and location(s) via model optimization that might improve kinematic symmetry of the hip and knee during swing.

Single- (thigh only, shank only) and multi-segment (combined thigh and shank) optimizations were conducted, with potential counter-mass magnitude constrained to less than 2.0 kg. The potential locations were constrained to the thigh and shank segment lengths; anterior/posterior and radial locations of up to 10 cm from the central axis of the respective segments to minimize negative aesthetic impact. Results indicated that knee

symmetry during swing was improved when a 2.0 kg mass was positioned 8 cm distally and 10 cm posterior to the distal end of knee unit, within the shank segment. This location, however, induced a hip torque artifact that reduced that adversely affected hip kinematic symmetry.

These preliminary results indicate that it may not be possible to position a counter-mass within a TF prosthesis that will offset a heavy active ankle-foot and improve kinematic symmetry of the hip and knee. Additional simulations inclusive of pelvic motion and hip moments obtained during TFA gait with active ankle-foot units are needed to confirm this preliminary finding. Future simulations might also be conducted to investigate counter-mass effects for an active knee, not an active ankle-foot.

BIBLIOGRAPHY

[1] K. W. Hollander, R. Ilg, T. G. Sugar and D. Herring, "An Efficient Robotic Tendon for Gait Assistance," *Journal of Biomechanical Engineering,* vol. 128, pp. 788-791, 2006.

[2] D. Bellman, M. A. Holgate and T. G. Sugar, "PARKy 3: Design of an Active Robotic Ankle Prosthesis with Two Actuated Degrees of Freedon Using Regenerative Kinetics," in *Second Biennial IEEE/RAS-EMBS International Conference on Biomedical Robotics and Biomechatronics*, 2008.

[3] B. J. Bergelin, J. O. Mattos, J. G. Wells Jr. and P. A. Voglewede, "Concept Through Preliminary Bench Testing of a Powered Lower Limb Prosthetic Device," *Journal of Mechanisms and Robotics,* vol. 2, 2012.

[4] B. J. Bergelin and P. A. Voglewede, "Design of an Active Ankle-Foot Prosthesis Utilizing a Four-Bar Mechanism," *Journal of Mechanical Design,* vol. 137, pp. 2-7, 2012.

[5] S. K. Au, J. Weber and H. Herr, "Biomechanical Design of a Powered Ankle-Foot Prostesis," *IEEE,* pp. 298-303, 2007.

[6] S. K. Au, H. Herr, J. Weber and E. C. Martinez-Villalpando, "Powered Ankle-Foot Prosthesis for the Improvement of Amputee Ambulation," in *Proceedings of the 29th Annual International Conference of the IEEE/EMBS* , 2007.

[7] S. K. Au, M. Berniker and H. Herr, "Powered ankle-foot prosthesis to assist level-ground and stair descent gaits," *Neural Networks,* vol. 21, pp. 654-666, 2008.

[8] S. K. Au, J. Weber and H. Herr, "Powered Ankle-Foot Prosthesis Improves Walking Metabolic Economy," *IEEE Transactions of Robotics,* vol. 25, no. 1, pp. 51-66, 2009.

[9] F. Sup, H. A. Varol and M. Goldfarb, "Upslope Walking With a Powered Knee and Ankle Prosthesis: Initial Results With an Amputee Subject," *IEEE: Transactions on Neural Systems and Rehabilitation Engineering,* vol. 19, pp. 71-78, 2011.

[10] F. Sup, H. A. Varol, J. Mitchell and T. Withrow, "Design and Control of an Active Electrical Knee and Ankle Prosthesis," in *2nd Biennial IEEE/RAS-EMBS Internaltion Conference on Biomedical Robotics and Biomechatronics,* 2008.

[11] F. Sup, H. A. Varol, J. Mitchell and T. Withrow, "Preliminary Evaluations of a Self-Contained Anthropomorphic Trans-femoral Prosthesis," *IEEE/ASME Transactions on Mechatronics,* vol. 14, pp. 667-676, 2009.

[12] D. Mena, J. M. Mansour and S. R. Simon, "Analysis and Synthesis of Human Swing Leg Motion During Gait and Its Clinical Applications," *Journal of Biomechanics,* vol. 14, pp. 823-832, 1980.

[13] C. S. Tsai and J. M. Mansour, "Swing Phase Simulation and Design of Above Knee Prostheses," *Journal of Biomechanical Engineering,* vol. 108, pp. 65-72, 1986.

[14] S. Tashman, R. Hicks and D. Jendrzejczyk, "Evaluation of a Prosthetic Shank with Variable Inertial Properties," *Clinical Prosthetics and Orthotics,* vol. 9, pp. 23-28, 1985.

[15] S. A. Hale, "Analysis of the Swing Phase Dynamics and Muscular Effort of the Above-Knee Amputee for Varying Prosthetic Shank Loads," *Prosthetics and Orthotics International,* vol. 14, pp. 125-134, 1990.

[16] A. Gitter, J. Czerniecki and M. Meinders, "Effect of Prosthetic Mass on Swing Phase Work During Above-Knee Amputee Ambulation," *American Journal of Physical Medicine & Rehabilitation,* vol. 76, pp. 114-121, 1997.

[17] J. C. Beck and J. Czerniecki, "A method for optimization of above-knee prosthetic shank-foot inertial characteristics," *Gait & Posture,* vol. 2, pp. 75-84, 1994.

[18] J. M. Czerniecki, A. Gitter and K. Weaver, "Effects of Alterations in Prosthetic Shank Mass on the Metabolic Costs of Ambulation in Above-Knee Amputees," *American Journal of Physical Medicine & Rehabilitation,* vol. 73, pp. 338-342, 1994.

[19] R. W. Selles, A. Buss, B. J. Johammes, R. C. Wagenaar and H. J. Stam, "Effects of Prosthetic Mass and Mass Distribution on Kinematics and Energetics of Prosthetic Gait: A Systemic Review," *Archives of Physical Medicine and Rehabilitation,* vol. 80, pp. 1593-1599, 1999.

[20] D. A. Winter, Biomechanics and Motor Control of Human Movement, 2nd ed., New York: Wiley, 1990, pp. 56-57.

[21] M. W. Whittle, Gait Analysis: An Introduction, 3rd ed., Woburn, Massachusetts: Butterworth-Heinemann, 2002.

[22] J. Perry and J. M. Burnfiend, Gait Analysis: Normal and Pathological Function, Thorofare, N.J.: SLACK inc., 2010.

[23] G. Malanga and J. A. Delisa, "Clinical Observation," in *Gait Analysis in the Science of Rehabilitation*, Washington DC, Department of Veterans Affairs, 1998, pp. 1-11.

[24] D. A. Winter, "Biomechanical Motor Patterns in Normal Walking," *Journal of Motor Behavior,* vol. 15, pp. 302-330, 1983.

[25] R. E. Seroussi, A. J. Gitter, J. M. Czerniecki and K. Weaver, "Mechanical work adaptations of above knee amputee ambulation," *Archives of Physical Medicine and Rehabilitation,* vol. 77, pp. 1209-1214, 1996.

[26] J. M. Czerniecki and A. J. Gitter, "Gait Analysis in the Amputee: Has it helped the amputee or contributed to development of improved prosthetic components?," *Journal of Biomechanics,* vol. 22, pp. 258-268, 1989.

[27] R. L. Waters and S. Mulroy, "The energy expenditure of normal and pathologic gait," *Gait and Posture,* vol. 9, pp. 207-231, 1999.

[28] D. G. Shurr and T. M. Cook, Prosthetics & Orthotics, Norwalk, CN: Appleton & Lange, 1990.

[29] NLLIC, *Limb Loss in the United States Fact Sheet,* National Limb Loss Information Center and the Limb Loss Research and Statistics Program, 2008.

[30] T. R. Dillingham, L. E. Pezzin and E. J. MacKenzie, "Limb amputation and limb deficiency: the epidemiology and recent trends in the United States," *Southern Medical Journal,* vol. 95, pp. 875-883, 2002.

[31] P. Sugarbaker, J. Bickels and M. Malawer, "Above-knee Amputation," in *Treatment of Sarcomas and Allied Diseases,* Springer, 2001, pp. 349-360.

[32] M. P. Murray, S. B. Sepic, G. M. Gardner and L. A. Mollinger, "Gait Patterns of Above-Knee Amputees Using Constant Friction Knee Components," *Bulletin of Prosthetics Research,* vol. 10, no. 33, pp. 34-45, 1980.

[33] M. P. Murray, L. A. Mollinger, S. B. Sepic, G. M. Gardner and M. T. Linder, "Gait Patters in Above-Knee Amputee Patients: Hydraulic Swing Control vs Constant-friction Knee Components," *Archives of Physical Medicine and Rehabilitation,* vol. 64, pp. 329-333, 1983.

[34] M. Lusardi, Orthotics and Prosthetics in Rehabilitation, 3rd ed., Philadelphia, Pa.: Saunders, 2012.

[35] R. Seymour, Prosthetics and Orthotics Lower Limb and Spinal, New York: Lippincoot Williams & Wilkins, 2002.

[36] S. A. Gard and R. J. Konz, "The effect of a shock-absorbing pylon on the gait of persons with unilateral transtibial amputation," *Journal of Rehabilitation Research and Development,* vol. 40, no. 2, pp. 109-124, 2003.

[37] J. E. Edelstein and A. Moroz, Lower-Limb Prosthetics and Orthotics Clinical Concepts, New York: SLACK Inc., 2011.

[38] M. Y. Zarrugh and C. W. Radcliffe, "Simulation of swing phase dynamics in above-knee prostheses," *Journal of Biomechanics,* vol. 9, no. 5, pp. 283-292, 1976.

[39] M. B. Silver-Thorn, *Class Notes BIEN 5630: Rehabilitation Engineering: Prosthetics, Orthotics, Seating & Positioning,* Milwaukee: Marquette University, 2012.

[40] L. Nolan and A. Lees, "The functional demands on the intact limb during walking for active trans-femoral and trans-tibial amputees," *Prosthetics and Orthotics International,* vol. 24, pp. 117-125, 2000.

[41] A. M. Boonstra, V. Fidler and W. H. Eisma, "Walking speed of normal subjects and amputees: aspects of validity of gait analysis," *Prosthetics and Orthotics International,* vol. 17, pp. 78-82, 1993.

[42] R. L. Waters, J. Perry, E. Antonello and H. Hislop, "Energy Cost of Walking of Amputees: The Influence of Level of Amputation," *Journal of Bone and Joint Surgery,* Vols. 58-A, pp. 42-46, 1976.

[43] J. M. Czerniecki, "Rehabilitation in limb deficiency. 1. Gait and motion analysis," *Gait & Posture,* vol. 77, pp. S3-8, 1996.

[44] S. M. Jaegers, J. H. Arendzen and H. J. d. Jongh, "An Electromyographic Study of the Hip Muscles of Transfemoral Amputees in Walking," *Clinical Orthopaedics and Related Research,* vol. 328, pp. 119-128, 1996.

[45] R. L. Waters, H. J. Hislop, J. Perry, L. Thomas and J. Campbell, "Comparative cost of walking in young and old adults," *Journal of Orthopaedic Research,* vol. 1, no. 1, pp. 73-76, 1983.

[46] K. R. Kaufman, J. A. Levine, R. H. Brey, B. K. Iverson, S. K. McCrady and D. J. Padgett, "Gait and balance of trans-femoral amputees using passive mechanical and microprocessor-controlled prosthetic knees," *Gait & Posture,* vol. 26, pp. 489-493, 2007.

[47] P. A. Macflarlane, D. H. Nielsen and D. G. Shurr, "Mechanical Gait Analysis of Trans-femoral Amputees: SACH Foot Versus the Flex-Foot," *Journal of Prosthetics and Orthotics,* vol. 9, 1997.

[48] L. A. Miller and D. S. Childress, "Problems associated with the use of inverse dynamics in prosthetic applications: An example using polycentric prosthetic knee," *Robotica,* vol. 23, pp. 325-335, 2005.

[49] D. A. Winter, "Table A.3(a) Linear and Angular Kinematics – Hip," in *Biomechanics and Motor Control of Human Movement*, New York, Wiley, 1990, pp. 240-244.

[50] D. A. Winter, "Table A.3(a) Linear and Angular Kinematics - Leg," in *Biomechanics and Motor Control of Human Movement*, New York, Wiley, 1990, pp. 237-240.

[51] D. Russell, "Swing Weight of Baseball and Softball Bats," *The Physics Teacher,* vol. 48, pp. 471-474, 2012.

[52] "360 Orthotics and Prosthetics," Otto Bock, [Online]. Available: http://www.360oandp.com/products/192/Otto-Bock-Axtion%C2%AE.aspx. [Accessed 19 February 2013].

[53] "Total Knee® 2000," Össur, [Online]. Available: http://www.ossur.com/?PageID=13446. [Accessed 10 2 2013].

[54] "What are the details of the Woltring Filter?," Vicon, [Online]. Available: http://www.vicon.com/support/solution_view.php?id=1098. [Accessed 9 2 2013].

[55] C. L. Boyda Glaister, *A Functional Comparison of Two Types of Prosthetic Knee Designs,* Milwaukee: Unpublished Thesis, 2005.

[56] R. Walker, "Density of Materials," SImetric, 4 April 2011. [Online]. Available: http://www.simetric.co.uk/si_materials.htm. [Accessed 23 Februrary 2013].

[57] "PLASTER OF PARIS," International Programme on Chemical Safety, 24 October 2004. [Online]. Available: http://www.inchem.org/documents/icsc/icsc/eics1217.htm. [Accessed 23 February 2013].

[58] J. H. Hong and M. S. Mun, "Relationship between socket pressure and EMG of two

muscles in trans-femoral stumps during gait," *Prosthetics and Orthotics International,* vol. 29, no. 1, pp. 59-72, 2005.

[59] S. Srinivasan, E. R. Westervelt and A. H. Hansen, "A Low-Dimensional Sagittal-Plane Forward-Dynamic Model for Asymmetric Gait and Its Application to Study the Gait of Transtubial Prosthesis Users," *Journal of Biomechanical Engineering,* vol. 131, 2009.

[60] A. M. Boonstra, J. M. Schrama, W. H. Eisma, A. L. Hof and A. Fidler, "Gait Analysis of Trans-femoral Amputee Patients Using Prostheses With Two Different Knee Joints," *Archives of Physical Medicine and Rehabilitation,* vol. 77, pp. 515-520, 1996.

[61] J. Rose and J. G. Gamble, Eds., Human Wallking, Baltimore, Maryland: Williams and Wilkins, 1994.

[62] B. Bresler and F. JP, "The Forces and Moments in the Leg During Level Walking," *Trans ASME,* vol. 72, pp. 27-36, 1950.

[63] H. Van der Kooij, R. Jacobs, B. Koopman and F. Van der Helm, "An alternative approach to synthesizing bipedal walking," *Biological Cybernetics,* vol. 88, pp. 46-59, 2003.

[64] F. W. M. M. N.E. Bishop, "Friction moments of large metal-on-metal hip joint bearings and other modern designs," *Medical Engineering & Physics,* vol. 30, no. 8, pp. 1057-1064, 2008.

APPENDIX A: ACRONYMS

TFA	Transfemoral amputee
COM	Center of mass
ψ_T	Thigh segment angle defined with respect to the horizontal
ψ_S	Shank segment angle defined with respect to the horizontal
θ_H	Hip angle measure defined with respect to vertical
θ_K	Knee angle measure
RMS	Root mean square error
AB	Able-bodied
C_H	Viscous damping at the hip
C_K	Viscous damping at the knee
K_H	Rotational stiffness of torsion spring at the hip
K_K	Rotational stiffness of torsion spring at the knee
τ	Time at which damping coefficient changed
$M_{H\text{-static}}$	Static resistive moment acting at the hip
$M_{H\text{-kinetic}}$	Kinetic resistive moment acting at the hip
ROM	Range of motion

APPENDIX B: EQUATIONS ON MOTION FOR AB MODELS

$$L = \frac{1}{2}m_T {V_T}^2 + \frac{1}{2}m_S {V_S}^2 + \frac{1}{2}I_T {\omega_T}^2 + \frac{1}{2}I_S {\omega_S}^2 - m_T g y_T - m_S g y_S - \frac{1}{2}K_H {\theta_1}^2 - \frac{1}{2}K_K(\theta_2 - \theta_1)^2 \quad (10)$$

$$\frac{d}{dt}\left(\frac{\partial L}{\partial \dot{\theta_1}}\right) - \frac{\partial L}{\partial \theta_1} = -C_H \frac{d\theta_1}{dt} + C_K \frac{d\theta_2}{dt} - C_K \frac{d\theta_1}{dt} \quad (11)$$

$$\frac{d}{dt}\left(\frac{\partial L}{\partial \dot{\theta_2}}\right) - \frac{\partial L}{\partial \theta_2} = -C_K \frac{d\theta_2}{dt} + C_K \frac{d\theta_1}{dt} \quad (12)$$

L: Lagrangian

m_T: Mass of thigh (kg)

m_S: Mass of thigh (kg)

V_T: Linear velocity of thigh pinned at the hip $\left(\frac{m}{s}\right)$

V_S: Linear velocity of shank pinned at the knee $\left(\frac{m}{s}\right)$

I_T: Thigh moment of Inertia (kg m^2)

I_S: Shank moment of Inertia (kg m^2)

ω_T: Angular velocity of the thigh $\left(\frac{rad.}{s}\right)$

ω_S: Angular velocity of the shank $\left(\frac{rad.}{s}\right)$

g: gravitational constant $\left(\frac{m}{s^2}\right)$

y_T: Location of thigh mass center on y axis (m)

y_S: Location of shank mass center on y axis (m)

K_H: Constant for spring at hip $\left(\frac{N\,m}{rad.}\right)$

K_K: Constant for spring at knee $\left(\frac{N\,m}{rad.}\right)$

θ_2: Angular displacement of the knee (rad.)

θ_1: Angular displacement of the hip (rad.)

C_H: Coefficient of damper at hip $\left(\frac{kg\,m^2}{s\,rad.}\right)$

C_K: Coefficient of damper at knee $\left(\frac{kg\,m^2}{s\,rad.}\right)$

APPENDIX C: SIMMECHANICS MODEL OF TFA

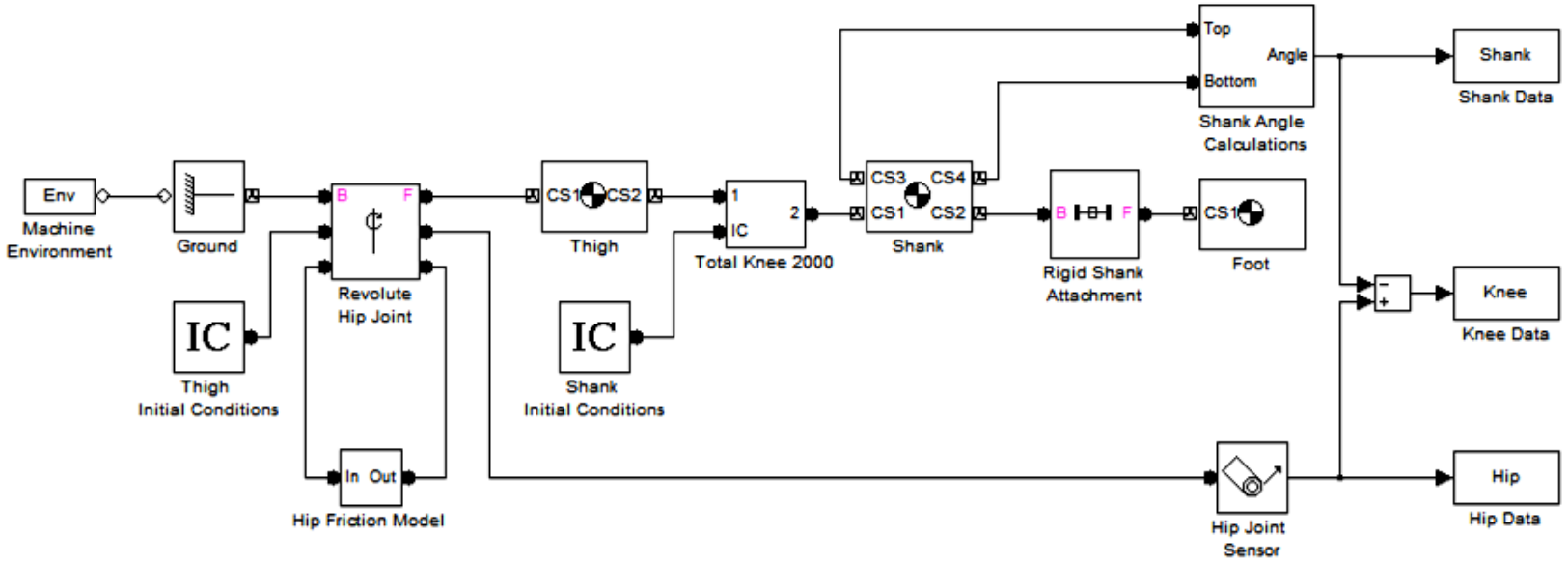

Figure 33: The SimMechanics block diagram of TFA-2 and TFA-3 models. The parameters of the foot and shank components were selected based on the physical models, as described in section 3.1.2.

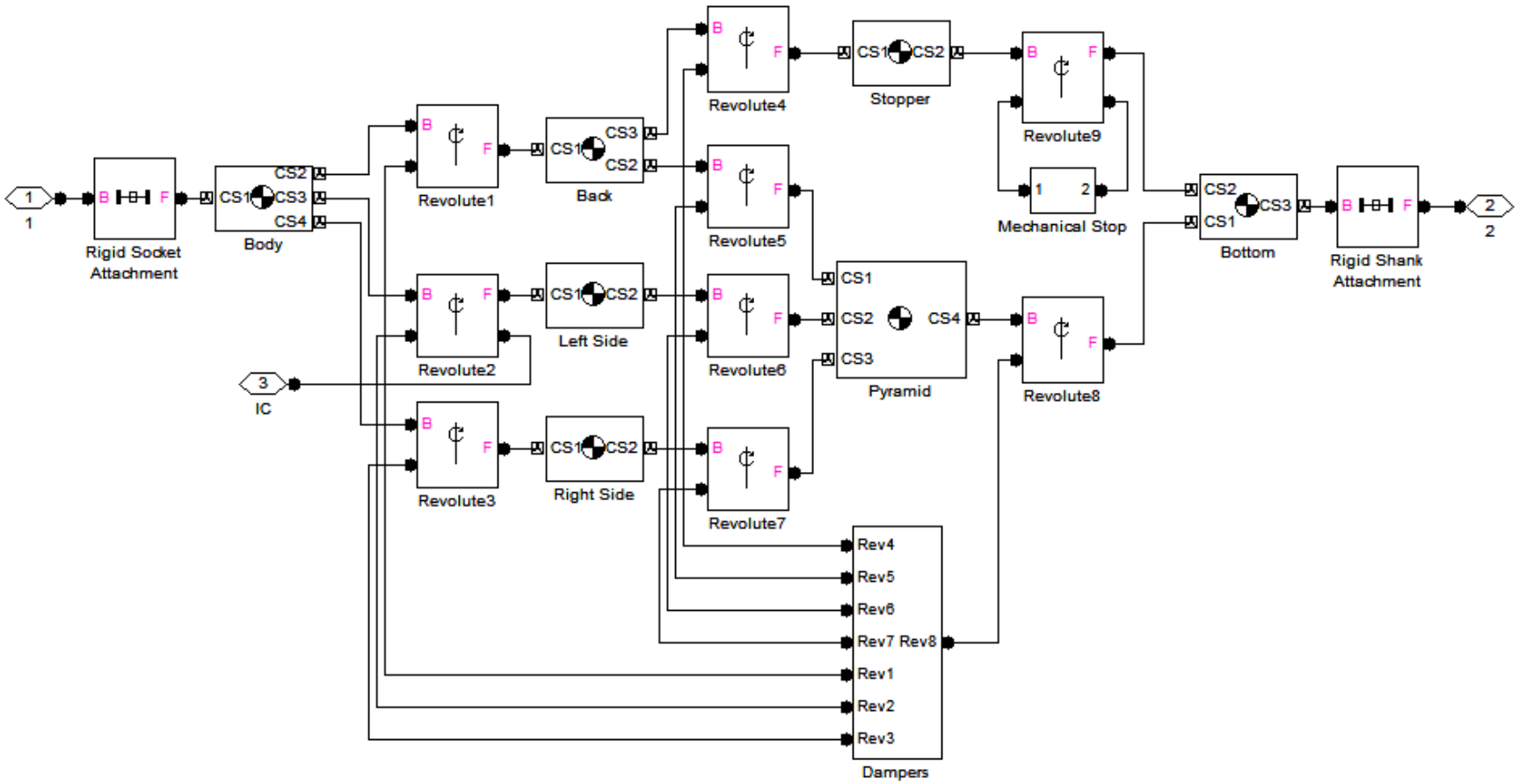

Figure 34: SimMechanics model of the Total Knee 2000 and its respective linkages. Connection point 1 indicates the proximal attachment to the thigh segment via the distal socket; connection point 2 indicates the distal attachment to the endoskeletal pylon of the shank (see Figure 33).

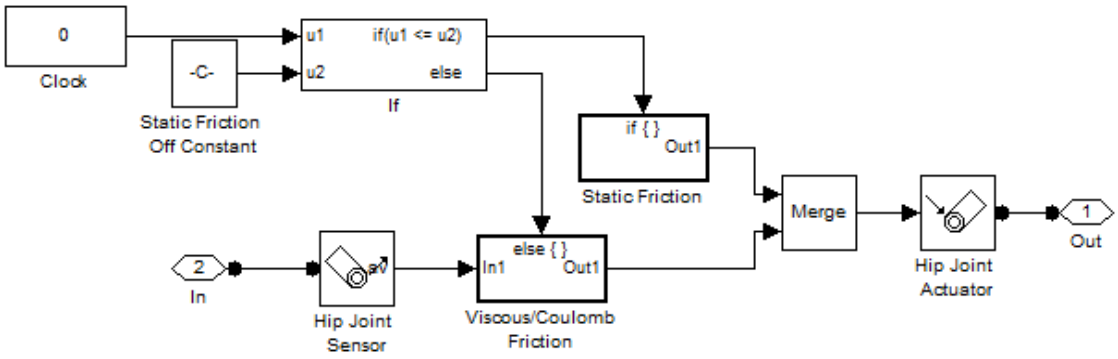

Figure 35: The static/viscous hip friction (models TFA-2 and TFA-3) was approximated using a conditional statement involving the time constant τ.

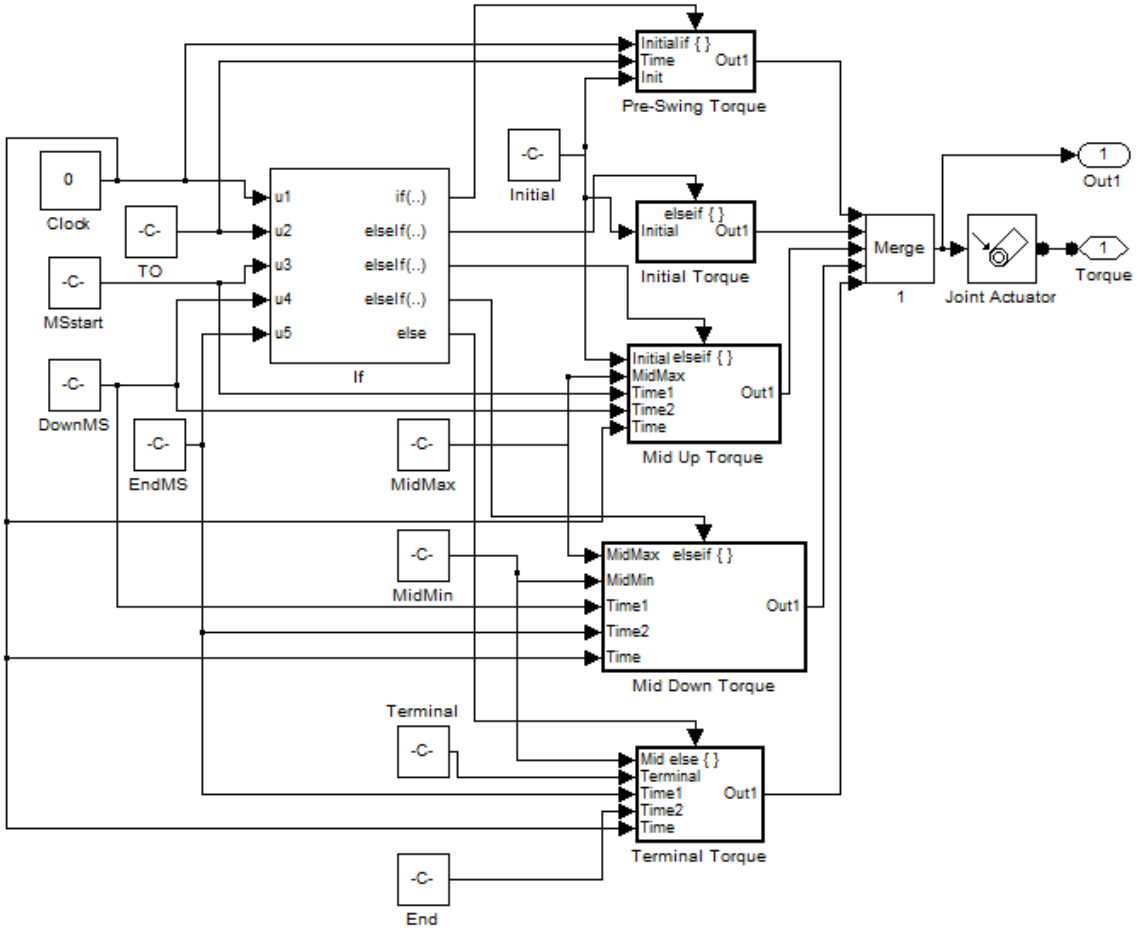

Figure 36: The piece-wise linear hip torque for the TFA-3 model was approximated using the logic in this block diagram.

APPENDIX D: OBJECTIVE FUNCTION RESULTS

Table 25: Optimized mechanical parameters for AB-2 and AB-3 models using alternative objective functions.

	Function	C_H $\left(\frac{kg\ m^2}{s\ rad.}\right)$	C_K $\left(\frac{kg\ m^2}{s\ rad.}\right)$	K_H $\left(\frac{N\ m}{rad.}\right)$	K_K $\left(\frac{N\ m}{rad.}\right)$	τ (s)
AB-2	$OF_{diff-hor}$ (°)	0	0.9714	0	0.1573	-
	$\overline{OF}_{ROM-hor}$ (-)	0	0.9585	0	0	-
	$\overline{OF}_{hor-ref}$ (-)	0	1.038	0	4.186	-
	$\overline{OF}_{vert-ref}$ (-)	0	0.9695	0	5.904	-
AB-3	$OF_{diff-hor}$ (°)	0	0/1.275*	0	7.358	0.1184
	$\overline{OF}_{ROM-hor}$ (-)	0	0/1.275*	0	7.358	0.1184
	$\overline{OF}_{hor-ref}$ (-)	0	0/1.275*	0	7.358	0.1184
	$\overline{OF}_{vert-ref}$ (-)	0	1.297/0.9325*	0	5.609	0.1199

*Values for before and after knee damper activation

Table 26: Hip, knee and shank RMS error values during swing for AB-2 and AB-3 models for the various objective functions.

		RMS Error		
	Function	θ_H	θ_K	ψ_S
AB-2	$OF_{diff-hor}$ (°)	1.896	9.058	10.62
	$\overline{OF}_{ROM-hor}$ (-)	1.523	9.885	11.01
	$\overline{OF}_{hor-ref}$ (-)	10.06	7.570	3.227
	$\overline{OF}_{vert-ref}$ (-)	12.74	12.86	1.776
AB-3	$OF_{diff-hor}$ (°)	11.18	9.729	2.070
	$\overline{OF}_{ROM-hor}$ (-)	11.18	9.729	2.070
	$\overline{OF}_{hor-ref}$ (-)	11.18	9.729	2.070
	$\overline{OF}_{vert-ref}$ (-)	12.89	13.18	1.981

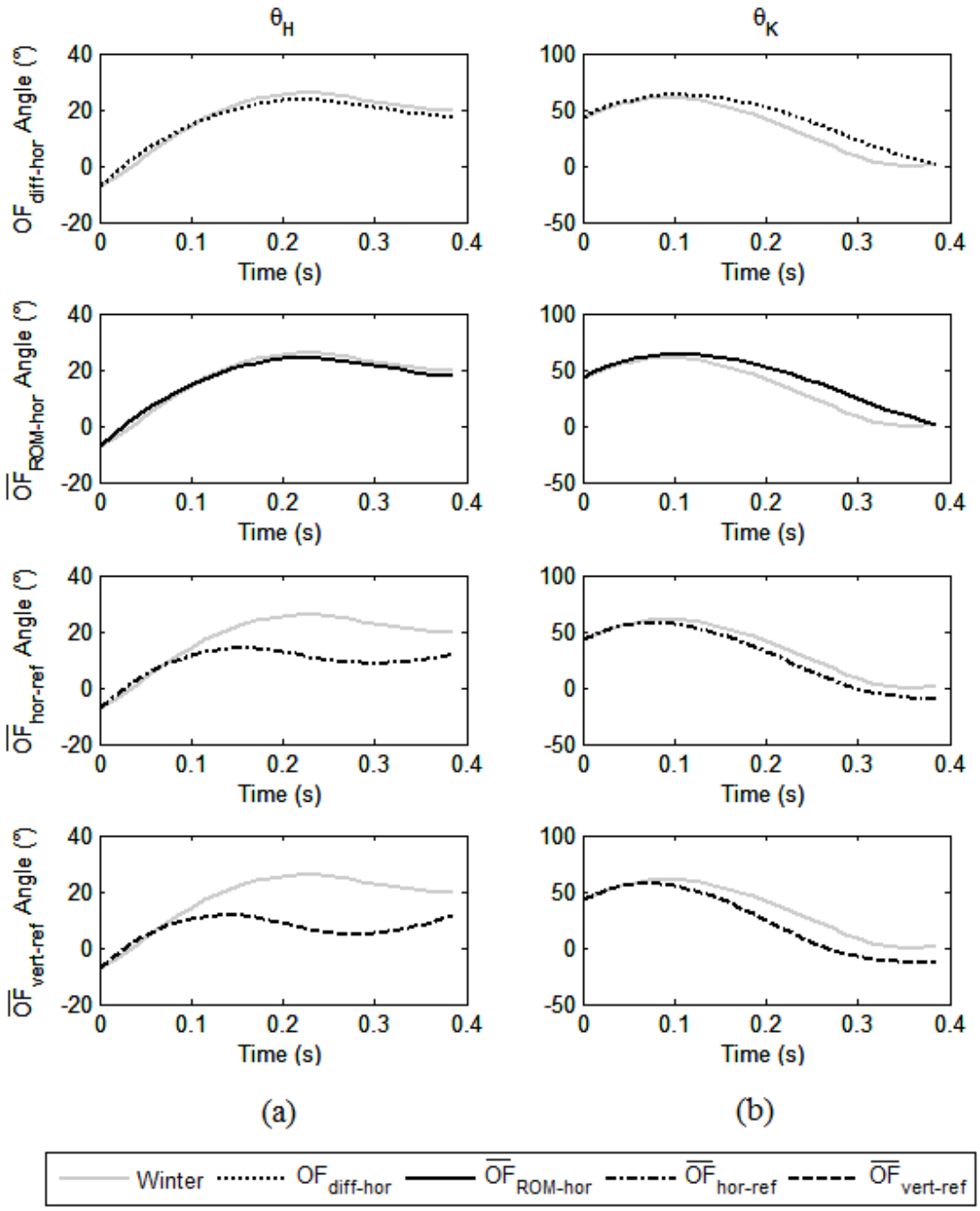

Figure 37: Comparison of simulated sagittal plane hip (right) and knee (left) joint motion during swing for the AB-2 model for each objective function compared with Winter [20] data. Positive angles indicate flexion; negative angles indicate extension.

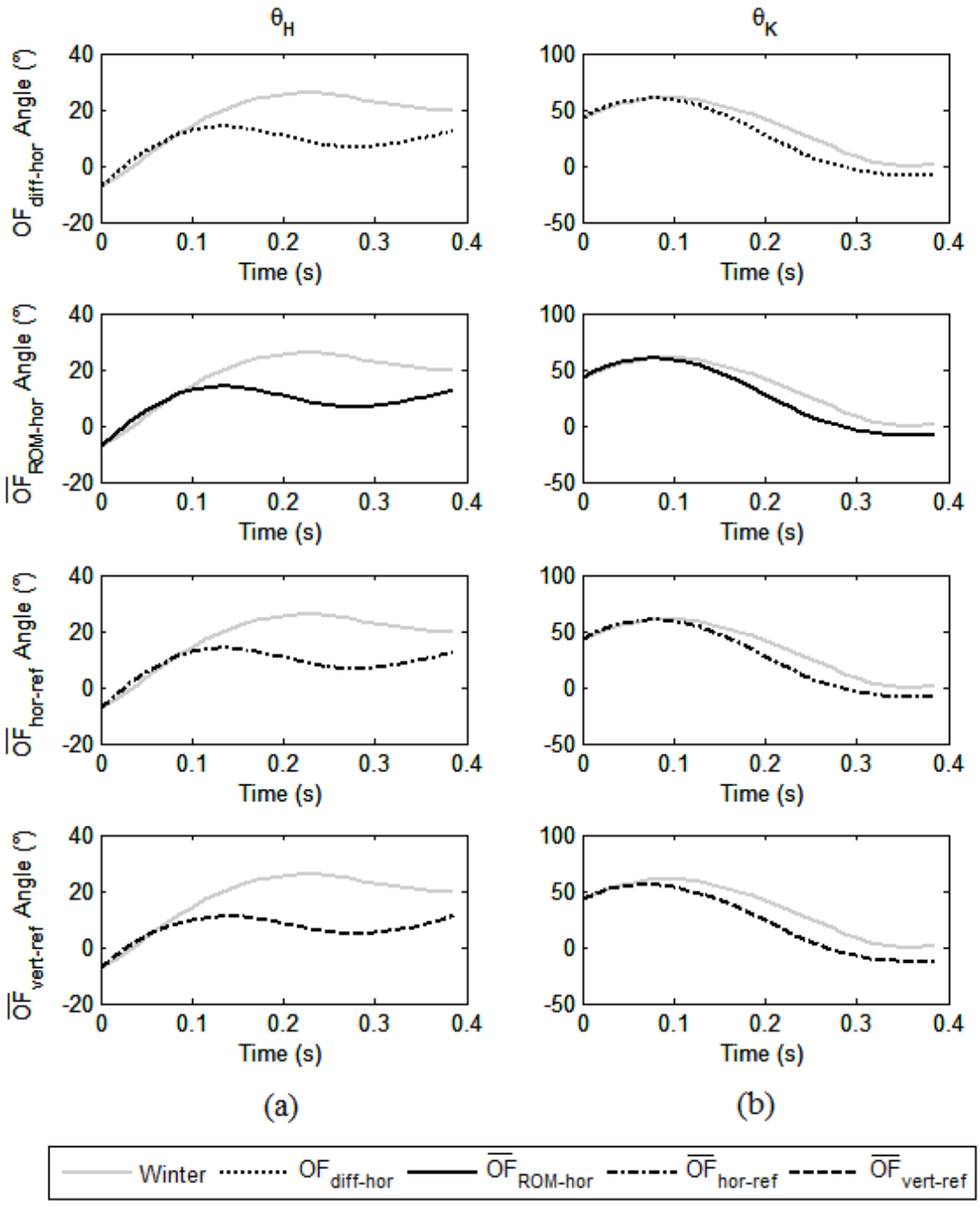

Figure 38: Comparison of simulated sagittal plane hip (left) and knee (right) joint motion during swing for the AB-3 model for each objective function compared with Winter [20] data. Positive angles indicate flexion; negative angles indicate extension.

Table 27: Optimized mechanical parameters for TFA-1 and TFA-2 models using alternative objective functions.

	Function	C_H $\left(\frac{kg\,m^2}{s\,rad.}\right)$	C_K $\left(\frac{kg\,m^2}{s\,rad.}\right)$	τ (s)	$M_{H\text{-static}}$ (N m)	$M_{H\text{-kinetic}}$ (N m)
TFA-1	$OF_{diff-hor}$ (°)	4.028	0.2086	-	-	-
	$\overline{OF}_{ROM-hor}$ (-)	3.881	0.2066	-	-	-
	$\overline{OF}_{hor-ref}$ (-)	4.149	0.2067	-	-	-
	$\overline{OF}_{vert-ref}$ (-)	3.114	0.2177	-	-	-
TFA-2	$OF_{diff-hor}$ (°)	0.3707	$6.44\text{x}10^{-4}$	0	$2.04\text{x}10^{-3}$	1.073
	$\overline{OF}_{ROM-hor}$ (-)	0.2638	$6.30\text{x}10^{-4}$	0	$2.26\text{x}10^{-5}$	1.108
	$\overline{OF}_{hor-ref}$ (-)	0.5540	$7.03\text{x}10^{-4}$	0	$2.48\text{x}10^{-4}$	1.058
	$\overline{OF}_{vert-ref}$ (-)	0	$5.38\text{x}10^{-4}$	0	$3.39\text{x}10^{-6}$	1.106

Table 28: Hip, knee, and shank RMS error values for TFA-1 and TFA-2 models using alternative objective functions.

		RMS Errors		
	Function	θ_H	θ_K	ψ_S
TFA-1	$OF_{diff-hor}$ (°)	0.5842	0.8539	0.3116
	$\overline{OF}_{ROM-hor}$ (-)	0.5774	0.8653	0.3230
	$\overline{OF}_{hor-ref}$ (-)	0.5997	0.8690	0.3067
	$\overline{OF}_{vert-ref}$ (-)	0.6537	1.254	0.6888
TFA-2	$OF_{diff-hor}$ (°)	0.1159	0.8781	0.9097
	$\overline{OF}_{ROM-hor}$ (-)	0.1047	0.9245	0.9264
	$\overline{OF}_{hor-ref}$ (-)	0.1389	0.8549	0.9115
	$\overline{OF}_{vert-ref}$ (-)	0.1085	1.029	1.011

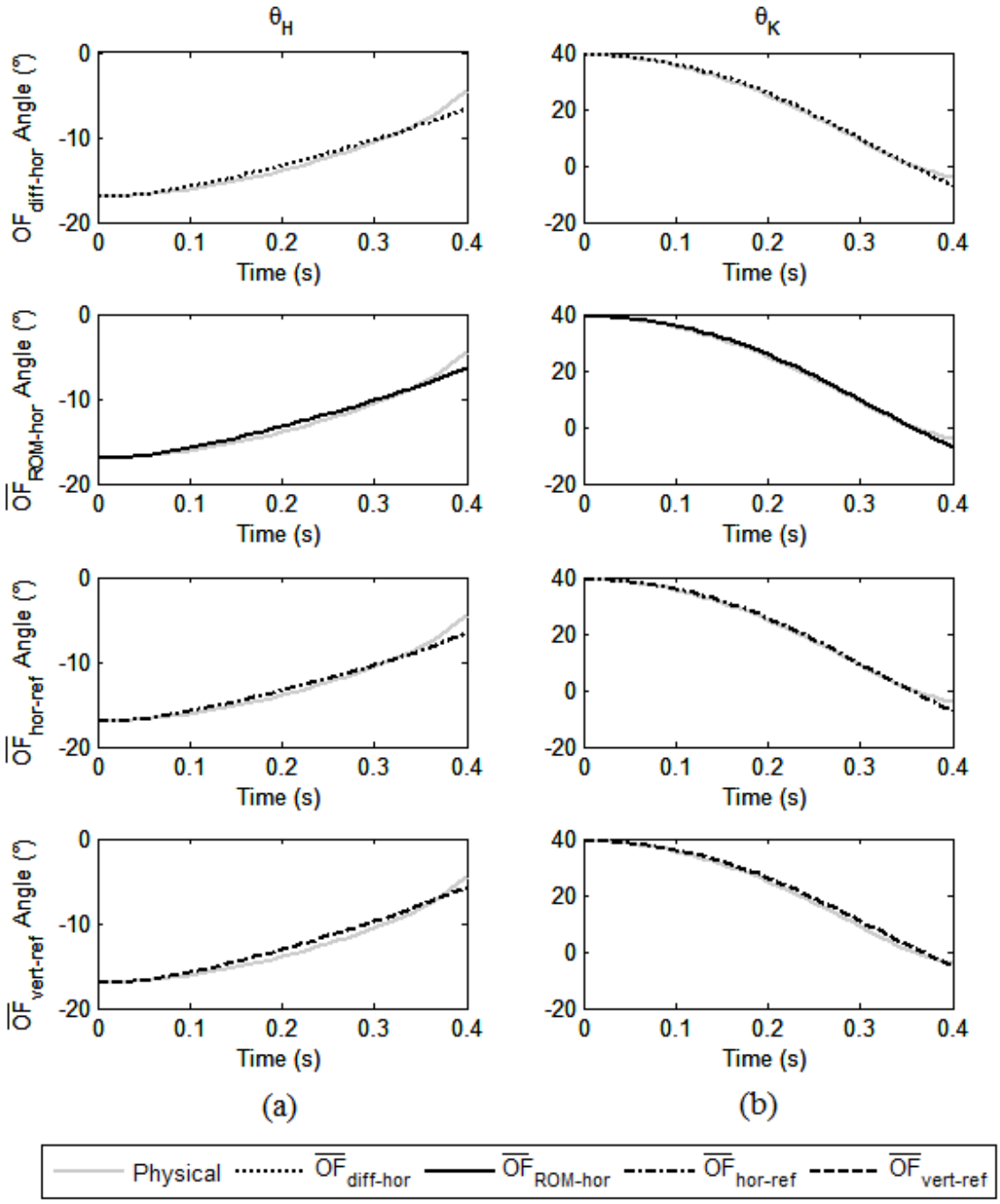

Figure 39: Comparison of simulated sagittal plane hip (left) and knee (right) joint motion during swing for the TFA-1 model for each objective function compared with the corresponding physical model. Positive angles indicate flexion; negative angles indicate extension.

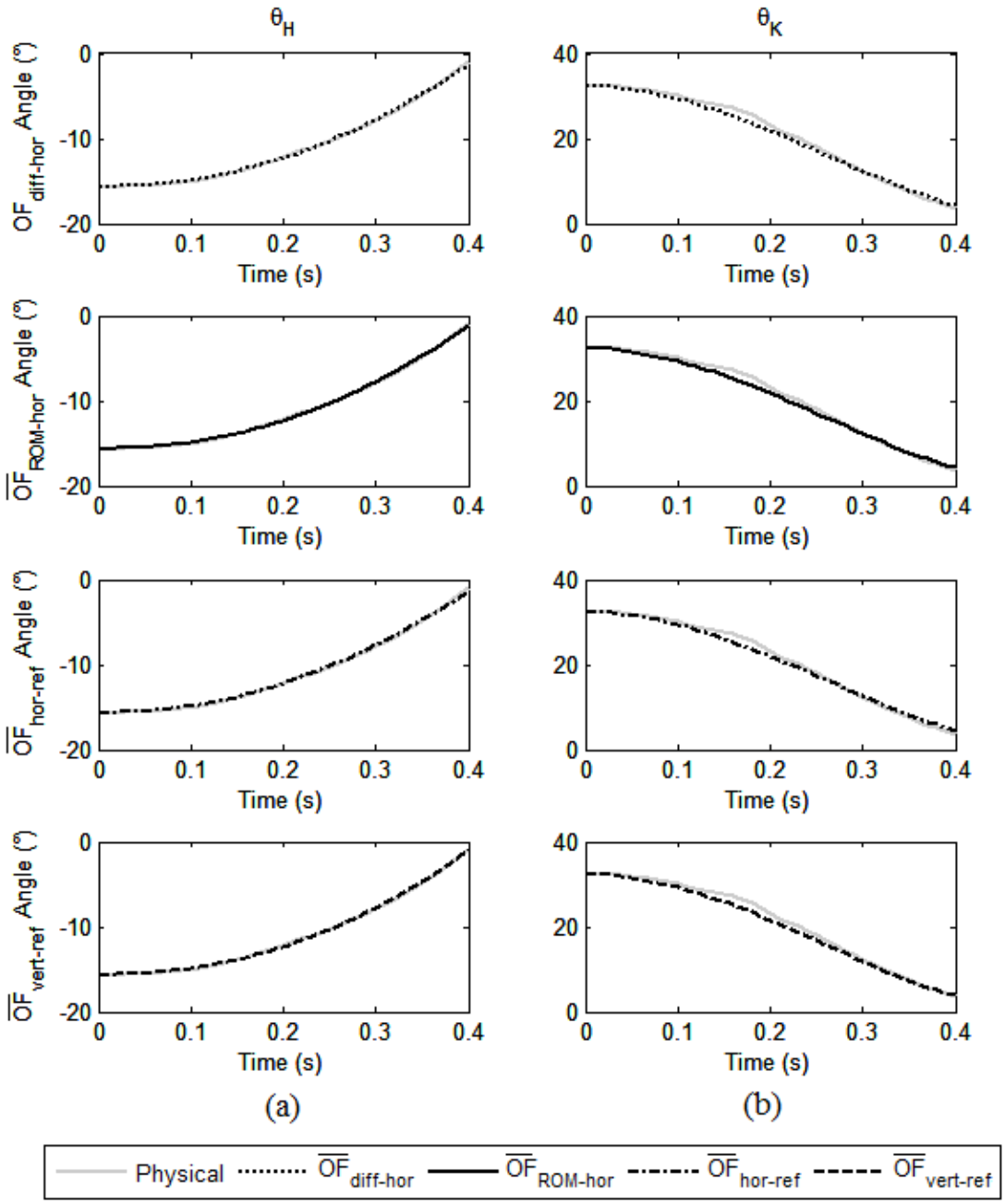

Figure 40: Comparison of simulated sagittal plane hip (left) and knee (right) joint motion during swing for the TFA-2 model for each objective function compared with the corresponding physical model. Positive angles indicate flexion; negative angles indicate extension.